CHARACTERIZATION AND DESIGN OF *SHEWANELLA ONEIDENSIS* AND *ESCHERICHIA COLI* AS CHASSIS FOR BIOELECTROCHEMICAL SYSTEMS

By

Megan Caroline Gruenberg Cross

A DISSERTATION

Submitted to
Michigan State University
in partial fulfillment of the requirements
for the degree of

Biochemistry and Molecular Biology – Doctor of Philosophy

2024

ABSTRACT

Microbial electrosynthesis (MES) is an emerging technology which, in the most extreme cases, uses an electroautotrophic biocatalyst to convert CO_2 and clean electricity into value-added products. Technologies that combine CO_2 remediation efforts with chemical production from fossil-fuel alternatives are promising contributors to the fight against climate change. MES is limited by presently available biocatalysts, which have small product scopes and few genetic engineering tools to improve them. For MES to be an industrially competitive technology, a robust biocatalyst which can be engineered to have a large product scope with high titers must be implemented. This dissertation describes progress toward the development of *Shewanella oneidensis* and *Eschericahia coli* as MES hosts.

MES uses clean electricity to power the unfavorable reduction reactions that take place in carbon fixation and conversion to fuels and chemicals. Thus, an important aspect of a MES biocatalyst is electroactivity. *S. oneidensis* is a metal-reducing bacteria that can respire extracellular metals and electrodes. It has a well-characterized extracellular electron transfer pathway, the Mtr pathway, and established genetic engineering tools which make it an attractive candidate for MES. However, *S. oneidensis* cannot fix CO_2.

CO_2-derived formate assimilation is considered for a CO_2-fixing *S. oneidensis* strain. Formatotrophy would need to be engineered; however, formate is toxic to this organism. As a first step toward engineering formatotrophy in *S. oneidensis*, several formate tolerant strains were evolved and mutations were characterized (Chapter 2).

To drive formate assimilation pathways, low potential electron carriers, such as reduced ferredoxin will be required. Therefore, we characterized the Rnf complex in *S.*

oneidensis, a potential source of low potential electrons, which led to the discovery that Rnf is essential for iron-sulfur cluster biosynthesis and repair in this organism (Chapter 3). This work confirmed that the Rnf complex is a source of reduced ferredoxins in *S. oneidensis* and could serve as a power source for carbon fixation pathways in the future.

In the course of our study of the *S. oneidensis* Rnf complex, the unusual observation that isopropyl β-D-1-thiogalactopyranoside (IPTG) altered growth of the organism was made. IPTG is often used to induce gene expression in engineered systems and is assumed to have no off-target effects on metabolism or regulation. However, in this work IPTG was found to improve growth of *S. oneidensis* cultivated with sugar substrate N-acetylglucosamine (Chapter 4). As the use of IPTG is so widespread, researchers in this field should be mindful of our results so false positive correlations can be avoided.

Another interesting candidate for a MES biocatalyst is *Escherichia coli*, one of the most well-studied microorganisms that has been engineered for fermentative biosynthesis of a vast array of compounds. The ability to connect these reactions to CO_2 fixation would offer viable means of production of such compounds from a fossil-fuel alternative while helping prevent release of CO_2. *E. coli* requires both the engineering of electroactivity and CO_2 fixation to be considered a viable option for MES, as the organism does not natively have either capability. In this work, the biotechnological potential of an electroactive strain of *E. coli* expressing the Mtr pathway from *S. oneidensis* is explored (Chapter 5).

Overall, this dissertation describes four experimental studies which contribute to overcoming the technical barriers of using *S. oneidensis* and *E. coli* as MES biocatalysts.

This work is dedicated to my husband and our growing family.

ACKNOWLEDGEMENTS

Graduate school can be a tough time. Ideally, you leave with much more knowledge and practical experience than you started with, and getting there is not an easy task. I am incredibly lucky and grateful that I had support from every front during the completion of my PhD that did away with the stereotype that graduate school can be one of the most difficult times of an academic's life.

My advisor, Michaela, was the foundation of my daily academic support. First, she took a chance, and accepted me into her lab during the first summer of COVID. Due to safety regulations in place at the time, I wasn't even allowed in the lab for a few months. That time wasn't wasted. I spent these months reading the literature and creating plans for when I would be allowed to start bench work. Michaela never let me fall between the cracks, even when we only existed to each other on Zoom and Slack. During the course of my PhD, she was always able to give me ideas and papers to read when I was feeling stuck. Michaela was always supportive in the lab, and she was also supportive of my personal goals. For example, when I wanted to take a few weeks off for my wedding and honeymoon during my final year, she was supportive, even though that meant I would be pausing a months-long experiment. The culture of growth and support Michaela cultivated in the lab set the standard for how lab members were expected to treat one another. I worked alongside people who warmly welcomed me and were always willing to help, including Dr. Kody Duhl, Dr. Magdalena Felczak, Dr. Kathryne Ford, Dr. Elhussiny Aboulnaga, Nicholas Tefft, Shaylynn Miller, and Emma Boismier. I will truly miss working with this team of dedicated scientists.

I also received much appreciated support from my committee members, Dr. Robert Hausinger, Dr. Claire Vieille, Dr. Daniel Ducat, and Dr. Bjoern Hamberger. I always felt as though committee meetings were a productive exchange of ideas that gave me new directions to explore in my research. I am especially grateful to my committee members for advising me more frequently during the summer that Michaela was on maternity leave. While I was pretty confident in my direction at the beginning of the summer, research always has a way of throwing your plans out of the window. Their guidance was instrumental in keeping me productive that summer.

Finally, I would like to thank my friends and family for their support from home. They stood behind me when I decided to change directions for my PhD that was going to add a few years onto my time in graduate school. While that was a difficult decision, I am ultimately a more capable scientist with a new outlook on what successful science looks like. My husband, parents, siblings, and close friends all served as much needed personal advisors during that time. I am so grateful that they supported me in taking a leap of faith and that the support I was receiving from my new environment lessened their burden.

I am very proud of the work I've done over the last four years, especially because of all the wonderful memories that came with it. Thank you to everyone who made my PhD experience so fulfilling. I couldn't have done it without you.

TABLE OF CONTENTS

LIST OF TABLES

LIST OF FIGURES

LIST OF ABBREVIATIONS

2xYT	2x yeast extract tryptone media
3P-glycerate	3-phosphoglycerate
Ace	pyruvate dehydrogenase
aceA	gene encoding isocitrate lyase
ackA	gene encoding acetate kinase
AckA	acetate kinase
AdhE	bifunctional aldehyde-alcohol dehydrogenase
ADP	adenosine diphosphate
agxT	gene encoding serine-pyruvate aminotransferase
AMP	adenosine monophosphate
apo	protein without its prosthetic group
ATP	adenosine triphosphate
BES	bioelectrochemical system
C1	one carbon
CA	carbonic anhydrase
caa	casamino acids
CBB	Calvin Benson Bassham
CCCP	carbonyl cyanide m-chlorophenyl hydrazone
CctA	periplasmic tetraheme cytochrome *c*
c-di-GMP	bis-(3′–5′)-cyclic-dimeric guanosine monophosphate
CDP-ME	4-diphosphocytidyl-2-C-methyl-D-erythritol-2-phosphate
CDP-MEP	methylerythritol cytidyl diphosphate
CFU	colony forming unit
cMEPP	2-C-methyl-D-erythritol-2,4- cyclodiphosphate
CMP	cytidine monophosphate
CoA	coenzyme A

CRISPRi	clustered regularly interspaced short palindromic repeats interference
crp	cAMP-responsive regulator of catabolite repression
CTP	cytidine triphosphate
CymA	cytochrome c-type protein
DAHP	3-Deoxy-D-arabinoheptulosonate 7-phosphate
DAP	2,6-diaminopimelic acid
dCas9	inactivated Cas9
dCTP	deoxycytidine triphosphate
dGMP	deoxyguanosine monophosphate
DMAPP	dimethylallyl diphosphate
DNA	deoxyribonucleic acid
dTTP	deoxythymidine triphosphate
DUF	domain of unknown function
DXP	1-deoxy-D-xylylose-5-phosphate
Dxr	1-deoxy-D-xylulose 5-phosphate reductoisomerase
Dxs	1-deoxy-D-xylulose-5-phosphate synthase
e^-	electron
$E^{o'}$	standard reduction potential
EET	extracellular electron transfer
Eno	enolase
FAD	flavin adenine dinucleotide
FccA	fumarate reductase flavoprotein
Fch	methenyltetrahydrofolate cyclohydrolase
FDH	formate dehydrogenase
Fhs	formate tetrahydrofolate ligase
FocA	bidirectional formate transporter

FolD	10-formyltetrahydrofolate synthase
Fpr	ferredoxin-NADP reductase
FrdABCD	fumarate reductase
FtfL	formate tetrahydrofolate ligase
FumBC	fumarate hydratase
Fur	ferric uptake regulation protein
G3P	glyceraldehyde 3-phosphate
GapA	glyceraldehyde-3-phosphate dehydrogenase
GCS	glycine cleavage system
GlyA	serine hydroxymethyltransferase
gmpA	gene encoding phosphoglycerate mutase
Gpm	phosphoglycerate mutase
GTP	guanosine monophosphate
H_4F	tetrahydrofolate
HEPES	4-(2-hydroxyethyl)-1-piperazineethanesulfonic acid
HexR	2-keto-3-deoxy-6-phosphogluconate-responsive transcriptional regulator
HMBPP	4-hydroxy-3-methyl-butenyl-1-diphosphate
HPLC	high performance liquid chromatography
IDI	Isopentenyl-diphosphate delta-isomerase
IET	inward electron transfer
IMP	inosine monophosphate
IPP	isopentyl diphosphate
IPTG	Isopropyl β-D-1-thiogalactopyranoside
ISC	iron sulfur cluster
IspD	2-C-methyl-D-erythritol 4-phosphate cytidylyltransferase
IspE	4-diphosphocytidyl-2-C-methyl-D-erythritol kinase

IspF	2-C-methyl-D-erythritol 2,4-cyclodiphosphate synthase
IspG	4-hydroxy-3-methylbut-2-en-1-yl diphosphate synthase
IspH	4-hydroxy-3-methylbut-2-enyl diphosphate reductase
kbl	gene encoding 2-amino-3-ketobutyrate coenzyme A ligase
LacI	lac repressor
LB	Lysogeny broth
LC-MS	liquid chromatography mass spectrometry
LdhA	lactate dehydrogenase
M5	minimal medium
mC	millicoulombs
Mdh	malate dehydrogenase
MEP	methylerythritol phosphate
MES	microbial electrosynthesis
ml	milliliter
mM	millimolar
mmol	millimole
MSA	multiple sequence alignment
MtdA	methylene tetrahydromethanopterin dehydrogenase
mV	millivolt
NAD	nicotinamide adenine dinucleotide
$NADP^+$	nicotinamide adenine dinucleotide phosphate
NAG	N-acetylglucosamine
nagR	gene encoding transcriptional repressor of N-acetylglucosamine utilization
NagR	transcriptional repressor of N-acetylglucosamine utilization
NEB	New England Biolabs
Nif	nitrogenase

NTA	nitrilotriacetic acid
NTF2	nuclear transport factor 2
Nth	endonuclease III
OD_{600}	optical density at 600 nanometers
OET	outward electron transfer
PCR	polymerase chain reaction
PDH	pyruvate dehydrogenase
pdhR	gene encoding pyruvate dehydrogenase
PEC	periplasmic electron carrier
PEP	phosphoenol pyruvate
pfkA	gene encoding ATP-dependent 6-phosphofructokinase isozyme 1
pfkB	gene encoding ATP-dependent 6-phosphofructokinase isozyme 2
PflB	pyruvate formate lyase
pgi	gene encoding glucose-6-phosphate isomerase
Pgk	phosphoglycerate kinase
pLDDT	predicted local distance difference test
PMF	proton motive force
pntAB	genes encoding NAD(P) transhydrogenase
Ppc	phosphoenolpyruvate carboxylase
ppsR	gene encoding phosphoenolpyruvate synthase regulatory protein
Prk	phosphoribulokinase
Prs	gene encoding ribose-phosphate pyrophosphokinase
Pta	phosphate acetyltransferase
Pyk	pyruvate kinase
Q	quinone
QH_2	quinol
Rf	riboflavin

rGly	reductive glycine
RID	refractive index
Rnf	*Rhodobacter* nitrogen fixation
RnfB	*Rhodobacter* nitrogen fixation subunit B
RnfC	*Rhodobacter* nitrogen fixation subunit C
Rpm	rotations per minute
rpoC	gene encoding DNA-directed RNA polymerase subunit beta
RuBisCO	ribulose-1,5-bisphosphate carboxylase/oxygenase
SbtA	sodium-dependent bicarbonate transporter
SdaA	serine dehydratase
serA	gene encoding serine dehydratase
sgRNA	single guide ribonucleic acid
Shikimate 3P	shikimate 3-phosphate
SoxR	redox-sensitive transcriptional activator
SUF	sulfur mobilization
TCA	tricarboxylic acid
TEA	terminal electron acceptor
ThT	thiflavin T
TRIC	trimeric intracellular cation
UDP	uridine diphosphate
UTP	uridine triphosphate
WT	wild type
yadS	gene encoding homotrimeric cation channel (TRIC) family protein
ybjU	gene encoding threonine aldolase
zwf	glucose-6-phosphate 1-dehydrogenase
µg	microgram
µl	microliter

μM	micromolar
σ	sigma factor

CHAPTER 1:

INTRODUCTION

CLIMATE CHANGE

Drilling for and burning fossil fuels is one of the greatest contributors to climate change and has led to a 1.1 °C increase in global temperatures since the pre-industrial era.[1] Climate change has widespread detrimental effects on the planet, such as changes in global temperatures, ocean acidification, melting glaciers, and extreme weather. Biodiversity loss is a major concern of climate change,[2,3] with some arguing that we are heading toward the Earth's sixth mass extinction.[4,5]

Plants and animals are not alone – humans are also paying the toll of a changing climate. Wildfires release fine particulate matter which pollutes the air and can cause both long and short-term health issues such as respiratory or cardiovascular complications, eye irritation, and corneal abrasions.[6,7] Heat waves can lead to heat stroke, heat exhaustion, cardiovascular complications, and death.[8,9] The World Health organization reports that heat-related deaths have increased by 70% in people 65 and older since 2000.[10] Disruptions in phenomena such as the timing of flower blooms,[11,12] declining bee populations,[13,14] and their effect on pollination can lead to difficulties in growing the food required for human and livestock sustenance.[15–17] The World Health Organization estimates that 98 million more people experienced food insecurity in 2020 than the average during 1981 – 2010.[10] An increase in extreme weather events such as hurricanes, floods, tsunamis, wildfires, and tornadoes have led to humanitarian crises across the globe.[18,19] Countries with low emission levels and few means to invest in preventative measures face the worst of this effect, paying the penalties for countries with highest emissions which do not feel the effects as strongly due to greater access to preventative

measures and aid.[20,21] To prevent the worst effects of climate change, the International Panel on Climate Change recommends limiting warming to below 2 °C.[1]

The warming of the planet comes from the accumulation of greenhouse gases in the atmosphere. These greenhouse gasses act as a heat trap, keeping energy from the sun in the Earth's atmosphere.[22] Burning of fossil fuels releases greenhouse gases like carbon dioxide (CO_2), which is one of the greatest drivers of climate change (**Figure 1**).[1] To limit climate change effects, greenhouse gas emissions must be significantly reduced to prevent their continued accumulation in the atmosphere.[1] The challenge with this goal is that CO_2 emissions are inevitable. Even a switch to burning renewably derived hydrocarbon fuels would result in the release of CO_2, as it is always a product in the combustion of hydrocarbons.[23] Therefore, CO_2 fixation and recycling are imperative efforts for climate change mitigation.[24]

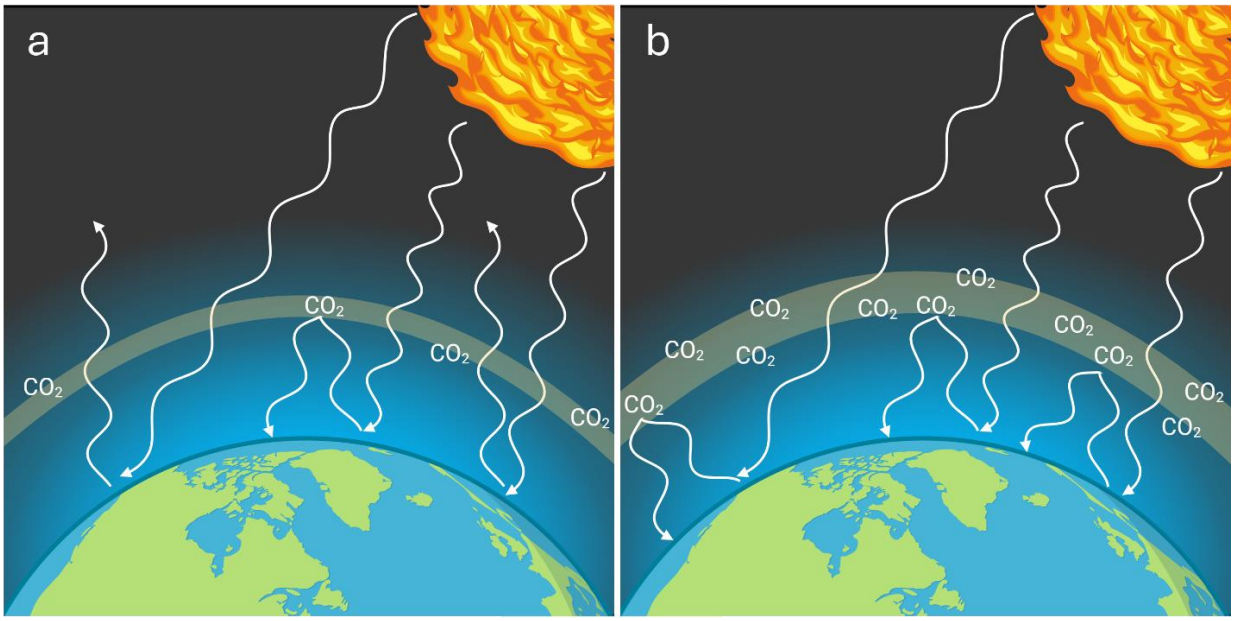

Figure 1. The greenhouse gas effect. a) Greenhouse gases help keep the planet warm by trapping heat from the sun. At appropriate levels, the greenhouse gases strike a balance between heat escape into space and heat retention which maintains healthy global temperatures. b) Increased greenhouse gas levels in the atmosphere traps more heat, which raises global temperatures. Created with BioRender.com.

If the threat of climate change wasn't enough to promote development and implementation of greener technology, a 2009 study using a modified Klass model estimated that coal, oil, and natural gas sources will be depleted by 2112, 2040, and 2042, respectively.[25] Shifting to new technologies that can produce energy and chemicals from renewable carbon sources must be a priority to keep meeting our energy needs on a planet that's fit to support life for centuries to come.[1,26]

RENEWABLE ENERGY

Electrical energy is a top contender for replacing fossil fuels. The transition to electrical energy can be seen most prominently with the push towards electric vehicles. For example, the major United States auto manufacturer Chrysler has announced that it plans for 100% of its fleet to be all-electric vehicles by 2028.[27] General Motors is expected to do the same by 2035;[28] and with the same target date, Ford has pledged for 40 – 50% of its fleet to be electric.[29] The Biden Administration also has plans for supporting a multi-million dollar effort to build an electric vehicle charging network across the country.[30] Even so, electrical energy cannot fully replace hydrocarbon fuel, especially in the cases of aviation and heat-intensive industrial processes.[31,32] Green production of biofuels from renewable carbon sources therefore remains an integral component of the shift away from fossil fuels.

Wind, solar, and hydroelectric power have long promised to be renewable, fossil-fuel-free methods of electrical energy generation. While there have been great advancements in these technologies, they are not capable of meeting our electrical energy demands, with over 62% of global electricity still being generated from coal and natural gas.[33] Power plants generate electricity as it is needed, with demand driving the real-time

production quantities.[34] This type of control does not exist with renewable electrical sources because of the intermittent forces that power them.[35] If the wind is not blowing or the sun is not shining, there is no electrical output whether there is demand or not. This poses a huge challenge to overcome with the feasibility of replacing fossil-fuel derived electrical energy with renewable sources.

Storage of clean electrical energy as chemical bonds in biofuels is a promising method to address two issues. First, the continuing demand for hydrocarbon fuels, and second, the intermittence of electrical energy production from renewable sources. Energy storage is a powerful tool which would allow clean energy to be used even during times when receiving electricity directly from these sources is not possible.

MICROBIAL ELECTROSYNTHESIS

Microbial electrosynthesis (MES) is a promising technology that has the potential to combine CO_2 remediation and clean electricity with the production of biofuels and other useful chemicals (**Figure 2**).[36,37] In this system, carbon from CO_2 is fixed by electroactive, autotrophic biocatalysts using clean electricity to power intracellular reduction reactions in a bioelectrochemical system (BES). In this system, electrical input from clean energy sources power the storage of electrons as chemical bonds in the resulting metabolic products. Genetic engineering of these biocatalyst can program biofuels or useful chemicals to be the main metabolic product from CO_2 and clean electricity.

MES biocatalysts are mainly acetogenic bacteria.[38] Acetogens are carbon-fixing microbes, some of which can use electron donors such as hydrogen or a cathode to power the reduction of CO_2 via the Wood-Ljungdahl pathway. Acetogens produce acetate as their main metabolic product from acetyl-CoA via substrate level phosphorylation.[38,41] As

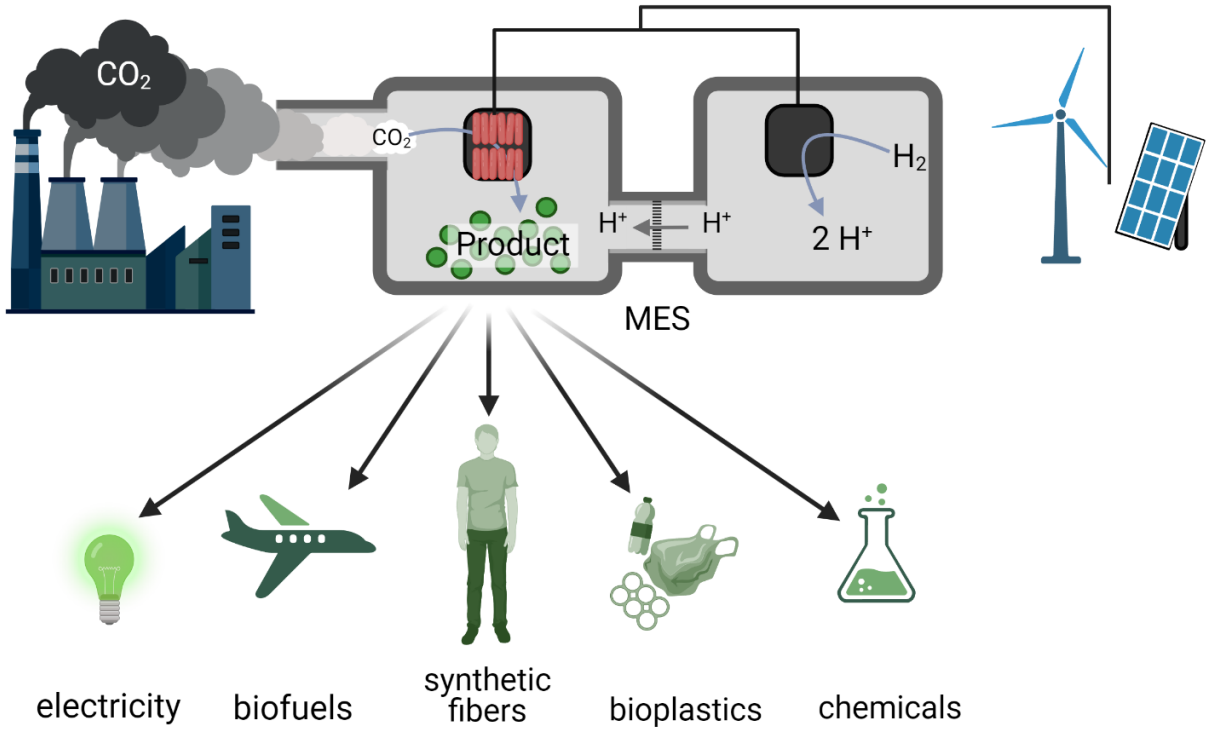

Figure 2. Microbial electrosynthesis. Microbial electrosynthesis converts CO_2 and clean electricity into useful chemical products that can be used for replacing hydrocarbons derived from fossil fuels. They could be used in production of biofuels, bioplastics, chemicals, synthetic fibers, and storage of electrical energy. Created with BioRender.com.

acetate is a low value and low energy density compound, metabolic engineering would be required to improve product scope and yields for these organisms to be competitive MES hosts.[38] Additionally, the mechanism of electron uptake by acetogens is not well understood, and different species may have different mechanisms.[41] Due to their limited product scope, little understanding of their electron transfer pathways, and limited genetic engineering tools, acetogens do not provide the power and flexibility required for commercially competitive industrial-scale MES, necessitating improvement to the system.[38–41]

Some success has been found in supplementing acetogens with mixed bacterial cultures; however, high acetate production remains an issue, and the mixed culture

composition is usually unknown, which significantly hampers the possibilities for targeting specific products.[42–44] Another issue with mixed cultures is that they are prone to off-target methane production due to increased methanogen populations in the reactors over time.[38] More information on current MES biocatalysts can be found on page 38. To overcome challenges with MES, a suitable biocatalyst must be engineered from organisms which have electroactivity, accessible genetic engineering tools, and well understood metabolisms and electron transfer pathways.

This dissertation explores two model organisms which have unique strengths for conversion to MES biocatalysts. The first is *Shewanella oneidensis*, a heterotrophic, facultative anaerobe with the capability of respiring solid, extracellular metals via its well-studied extracellular electron transfer (EET) pathway.[45–47] This EET pathway in *S. oneidensis* makes it capable of interfacing with an electrode.[46,47] *S. oneidensis*'s EET pathway, a good knowledge base of its metabolism, and established genetic engineering tools make this organism an attractive host for use in MES.[47–57] The second potential host for improved MES explored in this dissertation is *Escherichia coli*. As one of the most studied bacterial species, it has a plethora of genetic engineering tools which can be exploited for heterologous expression of CO_2 fixation and EET pathways.[58–64] *E. coli* has long been a host for fermentative biosynthesis of biofuels and chemicals.[64–70] Transfer of these fermentative biosynthesis systems into an electroautotrophic strain would be a monumental step toward realization of optimizing both the MES host and the possible product scope.

SHEWANELLA ONEIDENSIS AS A MES HOST

S. oneidensis MR-1 is a dissimilatory metal-reducing bacterium which can respire extracellular heavy metals such as iron, cobalt, and manganese.[71–73] This process is conducted by its EET pathways, with the major contributor being the Mtr pathway.[51,74,75] Electrons in the inner membrane quinone pool are used for EET. These electrons originate from substrates oxidized by quinone-linked oxidoreductases (e.g. NADH dehydrogenase). The Mtr pathway is initiated by inner membrane protein CymA, which transfers electrons from the quinone pool to the periplasm where they are deposited onto periplasmic electron carriers (PECs).[76-79] These PECs shuttle electrons to the other side of the periplasm where the MtrCAB complex transports the electrons across the outer membrane and deposits the electrons on an extracellular terminal electron acceptor (TEA) (**Figure 3a**).[51,78–81] For more information on the function of each component of the Mtr pathway, see pages 39 and 141.

Outward electron transfer (OET) is a native capability of *S. oneidensis* MR-1 which has allowed it to have great respiratory flexibility and gives it the ability to respire solid extracellular TEAs.[47,82,83] When cultivated in a BES, an anode can act as the TEA, and the pathway activity generates a current.[75,84] This capability has been harnessed for *S. oneidensis* use as a microbial fuel cell host.[46,53,85–87] In these systems, electricity is generated from the cellular oxidation of a substrate.[88,89] As a source of clean, renewable electricity, this technology is of great interest, especially when waste can be used as the substrate. For example, *S. oneidensis* has been used for electricity generation using wastewater in microbial fuel cells.[90,91]

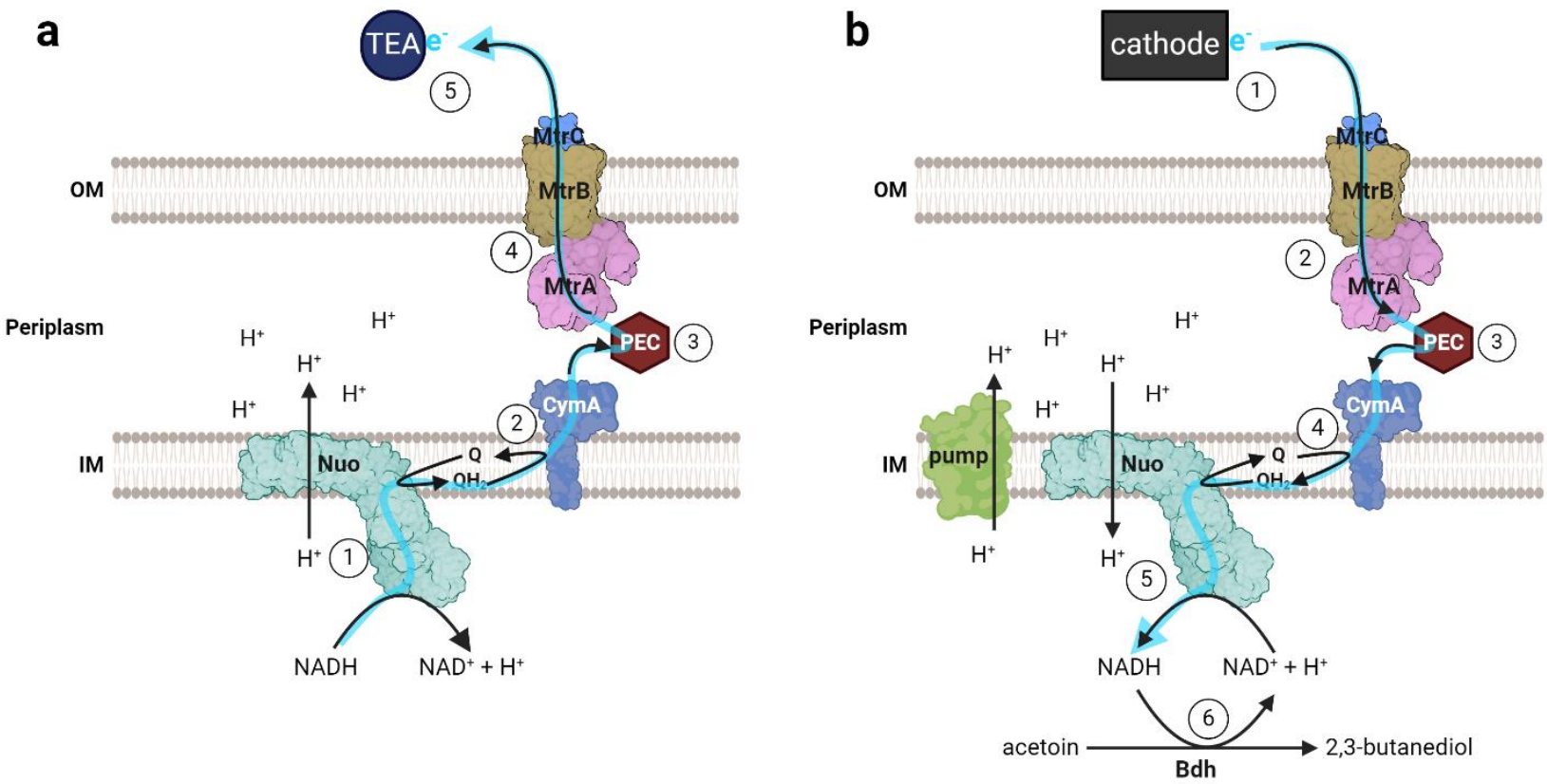

Figure 3. Extracellular electron transfer in *S. oneidensis*. a) Native outward electron transfer. Electrons are acquired through substrate oxidation by quinone-linked oxidoreductases like NADH dehydrogenase (Nuo) and are passed to the inner membrane quinone pool. CymA transfers electrons from the inner membrane quinone pool to periplasmic electron carriers (PEC). PECs deposit electrons with the outer membrane complex MtrCAB, which exports the electrons to the outer surface of the cell. Electrons are deposited on a terminal electron acceptor (TEA). b) Engineered inward electron transfer. The Mtr pathway is reversed when cultivated under cathodic conditions. The cathode can act as an electron source for the pathway. Electrons are transferred in the reverse order of inward electron transfer, with electrons from NADH being used to catalyze acetoin reduction via a heterologously expressed butanediol dehydrogenase (Bdh). Butanediol levels can act as an indicator of pathway function and efficiency. Reversed activity of proton-pumping Nuo depleted proton motive force (PMF). To replenish PMF, another proton pump must be used. This has been successful with green light-activated proteorhodopsin and native oxidases.

Wild-type *S. oneidensis* is also capable of inward electron transfer (IET). During IET, the electrons follow the same path as the native OET pathway in reverse. This has been demonstrated by applying a negative potential to *S. oneidensis* biofilm on a graphite electrode and monitoring reduction of exogenously added fumarate.[124] The reduction of fumarate was determined to be biotic activity, as shown by the deletion of Mtr pathway components *mtrA* and *cymA* decreasing fumarate reduction by 97% and 85%, respectively.[124] In this system, electrons derived from EET act as the electron donor for fumarate reduction to succinate by fumarate reductase. Oxygen can also act as a terminal electron acceptor for electrons taken up by IET.[48,96] Electrons in the quinone pool derived from EET follow two paths. First, they are used by NADH dehydrogenase to reduce NAD^+, a reaction which is coupled with consumption of proton motive force (PMF).[96] Second, the electrons are also used by terminal oxidases to generate PMF, complementing the activity of NADH dehydrogenase.[48,96]

Methods for IET optimization and IET tracking have been engineered in *S. oneidensis*.[48,92–95] Feeding of acetoin and expression of a heterologous butanediol dehydrogenase allows for NADH produced from IET to be monitored as 2,3-butanediol (**Figure 3b**).[93] This serves as proof-of-concept that IET can power intracellular reduction reactions as well as provide a quantifiable readout of the efficiency of the pathway. An important constraint to the IET pathway is the depletion of PMF. In the OET direction, NADH dehydrogenase acts as a proton pump, contributing to PMF. In the IET direction, NADH dehydrogenase uses PMF to power the reduction of NAD^+ to NADH (**Figure 3**).[93] If left uncorrected, IET would stop almost immediately because as soon as PMF was depleted, the reaction could no longer proceed. Therefore, another source of PMF is

required. This was accomplished in our lab with two methods. The first was the expression of a green light-driven proteorhodopsin.[93] This protein localizes to the inner membrane and pumps protons into the periplasm when illuminated with green light. While effective, light penetration decreases with increasing reactor volumes, which would make this technology difficult to scale up. To overcome this limitation, PMF can also be generated with native oxidases.[48,96] Since the Mtr pathway is an anaerobic respiration pathway, and because high oxygen levels cause reactive oxygen species formation in BESs, cultivation takes place in anoxic conditions. These anoxic conditions were previously thought to limit the contribution of PMF by oxidases. However, reactor dissolved oxygen concentrations were found to be ~1%, which is enough oxygen for the oxidases to generate PMF.[48] Therefore, the use of green light for *S. oneidensis* IET can be eliminated in microaerobic conditions, a potentially achievable scale-up requirement as complete anaerobic systems are difficult to maintain.

The IET pathway in *S. oneidensis* makes this organism an attractive potential host for MES. The missing component is CO_2 fixation. With an accessible genetic toolbox, engineering CO_2 fixation could be an achievable feat. There are many natural and synthetic options for engineering CO_2 fixation, including carboxylation-first pathways such as the reductive tricarboxylic acid (TCA) cycle and the Calvin Benson Bassham (CBB) cycle, and reduction-first pathways like the reductive glycine (rGly) pathway.[97,98] A reduction-first approach has the potential to make CO_2 fixation more feasible in *S. oneidensis*, as reduction-first pathways support greater biomass production and more efficient ATP utilization.[98,99] CO_2 reduction to formate, where formate is the one-carbon molecule which is assimilated into central metabolism, is an attractive option because

engineering CO_2 fixation through means such as the reductive TCA cycle or the CBB cycle can be a mountainous task.[100] In a reduction-first approach the metabolic engineering of formate assimilation can still be useful if CO_2 reduction cannot be achieved in *S. oneidensis* outright. For example, CO_2 could be pre-treated through its electrochemical reduction to formate, and subsequently the formate can act as the substrate for MES. Electrochemical reduction of CO_2 is a process which can be conducted at room temperature and pressure, which makes it feasible for inclusion in the MES bioreactor.[101]

Efforts toward both of these approaches in *S. oneidensis* are underway. The carboxylation route by RuBisCO and the CBB cycle are being modeled after CO_2 efforts in *E. coli*, which are described in detail on page 20.[50,125] Briefly, this approach separates upper and lower glycolysis at the step catalyzed by phosphoglycerate mutase (Gpm) in order to promote CO_2 assimilation via heterologously expressed RuBisCO, upper glycolysis, and the pentose phosphate pathway while cellular energy is produced from pyruvate via lower glycolysis and the TCA cycle (**Figure 4a**).[110-112] In *S. oneidensis*, the first step in separating these components of metabolism was accomplished through the use of CRISPRi and flux balance analysis modeling.[125] While Gpm was not essential in *E. coli*, initial efforts in making *gpmA* knockouts were unsuccessful. CRISPRi targeting *gpmA* and flux balance analysis modeling allowed for optimal knockout conditions to be uncovered and used for successful deletion of this conditionally essential gene.[125] *S. oneidensis* Δ*gpmA* harboring pCBB (a vector which expresses RuBisCO, phosphoribulokinase, and carbonic anhydrase) can grow on a combination of lactate and uridine, which will be utilized for chemostat evolution in a CO_2-containing atmosphere.[50] Lactate is converted to pyruvate which is used for energy production via the TCA cycle,

whereas uridine is used for biomass production in upper glycolysis and the pentose phosphate pathway. By restricting growth through limiting uridine concentrations, pressure will be provided to encourage CO_2 assimilation via RuBisCO.[50]

The reduction-first approach for CO_2 assimilation in *S. oneidensis* is modeled after the rGly pathway engineered in *E. coli*, which is described in detail on page 21. Briefly, the rGly pathway is a short, linear, energetically favorable pathway which uses CO_2-derived formate to generate serine (**Figure 4b**).[100] Conversion of serine to acetyl-CoA by serine dehydratase and pyruvate dehydrogenase can feed the CO_2-derived carbon into the TCA cycle. While the rGly pathway generally runs in the oxidative direction for glycine catabolism, all enzymatic steps from formate to serine are reversible.[110] The overall Δ_rG of this pathway at 1 mM concentrations of formate and CO_2 is approximately -6 kJ mol^{-1}, indicating that conversion of formate to serine is dependent upon adequate pathway substrate concentrations.[126] In *E. coli*, cellular growth coupled to reversed action of the rGly pathway was achieved with 30 mM formate and 10% CO_2.[117-119] This was achieved after streamlining the pathway by deleting all genes whose protein products siphon carbon away from the pathway, expressing missing rGly pathway enzymes, overexpressing limiting native rGly pathway enzymes, and short term adaptive laboratory evolution (see page 21).

All the proteins required for a functioning rGly pathway are encoded on the *S. oneidensis* MR-1 genome and have been detected by transcriptome analysis[127,128], indicating this method of CO_2 assimilation could be feasible in *S. oneidensis*. Most of the work toward implementing the rGly pathway in *S. oneidensis* has been focused on generating the necessary background strain – the glycine auxotroph. Glycine auxotrophy

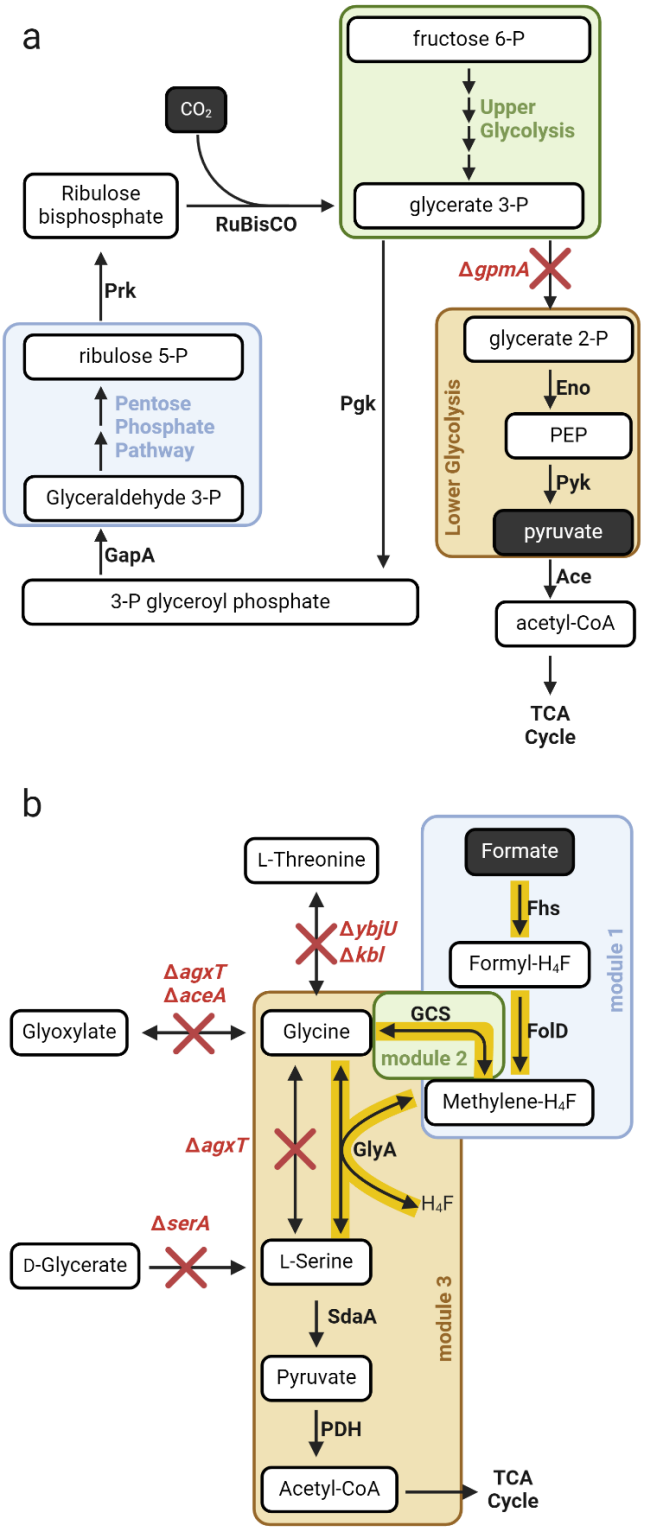

Figure 4. Proposed pathways for CO_2 fixation in *S. oneidensis*. a) Proposed pathway for engineering CO_2 fixation via the CBB cycle in *S. oneidensis*. Pathway substrates are highlighted in black. b) Proposed pathway for engineering formate assimilation via the rGly pathway in *S. oneidensis.* Arrows highlighted in yellow represent the rGly pathway. Pathway substrate highlighted in black. GCS – glycine cleavage system.

is achieved in *S. oneidensis* through the deletion of genes encodinng threonine aldolase, isocitrate lyase, 2-amino-3-ketobutyrate coenzyme A ligase, serine-pyruvate aminotransferase, and 3-phosphoglycerate dehydrogenase. *S. oneidensis* becomes more and more resistant to the homologous recombination deletion method after each gene deletion, which makes generating a five-gene knockout strain quite the feat. The glycine auxotroph strain was successfully generated after two years of genetic engineering. This glycine auxotroph cannot use formate to relieve the glycine auxotrophy, indicating that there is not enough reverse activity of the rGly pathway enzymes to support formate assimilation. Therefore, the next necessary step for implementing the rGly pathway in *S. oneidensis* is to express readily reversible rGly pathway enzymes in a modular format (**Figure 4b**). The approach taken will be similar to that of the *E. coli* model, details of which can be found on page 21.

S. oneidensis has three quinone-linked formate dehydrogenases and there is some evidence supporting their reversibility under cathodic potentials.[102] These promising data indicate that CO_2 reduction could occur *in vivo* and generate the formate required to feed the rGly pathway once it is established in *S. oneidensis* (**Figure 5**). As a cathode is already to be used for generating value-added products during MES, it can be used for powering CO_2 reduction, NADH generation, and downstream reduction reactions. For this reason, a cathode-driven biotic CO_2 reduction method is ideal for pairing with MES technology. Whether CO_2 reduction is achieved electrochemically or metabolically, it is clear that formate assimilation would provide *S. oneidensis* with the ability to utilize CO_2 derived compounds as a carbon and electron source for MES. In Chapter 2, progress toward this goal through generation of formate-tolerant *S. oneidensis* strains is discussed.

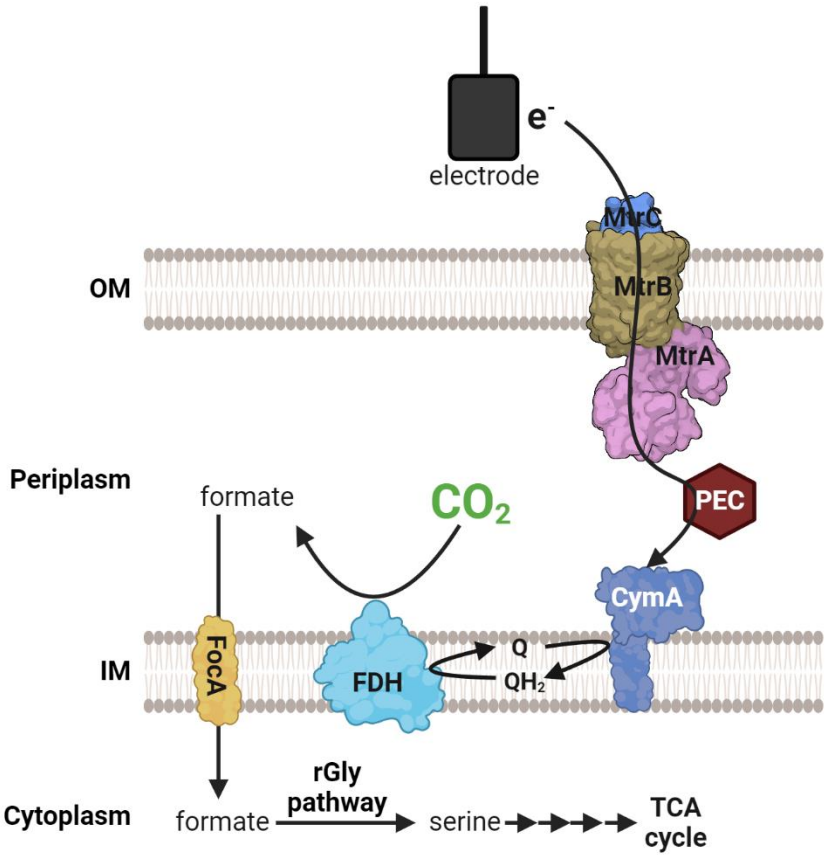

Figure 5. Schematic for using cathodic potentials to drive CO_2 assimilation in *S. oneidensis* via the rGly pathway.

OTHER CONSIDERATIONS FOR *S. ONEIDENSIS* AS A MES HOST

The *S. oneidensis* respiratory chain is highly branched, with the Mtr pathway being a critical component of anaerobic respiration via EET.[74,103] While many aspects of the respiratory chain have been explored, gaps in the literature still remain. For optimal performance of *S. oneidensis* as an MES host, the electron transfer pathways should be well understood so their influence on EET can be controlled. For example, low potential electrons such as those carried by ferredoxins or flavodoxins could act as yet-unidentified electron donors to the OET pathway. The Rnf complex has not been studied in *S.*

oneidensis. As a respiratory enzyme which connects the ferredoxin and NADH pools[104,105], Rnf could be an important source of low-potential electrons that may have influence over EET. Additionally, low potential electrons are needed for processes like carbon and nitrogen fixation. As important reactions to consider for developing an MES-compatible *S. oneidensis* strain, the generation of low-potential electrons is an important factor to consider. Characterization of the *S. oneidensis* complex and its broader role across species is discussed in Chapter 3.

As discussed above, genetic engineering is required for *S. oneidensis* to be a suitable MES host. One of the most common methods for testing recombinant proteins for their utility in strain improvement is by overexpressing their genes in the host strain under control of an isopropyl β-D-1-thiogalactopyranoside (IPTG)-inducible promoter.[106] An in-depth description of this system can be found on page 114. Since it is such a highly used system, sometimes the influence of IPTG on other cellular components can be overlooked or forgotten.[106] For rigorous optimization of MES host strains, it is imperative to understand the effects of not only the heterologous proteins on the system, but also their inducers. In Chapter 4, the influence of IPTG on wild-type *S. oneidensis* cultivated on N-acetylglucosamine, a common sugar feedstock for this organism, is discussed.

ESCHERICHIA COLI AS A MES HOST

E. coli is one of the most well-studied microbial production hosts.[62,63,107] It is frequently used in fermentative biosynthesis studies with high yields and titers, making it an attractive option for engineering a more robust MES host.[108,109] Its success as a production host comes from years of research into its metabolism and gene regulation, giving researchers great insights into its inner workings.[63,107,109] Additionally, many robust

genetic engineering tools have been developed for this organism, making it easier than ever to control metabolic and regulatory events inside the cell.[107] Unlike *S. oneidensis*, *E. coli* would need both aspects of MES (CO_2 fixation and EET) recombinantly expressed. Efforts into both of these engineering feats have been successfully implemented.

CO_2 fixation has been difficult to engineer in *E. coli*. One example of CO_2 fixation in recombinant *E. coli* comes from the expression of RuBisCO[110–112], a CO_2 fixing enzyme that is responsible for fixing 90% of inorganic carbon globally.[113] RuBisCO carboxylates ribulose 1,5-bisphosphate and it is assimilated through the CBB cycle.[114] To engineer CO_2 fixation via the CBB cycle, upper and lower metabolism in *E. coli* were separated through the deletion of *gpmA* and *gpmM*.[110] Expression of RuBisCO, phosphoribulokinase, and carbonic anhydrase allowed for CO_2 assimilation via endogenous upper glycolysis and pentose phosphate pathway enzymes in upper metabolism. Pyruvate was used to feed the energy-producing module of lower metabolism comprised of lower glycolysis and the TCA cycle. Additional deletions in *pfkA*, *pfkB*, and *zwf* made the strain dependent on CO_2 fixation by RiBisCO for growth on xylose. This strain was continuously evolved on xylose, pyruvate, and CO_2. The isolated evolved strain was able to generate all sugars from CO_2, a first step in engineering autotrophy.[110] Mutations identified to be helpful for CO_2 assimilation occurred in genes whose protein products are involved in generating biomass from intermediates of the CBB cycle (*prs, serA,* and *pgi*) and in carbon metabolism regulators (*crp* and *ppsR*).[111] Finally, the energy module fed by pyruvate was replaced by a NAD^+-dependent formate dehydrogenase from *Pseudomonas sp. 101*.[112] This allowed all biomass to be generated from CO_2 and all energy to be derived from formate, which could eventually be produced from CO_2 via a reversible formate dehydrogenase or

electrochemical reduction.[101,115] The limitation to RuBisCO is its slow rate of activity[116], which may not lend itself well to fueling rapid microbial growth.

As discussed above, a reduction-first approach to CO_2 fixation could be a useful strategy. This method has also been explored in *E. coli* using the rGly pathway for formate assimilation.[117-119] This consisted of expressing reversible rGly pathway enzymes, FtfL, Fch, and MtdA from *Methylobacterium extorquens* in an *E. coli* glycine auxotroph.[117] This strain was capable of growth using co-substrates formate and glucose. The next iteration of this strain was developed through overexpression of the native glycine cleavage system for greater conversion of formate to glycine, strong expression of *glyA* and *sdaA* for pyruvate production from glycine, and a NAD^+-dependent formate dehydrogenase from *Pseudomonas sp. 101* for energy production from formate.[118] After a few rounds of subculturing in high formate concentrations, the strain evolved to grow robustly on formate and CO_2, a necessary substrate for the rGly pathway. Two mutations allowed growth on formate alone: one in the promoter of the exogenously expressed formate dehydrogenase which improved energy production and one in the promoter of *pntAB* which increased availability of the rGly pathway cofactor NADPH.[118] Adaptive evolution generated an even more robust strain. The new strain contained mutations in the promoter region of *ackA* which decreased acetate uptake, *pdhR* which decreased oxidative flux of the TCA cycle, and *rpoC* which provided some unknown benefit to the strain.[119]

These engineering successes show that CO_2 fixation by either a carboxylation or a reduction-first method could be a viable means for implementing *E. coli* as a MES host. EET has also been engineered in *E. coli* as well, including methods using nanowires or the *S. oneidensis* Mtr pathway.[80,120–122] *E. coli* MFe444 is a recombinant strain which can

participate in EET using the Mtr pathway.[122] For an in-depth history of the development of this strain, see page 141. MFe444 participates in both OET and IET using lactate as an electron donor, making the Mtr pathway a viable option for endowing a CO_2-fixing strain with electroactivity.[58,61,122,123] As *E. coli* cannot ferment lactate, MFe444 given lactate as an electron donor would be incapable of the fermentative biosynthesis pathways for biofuel or chemical production that make this host so powerful. Therefore, detailed exploration into fermentable carbon and electron sources is necessary to assess its potential utility for MES. In Chapter 5, use of MFe444 as a host for glucose anodic and cathodic electro-fermentation is explored and discussed.

REFERENCES

1. Calvin, K. *et al. IPCC, 2023: Climate Change 2023: Synthesis Report. Contribution of Working Groups I, II and III to the Sixth Assessment Report of the Intergovernmental Panel on Climate Change [Core Writing Team, H. Lee and J. Romero (Eds.)]. IPCC, Geneva, Switzerland.* (2023) doi:10.59327/IPCC/AR6-9789291691647.

2. Mantyka-pringle, C. S., Martin, T. G. & Rhodes, J. R. Interactions between climate and habitat loss effects on biodiversity: a systematic review and meta-analysis. *Glob Chang Biol* **18**, 1239–1252 (2012).

3. Mooney, H. *et al.* Biodiversity, climate change, and ecosystem services. *Curr Opin Environ Sustain* **1**, 46–54 (2009).

4. Barnosky, A. D. *et al.* Has the Earth's sixth mass extinction already arrived? *Nature* **471**, 51–57 (2011).

5. Cowie, R. H., Bouchet, P. & Fontaine, B. The Sixth Mass Extinction: fact, fiction or speculation? *Biol Rev* **97**, 640–663 (2022).

6. Kinney, P. L. Climate Change, Air Quality, and Human Health. *Am J Prev Med* **35**, 459–467 (2008).

7. Xu, R. *et al.* Wildfires, Global Climate Change, and Human Health. *NEJM* **383**, 2173–2181 (2020).

8. Luber, G. & McGeehin, M. Climate Change and Extreme Heat Events. *Am J Prev Med* **35**, 429–435 (2008).

9. Kenney, W. L., Craighead, D. H. & Alexander, L. M. Heat Waves, Aging, and Human Cardiovascular Health. *Med Sci Sports Exerc* **46**, 1891–1899 (2014).

10. World Health Organization. Climate change. https://www.who.int/news-room/fact-sheets/detail/climate-change-and-health (2023).

11. Borghi, M., Perez de Souza, L., Yoshida, T. & Fernie, A. R. Flowers and climate change: a metabolic perspective. *New Phytologist* **224**, 1425–1441 (2019).

12. Tun, W., Yoon, J., Jeon, J.-S. & An, G. Influence of Climate Change on Flowering Time. *J Plant Biol* **64**, 193–203 (2021).

13. Goulson, D., Lye, G. C. & Darvill, B. Decline and Conservation of Bumble Bees. *Annu Rev Entomol* **53**, 191–208 (2008).

14. Cameron, S. A. *et al.* Patterns of widespread decline in North American bumble bees. *PNAS* **108**, 662–667 (2011).

15. Walters, J., Zavalnitskaya, J., Isaacs, R. & Szendrei, Z. Heat of the moment: extreme heat poses a risk to bee–plant interactions and crop yields. *Curr Opin Insect Sci* **52**, 100927 (2022).

16. Klein, A.-M. *et al.* Importance of pollinators in changing landscapes for world crops. *Proc R Soc B*, 303–313 (2007).

17. Decourtye, A., Alaux, C., Le Conte, Y. & Henry, M. Toward the protection of bees and pollination under global change: present and future perspectives in a challenging applied science. *Curr Opin Insect Sci* **35**, 123–131 (2019).

18. Ebi, K. L. *et al.* Extreme Weather and Climate Change: Population Health and Health System Implications. *Annu Rev Public Health* **42**, 293–315 (2021).

19. Amirkhani, M., Ghaemimood, S., von Schreeb, J., El-Khatib, Z. & Yaya, S. Extreme weather events and death based on temperature and CO_2 emission – A global retrospective study in 77 low-, middle- and high-income countries from 1999 to 2018. *Prev Med Rep* **28**, 101846 (2022).

20. Berlemann, M. & Wenzel, D. Hurricanes, economic growth and transmission channels. *World Dev* **105**, 231–247 (2018).

21. Noy, I. The macroeconomic consequences of disasters. *J Dev Econ* **88**, 221–231 (2009).

22. NRDC. Greenhouse Effect 101. https://www.nrdc.org/stories/greenhouse-effect-101#whatis (2023).

23. Speight, J. G. Combustion of hydrocarbons. in *Handbook of Industrial Hydrocarbon Processes* 421–463 (Elsevier, 2020). doi:10.1016/B978-0-12-809923-0.00010-2.

24. Jeffry, L. *et al.* Greenhouse gases utilization: A review. *Fuel* **301**, 121017 (2021).

25. Shafiee, S., & Topal, E. When will fossil fuel reserves be diminished? *Energy Policy*, *37*(1), 181–189 (2009).

26. Moore, B. *et al.* Transformations for climate change mitigation: A systematic review of terminology, concepts, and characteristics. *WIREs Climate Change* **12**, (2021).

27. Wayland, M. Chrysler kicks off plans to go all-electric by 2028 with debut of Airflow EV concept car. *CNBC* (2022).

28. Boudette, N. E. & Davenport, C. G.M. Will Sell Only Zero-Emission Vehicles by 2035. *The New York Times* (2021).

29. Ford Newsroom. Ford to lead America's shift to electric vehicles with new mega campus in Tennessee and twin battery plants in Kentucky; $11.4B investment to create 11,000 jobs and power new lineup of advanced EVS.

https://media.ford.com/content/fordmedia/fna/us/en/news/2021/09/27/ford-to-lead-americas-shift-to-electric-vehicles.html (2021).

30. U.S. Department of Transportation. Biden-Harris Administration Announces $623 Million in Grants to Continue Building Out Electric Vehicle Charging Network. (2024).

31. Sarwer, A. *et al.* Suitability of Biofuels Production on Commercial Scale from Various Feedstocks: A Critical Review. *ChemBioEng Reviews* **9**, 423–441 (2022).

32. Thiel, G. P. & Stark, A. K. To decarbonize industry, we must decarbonize heat. *Joule* **5**, 531–550 (2021).

33. Leonard, M. D., Michaelides, E. E. & Michaelides, D. N. Energy storage needs for the substitution of fossil fuel power plants with renewables. *Renew Energy* **145**, 951–962 (2020).

34. United States Environmental Protection Agency. U.S. Electricity Grid & Markets. https://www.epa.gov/green-power-markets/us-electricity-grid-markets (2023).

35. Basit, M. A., Dilshad, S., Badar, R. & Sami ur Rehman, S. M. Limitations, challenges, and solution approaches in grid-connected renewable energy systems. *Int J Energy Res* **44**, 4132–4162 (2020).

36. Dessì, P. *et al.* Microbial electrosynthesis: Towards sustainable biorefineries for production of green chemicals from CO_2 emissions. *Biotechnol Adv* **46**, 107675 (2021).

37. Jourdin, L. & Burdyny, T. Microbial Electrosynthesis: Where Do We Go from Here? *Trends Biotechnol* **39**, 359–369 (2021).

38. Prévoteau, A., Carvajal-Arroyo, J. M., Ganigué, R. & Rabaey, K. Microbial electrosynthesis from CO_2: forever a promise? *Curr Opin Biotechnol* **62**, 48–57 (2020).

39. Katsyv, A. & Müller, V. Overcoming Energetic Barriers in Acetogenic C1 Conversion. *Front Bioeng Biotechnol* **8**, (2020).

40. Philips, J. Extracellular Electron Uptake by Acetogenic Bacteria: Does H_2 Consumption Favor the H_2 Evolution Reaction on a Cathode or Metallic Iron? *Front Microbiol* **10**, (2020).

41. Rosenbaum, M. A. & Henrich, A. W. Engineering microbial electrocatalysis for chemical and fuel production. *Curr Opin Biotechnol* **29**, 93–98 (2014).

42. Ganigué, R., Puig, S., Batlle-Vilanova, P., Balaguer, M. D. & Colprim, J. Microbial electrosynthesis of butyrate from carbon dioxide. *Chem Comm* **51**, 3235–3238 (2015).

43. Raes, S. M. T., Jourdin, L., Buisman, C. J. N. & Strik, D. P. B. T. B. Continuous Long-Term Bioelectrochemical Chain Elongation to Butyrate. *ChemElectroChem* **4**, 386–395 (2017).

44. Arends, J. B. A., Patil, S. A., Roume, H. & Rabaey, K. Continuous long-term electricity-driven bioproduction of carboxylates and isopropanol from CO_2 with a mixed microbial community. *J CO_2 Util* **20**, 141–149 (2017).

45. Fredrickson, J. K. *et al.* Towards environmental systems biology of *Shewanella*. *Nat Rev Microbiol* **6**, 592–603 (2008).

46. Ikeda, S. *et al. Shewanella oneidensis* MR-1 as a bacterial platform for electro-biotechnology. *Essays Biochem* **65**, 355–364 (2021).

47. Beblawy, S. *et al.* Extracellular reduction of solid electron acceptors by *Shewanella oneidensis*. *Mol Microbiol* **109**, 571–583 (2018).

48. Ford, K. C. & TerAvest, M. A. The electron transport chain of *Shewanella oneidensis* MR-1 can operate bidirectionally to enable microbial electrosynthesis. *Appl Environ Microbiol* **90**, (2024).

49. Brutinel, E. D. & Gralnick, J. A. Shuttling happens: soluble flavin mediators of extracellular electron transfer in *Shewanella*. *Appl Microbiol Biotechnol* **93**, 41–48 (2012).

50. Ford, K. C. Microbial Electrosynthesis in *Shewanella oneidensis* MR-1. (Michigan State University, East Lansing, 2023).

51. Breuer, M., Rosso, K. M., Blumberger, J. & Butt, J. N. Multi-haem cytochromes in *Shewanella oneidensis* MR-1: structures, functions and opportunities. *J R Soc Interface* **12**, 20141117 (2015).

52. Serres, M. H. & Riley, M. Genomic Analysis of Carbon Source Metabolism of *Shewanella oneidensis* MR-1: Predictions versus Experiments. *J Bacteriol* **188**, 4601 (2006).

53. Kouzuma, A., Kasai, T., Hirose, A. & Watanabe, K. Catabolic and regulatory systems in *Shewanella oneidensis* MR-1 involved in electricity generation in microbial fuel cells. *Front Microbiol* **6**, (2015).

54. Flynn, C. M., Hunt, K. A., Gralnick, J. A. & Srienc, F. Construction and elementary mode analysis of a metabolic model for *Shewanella oneidensis* MR-1. *Biosystems* **107**, 120–128 (2012).

55. Pinchuk, G. E. *et al.* Pyruvate and Lactate Metabolism by *Shewanella oneidensis* MR-1 under Fermentation, Oxygen Limitation, and Fumarate Respiration Conditions. *Appl Environ Microbiol* **77**, 8234–8240 (2011).

56. McLean, J. S. *et al.* Investigations of structure and metabolism within *Shewanella oneidensis* MR-1 biofilms. *J Microbiol Methods* **74**, 47–56 (2008).

57. Tang, Y. J., Meadows, A. L., Kirby, J. & Keasling, J. D. Anaerobic Central Metabolic Pathways in *Shewanella oneidensis* MR-1 Reinterpreted in the Light of Isotopic Metabolite Labeling. *J Bacteriol* **189**, 894–901 (2007).

58. TerAvest, M. A., Zajdel, T. J. & Ajo-Franklin, C. M. The Mtr Pathway of *Shewanella oneidensis* MR-1 Couples Substrate Utilization to Current Production in *Escherichia coli*. *ChemElectroChem* **1**, 1874–1879 (2014).

59. Goldbeck, C. P. *et al.* Tuning Promoter Strengths for Improved Synthesis and Function of Electron Conduits in *Escherichia coli*. *ACS Synth Biol* **2**, 150–159 (2013).

60. Jensen, H. M., TerAvest, M. A., Kokish, M. G. & Ajo-Franklin, C. M. CymA and Exogenous Flavins Improve Extracellular Electron Transfer and Couple It to Cell Growth in Mtr-Expressing *Escherichia coli*. *ACS Synth Biol* **5**, 679–688 (2016).

61. Lienemann, M. *et al.* Towards patterned bioelectronics: facilitated immobilization of exoelectrogenic *Escherichia coli* with heterologous pili. *Microb Biotechnol* **11**, 1184–1194 (2018).

62. Pontrelli, S. *et al. Escherichia coli* as a host for metabolic engineering. *Metab Eng* **50**, 16–46 (2018).

63. Hoesl, M. G. & Budisa, N. Recent advances in genetic code engineering in *Escherichia coli*. *Curr Opin Biotechnol* **23**, 751–757 (2012).

64. Liu, T. & Khosla, C. Genetic Engineering of *Escherichia coli* for Biofuel Production. *Annu Rev Genet* **44**, 53–69 (2010).

65. Yu, C., Cao, Y., Zou, H. & Xian, M. Metabolic engineering of *Escherichia coli* for biotechnological production of high-value organic acids and alcohols. *Appl Microbiol Biotechnol* **89**, 573–583 (2011).

66. Chen, X. *et al.* Metabolic engineering of *Escherichia coli*: A sustainable industrial platform for bio-based chemical production. *Biotechnol Adv* **31**, 1200–1223 (2013).

67. Wen, M., Bond-Watts, B. B. & Chang, M. C. Production of advanced biofuels in engineered E. coli. *Curr Opin Chem Biol* **17**, 472–479 (2013).

68. Huffer, S., Roche, C. M., Blanch, H. W. & Clark, D. S. *Escherichia coli* for biofuel production: bridging the gap from promise to practice. *Trends Biotechnol* **30**, 538–545 (2012).

69. Clomburg, J. M. & Gonzalez, R. Biofuel production in *Escherichia coli*: the role of metabolic engineering and synthetic biology. *Appl Microbiol Biotechnol* **86**, 419–434 (2010).

70. Koppolu, V. & Vasigala, V. K. Role of *Escherichia coli* in Biofuel Production. *Microbiol Insights* **9**, MBI.S10878 (2016).

71. Bücking, C., Schicklberger, M. & Gescher, J. The Biochemistry of Dissimilatory Ferric Iron and Manganese Reduction in *Shewanella oneidensis*. in *Microbial Metal Respiration* 49–82 (Springer Berlin Heidelberg, Berlin, Heidelberg, 2013). doi:10.1007/978-3-642-32867-1_3.

72. Hau, H. H., Gilbert, A., Coursolle, D. & Gralnick, J. A. Mechanism and Consequences of Anaerobic Respiration of Cobalt by *Shewanella oneidensis* Strain MR-1. *Appl Environ Microbiol* **74**, 6880–6886 (2008).

73. Cooper, R. E., Goff, J. L., Reed, B. C., Sekar, R. & Dichristina, T. J. Breathing Iron: Molecular Mechanism of Microbial Iron Reduction by *Shewanella oneidensis*. in *Manual of Environmental Microbiology* 5.2.1-1-5.2.1-13 (ASM Press, Washington, DC, USA, 2015). doi:10.1128/9781555818821.ch5.2.1.

74. Coursolle, D. & Gralnick, J. A. Modularity of the Mtr respiratory pathway of *Shewanella oneidensis* strain MR-1. *Mol Microbiol* **77**, 995–1008 (2010).

75. Coursolle, D., Baron, D. B., Bond, D. R. & Gralnick, J. A. The Mtr Respiratory Pathway Is Essential for Reducing Flavins and Electrodes in *Shewanella oneidensis*. *J Bacteriol* **192**, 467–474 (2010).

76. Marritt, S. J. *et al.* The roles of CymA in support of the respiratory flexibility of *Shewanella oneidensis* MR-1. *Biochem Soc Trans* **40**, 1217–1221 (2012).

77. Marritt, S. J. *et al.* A functional description of CymA, an electron-transfer hub supporting anaerobic respiratory flexibility in *Shewanella*. *Biochemical Journal* **444**, 465–474 (2012).

78. Sturm, G. *et al.* A dynamic periplasmic electron transfer network enables respiratory flexibility beyond a thermodynamic regulatory regime. *ISME J* **9**, 1802–1811 (2015).

79. Fonseca, B. M. *et al.* Mind the gap: cytochrome interactions reveal electron pathways across the periplasm of *Shewanella oneidensis* MR-1. *Biochemical Journal* **449**, 101–108 (2013).

80. Schuetz, B., Schicklberger, M., Kuermann, J., Spormann, A. M. & Gescher, J. Periplasmic Electron Transfer via the *c* -Type Cytochromes MtrA and FccA of *Shewanella oneidensis* MR-1. *Appl Environ Microbiol* **75**, 7789–7796 (2009).

81. Firer-Sherwood, M., Pulcu, G. S. & Elliott, S. J. Electrochemical interrogations of the Mtr cytochromes from *Shewanella*: opening a potential window. *JBIC Journal of Biological Inorganic Chemistry* **13**, 849–854 (2008).

82. Beblawy, S. *et al.* Extracellular reduction of solid electron acceptors by *Shewanella oneidensis*. *Mol Microbiol* **109**, 571–583 (2018).

83. Hernandez, M. E. & Newman, D. K. Extracellular electron transfer. *Cellular and Molecular Life Sciences* **58**, 1562–1571 (2001).

84. Roy, J. N. *et al.* Applied Electrode Potential Leads to *Shewanella oneidensis* MR-1 Biofilms Engaged in Direct Electron Transfer. *J Electrochem Soc* **160**, H866–H871 (2013).

85. Kumar, R., Singh, L., Wahid, Z. A. & Din, M. F. Md. Exoelectrogens in microbial fuel cells toward bioelectricity generation: a review. *Int J Energy Res* **39**, 1048–1067 (2015).

86. Leung, D. H. L. *et al.* Engineering *S. oneidensis* for Performance Improvement of Microbial Fuel Cell—a Mini Review. *Appl Biochem Biotechnol* **193**, 1170–1186 (2021).

87. Zou, L., Huang, Y. hong, Long, Z. er & Qiao, Y. On-going applications of *Shewanella* species in microbial electrochemical system for bioenergy, bioremediation and biosensing. *World J Microbiol Biotechnol* **35**, 1–9 (2019).

88. Liu, T. *et al.* Enhanced *Shewanella* biofilm promotes bioelectricity generation. *Biotechnol Bioeng* **112**, 2051–2059 (2015).

89. Wu, D. *et al.* Ferric iron enhances electricity generation by *Shewanella oneidensis* MR-1 in MFCs. *Bioresour Technol* **135**, 630–634 (2013).

90. Dai, H. N. *et al.* Power generation of *Shewanella oneidensis* MR-1 microbial fuel cells in bamboo fermentation effluent. *Int J Hydrogen Energy* **46**, 16612–16621 (2021).

91. Nimje, V. R. *et al.* Comparative bioelectricity production from various wastewaters in microbial fuel cells using mixed cultures and a pure strain of *Shewanella oneidensis*. *Bioresour Technol* **104**, 315–323 (2012).

92. Yang, Y. *et al.* Enhancing Bidirectional Electron Transfer of *Shewanella oneidensis* by a Synthetic Flavin Pathway. *ACS Synth Biol* **4**, 815–823 (2015).

93. Tefft, N. M. & Teravest, M. A. Reversing an Extracellular Electron Transfer Pathway for Electrode-Driven Acetoin Reduction. *ACS Synth Biol* **8**, 1590–1600 (2019).

94. Tefft, N. M., Ford, K. & TerAvest, M. A. NADHdehydrogenases drive inward electron transfer in *Shewanella oneidensis* MR-1. *Microb Biotechnol* **16**, 560–568 (2023).

95. Ross, D. E., Flynn, J. M., Baron, D. B., Gralnick, J. A. & Bond, D. R. Towards Electrosynthesis in *Shewanella*: Energetics of Reversing the Mtr Pathway for Reductive Metabolism. *PLoS One* **6**, e16649 (2011).

96. Rowe, A. R. *et al.* Tracking Electron Uptake from a Cathode into *Shewanella* Cells: Implications for Energy Acquisition from Solid-Substrate Electron Donors. *mBio* **9**, (2018).

97. François, J. M., Lachaux, C. & Morin, N. Synthetic Biology Applied to Carbon Conservative and Carbon Dioxide Recycling Pathways. *Front Bioeng Biotechnol* **7**, (2020).

98. Cotton, C. A., Edlich-Muth, C. & Bar-Even, A. Reinforcing carbon fixation: CO_2 reduction replacing and supporting carboxylation. *Curr Opin Biotechnol* **49**, 49–56 (2018).

99. Bar-Even, A., Noor, E. & Milo, R. A survey of carbon fixation pathways through a quantitative lens. *J Exp Bot* **63**, 2325–2342 (2012).

100. Bar-Even, A., Noor, E., Lewis, N. E. & Milo, R. Design and analysis of synthetic carbon fixation pathways. *PNAS* **107**, 8889–8894 (2010).

101. Philips, M. F., Gruter, G.-J. M., Koper, M. T. M. & Schouten, K. J. P. Optimizing the Electrochemical Reduction of CO_2 to Formate: A State-of-the-Art Analysis. *ACS Sustain Chem Eng* **8**, 15430–15444 (2020).

102. Davies, J. Characterisation of the reversible formate dehydrogenases of *Shewanella*. (University of East Anglia, 2017).

103. Duhl, K. Disentangling the Branched Respiratory Chain of *Shewanella oneidensis* MR-1. (Michigan State Univeristy, East Lansing, 2022).

104. Biegel, E., Schmidt, S., González, J. M. & Müller, V. Biochemistry, evolution and physiological function of the Rnf complex, a novel ion-motive electron transport complex in prokaryotes. *CMLS* **68**, 613–634 (2011).

105. Biegel, E., Schmidt, S., González, J. M. & Müller, V. Biochemistry, evolution and physiological function of the Rnf complex, a novel ion-motive electron transport complex in prokaryotes. *CMLS* **68**, 613–634 (2011).

106. Gruenberg, M. C. & TerAvest, M. A. A common inducer molecule enhances sugar utilization by *Shewanella oneidensis* MR-1. *J Ind Microbiol Biotechnol* **50**, (2023).

107. Idalia, V.-M. N. & Bernardo, F. Escherichia coli as a Model Organism and Its Application in Biotechnology. in *Escherichia coli - Recent Advances on Physiology, Pathogenesis and Biotechnological Applications* (ed. Samie, A.) 253–274 (IntechOpen, Rijeka, 2017). doi:10.5772/67306.

108. Huang, T. & Ma, Y. Advances in biosynthesis of higher alcohols in *Escherichia coli*. *World J Microbiol Biotechnol* **39**, 125 (2023).

109. Yang, D., Park, S. Y., Park, Y. S., Eun, H. & Lee, S. Y. Metabolic Engineering of *Escherichia coli* for Natural Product Biosynthesis. *Trends Biotechnol* **38**, 745–765 (2020).

110. Antonovsky, N. *et al.* Sugar Synthesis from CO_2 in *Escherichia coli*. *Cell* **166**, 115–125 (2016).

111. Herz, E. *et al.* The genetic basis for the adaptation of *E. coli* to sugar synthesis from CO2. *Nat Commun* **8**, 1705 (2017).

112. Gleizer, S. *et al.* Conversion of *Escherichia coli* to Generate All Biomass Carbon from CO2. *Cell* **179**, 1255-1263.e12 (2019).

113. Berg, I. A. Ecological Aspects of the Distribution of Different Autotrophic CO_2 Fixation Pathways. *Appl Environ Microbiol* **77**, 1925–1936 (2011).

114. Federici, F., Orsi, E. & Nikel, P. I. From Rags to Riches: Exploiting the Calvin-Benson-Bassham Cycle for Biomanufacturing. *ChemCatChem* **15**, (2023).

115. Calzadiaz-Ramirez, L. & Meyer, A. S. Formate dehydrogenases for CO_2 utilization. *Curr Opin Biotechnol* **73**, 95–100 (2022).

116. Prywes, N., Phillips, N. R., Tuck, O. T., Valentin-Alvarado, L. E. & Savage, D. F. Rubisco Function, Evolution, and Engineering. *Annu Rev Biochem* **92**, 385–410 (2023).

117. Yishai, O., Goldbach, L., Tenenboim, H., Lindner, S. N. & Bar-Even, A. Engineered Assimilation of Exogenous and Endogenous Formate in *Escherichia coli*. *ACS Synth Biol* **6**, 1722–1731 (2017).

118. Kim, S. *et al.* Growth of *E. coli* on formate and methanol via the reductive glycine pathway. *Nat Chem Biol* **16**, 538–545 (2020).

119. Kim, S. *et al.* Optimizing *E. coli* as a formatotrophic platform for bioproduction via the reductive glycine pathway. *Front Bioeng Biotechnol* **11**, (2023).

120. Lee, Y., Lee, J. & Kim, S. Direct extracellular electron transfer from *Escherichia coli* through modified carbon nanoparticles. *Electrochim Acta* **437**, 141497 (2023).

121. Gescher, J. S., Cordova, C. D. & Spormann, A. M. Dissimilatory iron reduction in *Escherichia coli*: identification of CymA of *Shewanella oneidensis* and NapC of *E. coli* as ferric reductases. *Mol Microbiol* **68**, 706–719 (2008).

122. Jensen, H. M., TerAvest, M. A., Kokish, M. G. & Ajo-Franklin, C. M. CymA and Exogenous Flavins Improve Extracellular Electron Transfer and Couple It to Cell Growth in Mtr-Expressing *Escherichia coli*. *ACS Synth Biol* **5**, 679–688 (2016).

123. Baruch, M., Tejedor-Sanz, S., Su, L. & Ajo-Franklin, C. M. Electronic control of redox reactions inside *Escherichia coli* using a genetic module. *PLoS One* **16**, e0258380 (2021).

124. Ross, D. E. *et al*. Towards Electrosynthesis in *Shewanella*: Energetics of Reversing the Mtr Pathway for Reductive Metabolism. *PLoS ONE*, *6*(2), e16649 (2011).

125. Ford, K. C., Kaste, J. A. M., Shachar-Hill, Y., & Teravest, M. A. Flux-Balance Analysis and Mobile CRISPRi-Guided Deletion of a Conditionally Essential Gene in *Shewanella oneidensis* MR-1. *ACS Synthetic Biology*, *11*(10), 3405–3413 (2022).

126. Yishai O, Bouzon M, Döring V, Bar-Even A In Vivo Assimilation of One-Carbon via a Synthetic Reductive Glycine Pathway in *Escherichia coli*. *ACS synthetic biology*, 7(9):2023–2028 (2018).

127. Beliaev, A. S. *et al.* Global Transcriptome Analysis of *Shewanella oneidensis* MR-1 Exposed to Different Terminal Electron Acceptors. *J Bacteriol* **187**, 7138–7145 (2005).

128. Gao H, Wang Y, Liu X, Yan T, Wu L, Alm E, Arkin A, Thompson DK, Zhou J Global transcriptome analysis of the heat shock response of *Shewanella oneidensis*. *J bacteriol*, 186(22):7796–7803 (2004).

CHAPTER 2:

A SMALL NUMBER OF POINT MUTATIONS CONFER FORMATE TOLERANCE IN *SHEWANELLA ONEIDENSIS*

PREFACE

The overarching goal for the *Shewanella* components of my doctoral work was to create a formatotrophic strain which would be able to use CO_2-derived formate for MES. It is not an easy feat to engineer autotrophy in a heterotroph, evidenced by the lack of successful examples in the literature. Since I had found a source describing the reversible activity of *S. oneidensis* formate dehydrogenases, I decided to start the engineering at developing formatotrophy, which would allow me to use a soluble source of carbon, making experimental set ups a bit easier.

I took two approaches for developing formatotrophy in *S. oneidensis*. One was an engineering approach in which I would use the *E. coli* model using rGly pathway for growth on formate for inspiration. I described this approach in the introductory chapter. As many deletions are required to generate the background strain for developing the rGly pathway, almost my entire PhD was complete before I had just the background strain. This is because each subsequent knockout in *S. oneidensis* using our homologous recombination method becomes more and more difficult and some resistance to the sucrose counterselection is gained while generating each deletion. Needless to say, generating the background strain was a lot of work.

As an alternative method, I decided to also attempt to evolve a formatotrophic phenotype. I did this in two different atmospheres. The first was in CO_2-enriched air, which was comprised of 10% CO_2 and 21% O_2 balanced with N_2. The strains were continuously subcultured in minimal medium containing lactate and increasing concentrations of formate. The goal was to improve formate tolerance and then start removing lactate. The elevated CO_2 levels were to promote reversal of the rGly pathway, as the glycine cleavage

system operating in the reductive direction requires CO_2 input. This evolution was extremely slow. I saved samples throughout the culturing period of one year (which was actually multiple years because I restarted this evolution twice), and that was imperative because the strains would often die off. This evolution experiment ended toward the end of my PhD with a few strains which were more tolerant to formate. Interestingly, they grew much better in regular air than in CO_2-enriched air. Therefore, out of curiosity, this same evolution was performed in regular air. To my great surprise, eight different lines of *S. oneidensis* were tolerant to 100 mM formate within 30 days.

This chapter describes the evolution which took place in a standard air atmosphere and the characterization of the resulting strains.

ABSTRACT

Microbial electrosynthesis (MES) is a sustainable approach to chemical production from CO_2 and clean electricity. However, limitations in the electron transfer efficiency and gaps in understanding of electron transfer pathways in MES systems prevents full realization of this technology. *Shewanella oneidensis* is a potential MES biocatalyst because it has a well-studied, efficient transmembrane electron transfer pathway. A key first step in MES in this organism could be CO_2 reduction to formate. However, wild-type *S. oneidensis* does not tolerate high levels of formate. In this work, we created and characterized formate-tolerant strains of *S. oneidensis* for further engineering and future use in MES systems through adaptive laboratory evolution. Separate point mutations in genes encoding a sodium-dependent bicarbonate transporter and a DUF2721-contianing protein separately confer formate tolerance in *S. oneidensis*. The mutations were further evaluated to understand their role in improving formate tolerance.

INTRODUCTION

Microbial electrosynthesis (MES) from CO_2 is a promising technology that utilizes clean electricity and water for the green production of biofuels, bioplastics, and platform chemicals.[1–3] MES is mediated by electrochemically active organisms, which can utilize reducing power from an electrode and carbon from CO_2 to generate target molecules through native or engineered metabolic reactions. Three different avenues of MES have been explored to date, each with their own limitations. The first method employs pure cultures of acetogens. At first glance, acetogens are an attractive MES catalyst, because they are autotrophic and some are electrochemically active; however, they suffer from a limited product scope, with acetate being the most abundant product.[4–6] Expansion of the product scope is hindered by the small synthetic biology toolbox for acetogens and their slow rate of electron uptake.[6,7] Another limitation of acetogens is the narrow understanding of their EET mechanism, which makes it difficult to engineer improvements. At least five mechanisms have been proposed for EET in acetogens, but experimental evidence supporting any of these mechanisms is lacking, and it is not known whether a single EET mechanism is shared by all electrochemically active acetogens.[8]

Some of these issues are addressed by the second major approach to MES, replacing the acetogen biocatalyst with mixed cultures. Mixed cultures have more success in producing a wider variety of products, although acetate production remains high.[9–11] However, utilizing mixed cultures for MES is plagued by off-target methane production due to rising methanogen populations in the reactors over time.[5] A third approach uses model organisms in conjunction with exogenous electron carriers for MES. Model organisms like *E. coli* are more versatile because of its well understood metabolism and abundance of

synthetic biology techniques.[12] However, scaling up MES reactions which require exogenous electron carriers is likely not feasible due to their cost. To make MES commercially competitive, a better microbial catalyst with well-understood EET mechanisms, metabolism, and synthetic biology tools is needed. One promising candidate is the electroactive bacterium *Shewanella oneidensis*. The discovery of the inward electron transfer pathway in this organism has shown that, if coupled to a C1 assimilation pathway, *S. oneidensis* would likely serve as an improved MES biocatalyst.[13-15]

S. oneidensis is a heterotrophic facultative anaerobe with the ability to utilize a wide variety of terminal electron acceptors (TEAs) including electrodes.[16,17] Extracellular electron transfer is made possible by the Mtr pathway which includes the Mtr complex (MtrCAB), CctA, FccA, and CymA.[18] Quinone-linked oxidoreductases such as NADH dehydrogenase, formate dehydrogenase, and lactate dehydrogenase pass electrons obtained from their respective oxidation reactions to inner membrane quinones.[19–21] CymA, an inner membrane tetraheme cytochrome *c*, receives electrons from the quinone pool and subsequently passes them to periplasmic *c*-type cytochromes FccA and CctA to traverse the periplasm.[22–24] On the other side of the periplasm, the cytochromes transfer the electrons to the outer membrane Mtr complex (MtrCAB) which transports the electrons to the outer surface of the cell.[18] The Mtr complex is composed of a porin (MtrB) which spans the outer membrane and encases two cytochromes *c*, one that interfaces with the periplasm (MtrA) and one that interfaces with the extracellular space (MtrC).[25,26] Once outside the cell, electrons can either directly reduce extracellular TEAs or be shuttled to TEAs via extracellular flavins.[16,17]

Its well-studied, reversible Mtr pathway makes *S. oneidensis* a promising host for

MES as it can efficiently exchange electrons with an electrode; however, this organism cannot fix CO_2. *S. oneidensis* requires engineered CO_2 fixation for its full potential as an effective MES biocatalyst to be realized. There are multiple potential methods for CO_2 fixation, with two possibilities for initial conversions: carboxylation, such as in the Calvin cycle and the reductive tricarboxylic acid cycle, and reduction, such as in the Wood-Ljungdahl pathway and the reductive glycine pathway.[27–29] Pathways which first reduce CO_2 to formate have been found to support higher biomass yields due to utilizing ATP more efficiently.[27,29] Because of this, engineering CO_2-fixation in *S. oneidensis* via a reduction-first pathway would be a promising strategy for generating an MES-compatible host. CO_2 can be reduced to formate via reversible formate dehydrogenases[30,31] and formate can be assimilated through a host of methods such as the reductive glycine pathway, the serine cycle, and reversed activity of pyruvate-formate lyase.[32] Additionally, formate-assimilating *S. oneidensis* could also be utilized for MES when an electrode with adsorbed formate dehydrogenase is supplied, as such electrodes have been shown to freely interconvert CO_2 and formate with low overpotentials.[31,33] *S. oneidensis* is not naturally tolerant of very high formate concentrations, necessitating greater tolerance to be acquired if a CO_2-reducing electrode is used or a reduction-first CO_2 fixation pathway is expressed. In this work, we utilized adaptive laboratory evolution to create formate-tolerant strains of *S. oneidensis* as a first step toward developing an MES-compatible host. We found two genes that are responsible for increasing formate tolerance in this organism and explore their application toward a future CO_2 fixing strain of *S. oneidensis*.

METHODS

Strains and Plasmids

Strains and plasmids used in this study are listed in **Table 1** and **Table 2**, respectively. Plasmids for mutant gene overexpression were prepared by cloning the wild-type (WT) or mutant gene from WT or mutant genomic DNA via PCR with primers (**Table 3**) that added regions homologous to the backbone vector pRL814[34] at the NdeI and HindIII restriction sites. WT copies of SO_3758 and SO_1320 were amplified from WT *S. oneidensis*, SO_3758_A269T was amplified from MGC002, SO_1320_V106I was amplified from MGC007, SO_1320_V106F was amplified from MGC003, and SO_1320_S52I was amplified from MGC008. Amplified genes were purified via the Wizard PCR clean-up kit (Promega). The pRL814 backbone was digested with NdeI and HindIII-HF (New England Biolabs (NEB)). The digested backbone and amplified genes were ligated using NEBuilder HiFi DNA Assembly Master Mix (NEB) and transformed into chemically competent *E. coli* WM3064. Plasmids were transferred to WT *S. oneidensis* via conjugal transfer using *E. coli* WM3064 as described previously.[25] CRISPRi knockdown vectors were prepared from the backbone pJMP2846 as described previously, with sgRNAs targeting *yadS*.[35,36] The CRISPRi vectors are kanamycin resistant and encode dCas9 and the sgRNA. The assembled CRISPRi vectors were transformed into chemically competent *E. coli* WM3064, a 2,6-diaminopimelic acid (DAP) auxotroph. The CRISPRi vectors were transferred to WT *S. oneidensis* via Tn7-based triparental conjugation using donor strains *E. coli* WM3064 with the CRISPRi vector and transposase-containing *E. coli* WM3064 pJMP2644 as described previously.[35] After the mating period, counter-selection was performed on lysogeny broth (LB) agar plates supplemented with 50 μg ml^{-1} of

kanamycin and without DAP. Single *S. oneidensis* colonies were screened for the correct sgRNAs by PCR using the sgRNA_check and related sgRNA reverse primers (**Table 3**).

Table 1. Strains used in experiments described in Chapter 2.

Strain	Description	Reference
Parent strains		
S. oneidensis MR-1	Wild-type	Lab stock
JG2957	*S. oneidensis* with deletion of SO_0101-SO_0103, SO_4509-SO_4511, and SO_4513-SO_4515	21
JG2955	*S. oneidensis* with deletion of SO_4509-SO_4511 and SO_4513-SO_4515	21
E. coli WM3064	Conjugal transfer donor, DAP auxotroph	Lab stock
Formate-tolerant strains		
MGC001	Formate-tolerant strain evolved from *S. oneidensis* MR-1. (Line A Colony 3)	This study
MGC002	Formate-tolerant strain evolved from *S. oneidensis* MR-1. (Line B Colony 1)	This study
MGC003	Formate-tolerant strain evolved from *S. oneidensis* MR-1. (Line C Colony 3)	This study
MGC004	Formate-tolerant strain evolved from *S. oneidensis* MR-1. (Line D Colony 1)	This study
MGC005	Formate-tolerant strain evolved from *S. oneidensis* JG2957. (Line A Colony 2)	This study
MGC006	Formate-tolerant strain evolved from *S. oneidensis* JG2957. (Line B Colony 1)	This study
MGC007	Formate-tolerant strain evolved from *S. oneidensis* JG2957. (Line C Colony 2)	This study
MGC008	Formate-tolerant strain evolved from *S. oneidensis* JG2955. (Colony 2)	This study

Table 2. Plasmids used in experiments described in Chapter 2.

Strain	Description	Reference
pRL814	Broad host plasmid expressing GFP under T7A1 promoter, spectomycin resistance	34
pJMP2846	CRISPRi vector expressing dCas9 and sgRNA, kanamycin resistance	35
pJMP2644	Transposase-containing vector, ampicillin resistance	35
pRL814-SO_3758	WT SO_3758 expression vector, derivative of pRL814, spectomycin resistance	This study
pRL814-SO_3758_A269T	SO_3758_A269T expression vector, derivative of pRL814, spectomycin resistance	This study
pRL814-SO_1320	WT SO_1320 expression vector, derivative of pRL814, spectomycin resistance	This study
pRL814-SO_1320_V106I	SO_1320_V106I expression vector, derivative of pRL814, spectomycin resistance	This study
pRL814-SO_1320_V106F	SO_1320_V106F expression vector, derivative of pRL814, spectomycin resistance	This study
pRL814-SO_1320_S52I	SO_1320_S52I expression vector, derivative of pRL814, spectomycin resistance	This study
pJMP2846-yadS-target_1	*yadS* knockdown vector target 1, derivative of pJMP2846, kanamycin resistance	This study
pJMP2846-yadS-target_2	*yadS* knockdown vector target 2, derivative of pJMP2846, kanamycin resistance	This study

Table 3. Primers used in experiments described in Chapter 2.

Primer	Sequence (5'->3')	Description
MG_203	ctttaagaaggagatatacatatgccagatattgtcattgca	SO_3758 cloning fwd
MG_204	aggaattcgatatcattatttatcatcatcatctttgtaatctcccgtaatttgcattac	SO_3758 cloning rev
MG_205	ctttaagaaggagatatacatatgcatgtttcattaacaac	SO_1320 fwd
MG_206	aggaattcgatatcattatttatcatcatcatctttgtaatctttactcatctctttgat	SO_1320 rev
MG_207	TAGTagcggctaaagcgccagaaa	CRISPRi yadS target 1 forward
MG_208	AAACtttctggcgctttagccgct	CRISPRi yadS target 1 reverse
MG_209	TAGTgtccatacggtggcgaccag	CRISPRi yadS target 2 forward
MG_210	AAACctggtcgccaccgtatggac	CRISPRi yadS target 2 reverse
sgRNA_check	GGTCCTTGAGCCCCATTATC	sgRNA foward

Culturing

Strains were precultured in 2 ml LB overnight at 30 °C with shaking at 250 rpm. The pre-cultures were washed three times and resuspended in basal M5-caa medium (1.29 mM K_2HPO_4, 1.65 mM KH_2PO_4, 7.87 mM NaCl, 1.70 mM NH_4SO_4, 475 µM $MgSO_4 \cdot 7H_2O$, 10 mM HEPES, pH 7.2). Minimal lactate medium was used for all experimental cultures unless otherwise stated and was comprised of basal M5-caa, supplemented with Wolfe's mineral solution, Wolfe's vitamin solution without riboflavin, and 20 mM D,L-lactate.

Formate and IPTG were added to the appropriate cultures at the specified concentrations. Cultivation took place at 30 °C with shaking at 250-275 rpm. Culture volumes are specified for each experiment.

Evolution of formate tolerance and genome sequencing

Formate tolerance was evolved by continuously subculturing the parent strains (WT, JG2957 JG2955) in 2 ml minimal lactate medium with increasing concentrations of formate. Pre-cultures of the parent strains were prepared as described above and were used to inoculate three 2 ml cultures of minimal lactate medium with 1 mM formate to an initial OD_{600} of 0.02. The three or four cultures for each parent strain represented a separate evolution line: line A, line B, line C, and line D. Cultures were incubated at 30 °C with shaking at 250 rpm. 2 µl aliquots were taken daily to monitor OD_{600} using an Eppendorf G1.0 microcuvette and an Eppendorf BioSpectrometer. When cultures reached an OD_{600} of 0.2 or higher, they were subcultured into a fresh 2 ml culture with minimal lactate medium and 5 mM formate. Strains were continuously cultured in this way with the formate concentration increasing in each subculture. The formate concentration progression was: 1 mM, 5 mM, 10 mM, 20 mM, 30 mM, 40 mM, 50 mM, 60 mM, 70 mM, 80 mM, 90 mM, 100 mM. Strains spent only one round of culturing in each formate concentration before moving to the next highest concentration. Cryogenic stocks were prepared from each of the populations when the 100 mM cultures reached an OD_{600} of 0.2 or higher. Cryogenic stocks from each evolution line were streaked onto LB agar plates, and multiple single colonies from each evolution line were saved as pure cryogenic stocks. Genome extraction, library preparation, and Oxford Nanopore sequencing was performed by Plasmidsaurus.

Bioinformatics

Raw genome sequencing reads were trimmed using Porechop v0.2.4 (https://github.com/rrwick/Porechop.git) to remove Nanopore sequencing adapters. Trimmed sequencing reads were aligned to the *S. oneidensis* MR-1 reference genome (Accession: NC_004347.2) and reference megaplasmid (Accession: NC_004349.1) and analyzed for mutations using Breseq v0.38.0.[37] Deviations of the evolved strains from the reference genome were compared to the deviations of the parent strains from the reference sequences. Deviations which appeared in the evolved strains but not in the parent strains were compiled in **Table 4** and classified as mutations. Mutations which appeared in multiple evolved strains were of particular interest. A sodium-dependent bicarbonate transporter (encoded by SO_3758) and a DUF2721-containing protein (encoded by SO_1320) were experimentally investigated for utility in formate tolerance.

iPro54-PseKNC and Sigma70Pred were used to search for *yadS* σ^{54} and σ^{70} promoters at the end of the SO_1320. An 81-nucleotide long sequence containing the end of SO_1320 and the first eight nucleotides of *yadS* were used as the query.[38,39]

Amino acid sequences of proteins encoded by the WT and mutant versions of SO_3758 were aligned to the sodium-dependent bicarbonate transporter SbtA from cyanobacteria *Synechocystis* sp. PCC 6803 substr. Kazusa (Accession: P73953) using T-coffee simple multiple sequence alignment.[40]

Tools DeepGO and DeepTMHMM were used to analyze the amino acid sequence of proteins encoded by SO_1320.[41,42] AlphaFold v2.3.2 was used to predict structures of proteins encoded by SO_3758_A269T, SO_1320_V106I, SO_1320_V106F, and SO_1320_S52I.[43] Predicted structures for proteins encoded by SO_3758 (Accession:

Q8EAY3) and SO_1320 (Accession: Q8EHA9) were downloaded from the AlphaFold database (https://alphafold.com/). Ligand binding prediction was performed with AutoDock Vina v1.1.2.[44] PyMOL v2.5.8 was used for visualization of protein and ligand models, identifying polar interactions between the ligand and surrounding amino acids, and calculating distances between interacting atoms.[45]

RESULTS

Two *S. oneidensis* strains were used in the testing and evolution of formate tolerance: WT and JG2957. *S. oneidensis* strain JG2957 has three major FDHs deleted (*fdhA1B1C1*, *fdhA2B2C2*, and *fdnGHI*) and was included to prevent loss of formate as CO_2 and provide a deeper understanding of formate tolerance.

First, to assess the native formate tolerance of *S. oneidensis*, WT and JG2957 were cultivated in 200 µl minimal lactate medium with varying concentrations of formate (**Figure 6**). Both strains had the shortest lag phase in medium without formate. With even as little as 1 mM formate, growth was impacted. With increasing formate concentrations, the

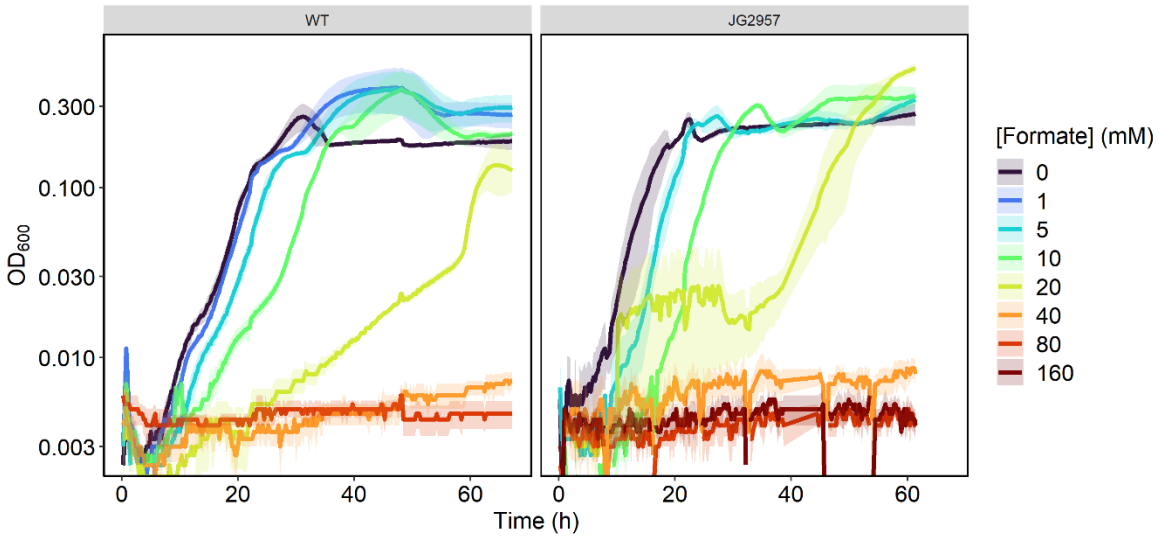

Figure 6. Growth curves of MR-1 and JG2957 in 200 µl minimal medium with 20 mM lactate and varying concentrations of formate.

strains' lag phase also increased. For WT, formate was tolerated up to a concentration of 10 mM, and for JG2957, formate was tolerated up to a concentration of 20 mM. Formate tolerance in these strains is low, and could present an issue in a *S. oneidensis* strain which has CO_2 reductase activity.

Formate toxicity can be a result of cytochrome *c* oxidase inhibition and/or reduction of proton motive force due to cytoplasm acidification from the protonated acid.[46–48] Since these issues are not easily solved with a genetic engineering approach, we opted to generate a formate-tolerant strain of *S. oneidensis* through adaptive laboratory evolution. This was accomplished through continuous subculturing of the parent strains (WT and JG2957) in minimal lactate medium while increasing the formate concentration in the medium for each subculture, with a goal of improving tolerance to 100 mM formate. Multiple separate evolution studies were conducted for each parent strain. Surprisingly, tolerance to 100 mM formate evolved within 30 days in seven evolution lines (**Figure 7**),

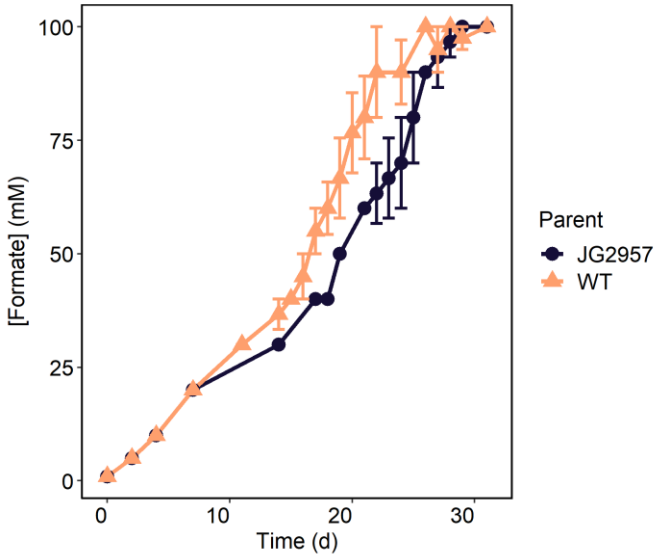

Figure 7. Length of subculturing each strain required for subculturing with increasing concentrations of formate.

with the subculturing frequency increasing in the later stages of the evolution, indicating acquired mutation(s) assisting with formate tolerance (**Figure 8**).

Single colonies from the seven evolution lines which could grow on 100 mM formate were isolated. Their formate tolerance was compared to the associated parent strain by culturing in 200 µl minimal lactate medium with 100 mM formate in triplicate (**Figure 9**). Both parent strains were incapable of growth on lactate when supplemented with 100 mM formate, while almost all the isolated evolved colonies were capable of growth, although not without a long lag phase of 60-90 hours. The evolution study from WT resulted in four lines (A, B, C, and D) which showed different growth phenotypes with lines A, C, and D having a shorter lag phase than line B. Less clear patterns emerge from strains evolved from JG2957. Two line A colonies and one line B colony could grow the most optimally under the conditions tested, while the other colonies from those lines more closely resembled the growth patterns of colonies from line C. One colony from each line was selected for further analysis. These seven new formate-tolerant S. oneidensis strains were renamed MGC001 through MGC007 (**Table 1**). Each formate-tolerant strain and the parent strains were cultivated in 50 ml minimal lactate medium with 100 mM formate and metabolites were analyzed via HPLC (**Figure 10**). Cultures were inoculated to a starting OD_{600} five times greater than previous cultures to allow the parent strains to grow under the high-formate conditions. This allowed comparison between the evolved and parent strains' metabolite concentrations (**Figure 11**). Even with the increased inoculum volume, WT and JG2957 had a longer lag phase than the evolved formate-tolerant strains. The evolved formate-tolerant strains did not have as long of a lag phase as when inoculated to a lower OD_{600}. All provided lactate was consumed in all strains. Formate levels remained

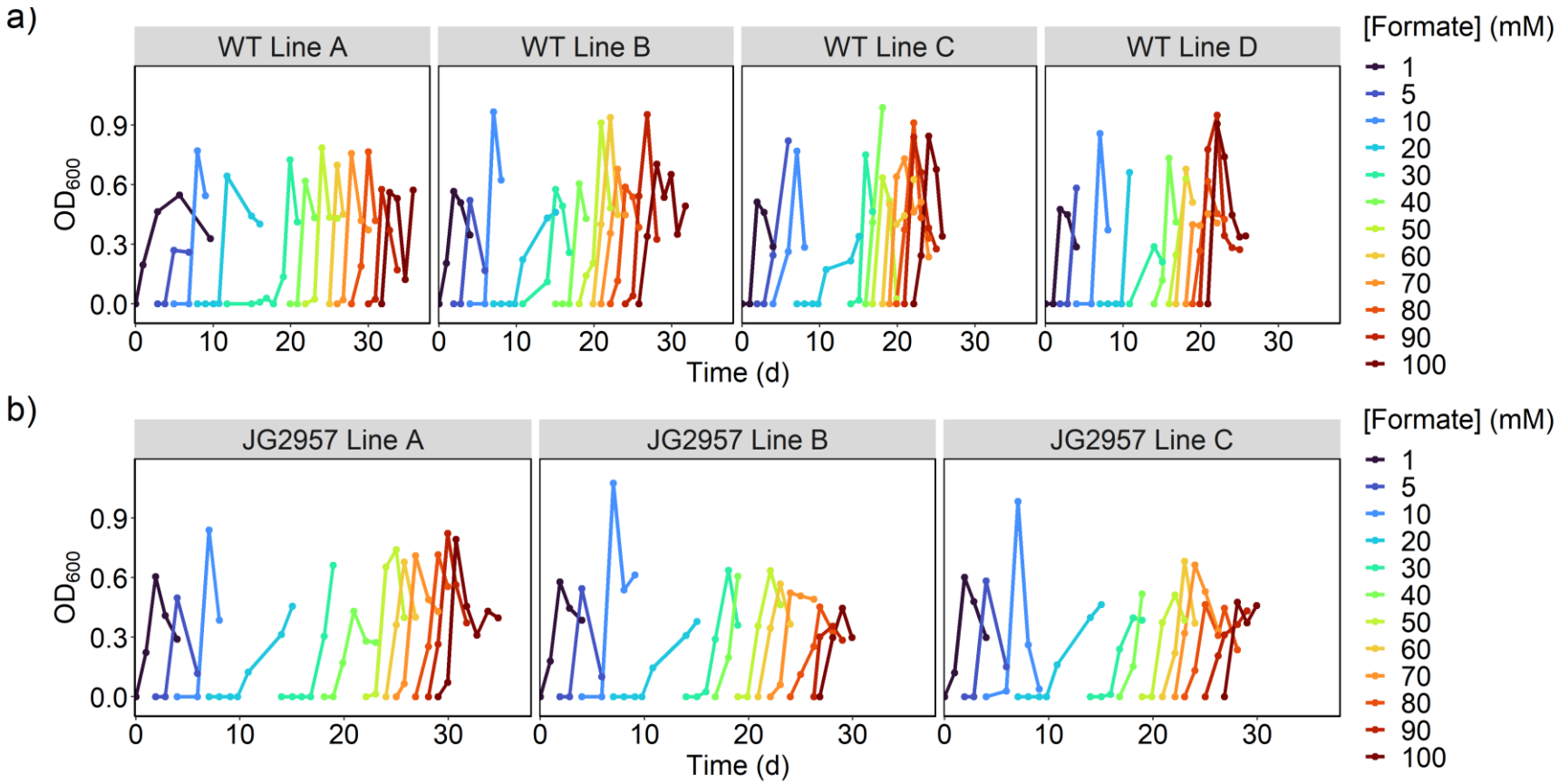

Figure 8. Growth curves of directed evolution subculturing in increasing formate concentrations of parent strains. a) WT and b) JG2957. Each panel displays growth curves of a replicate evolution line. Evolution experiments were halted after cells were able to tolerate a formate concentration of 100 mM.

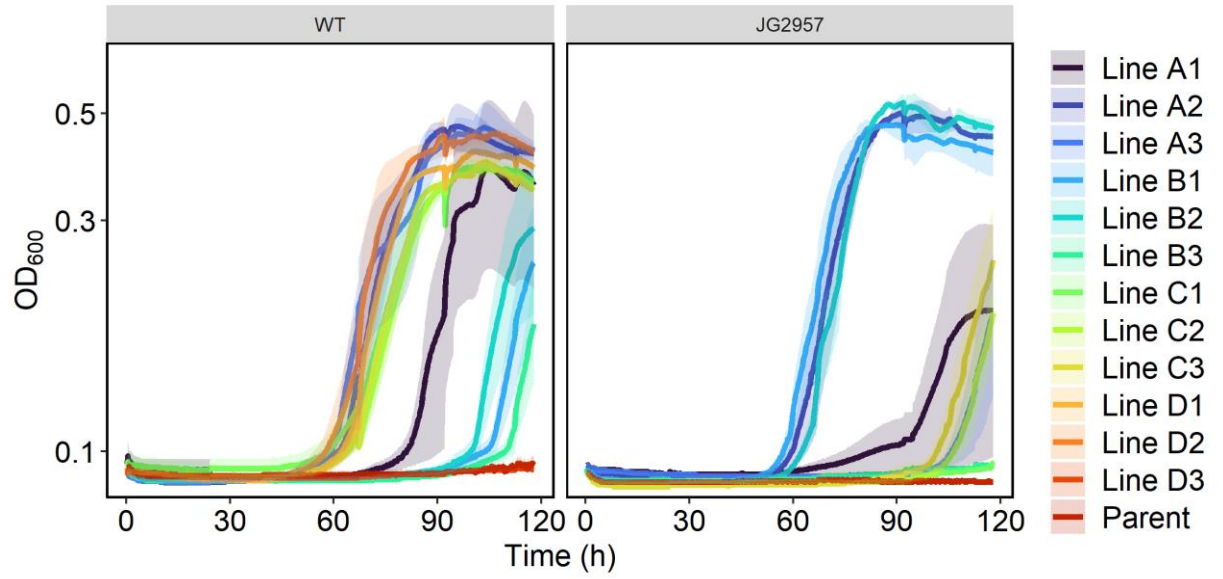

Figure 9. Growth curves of single colonies in triplicate isolated from the evolution experiments compared to their associated parent strain. Strains were cultured in 200 µl of minimal medium with 20 mM lactate and 100 mM formate.

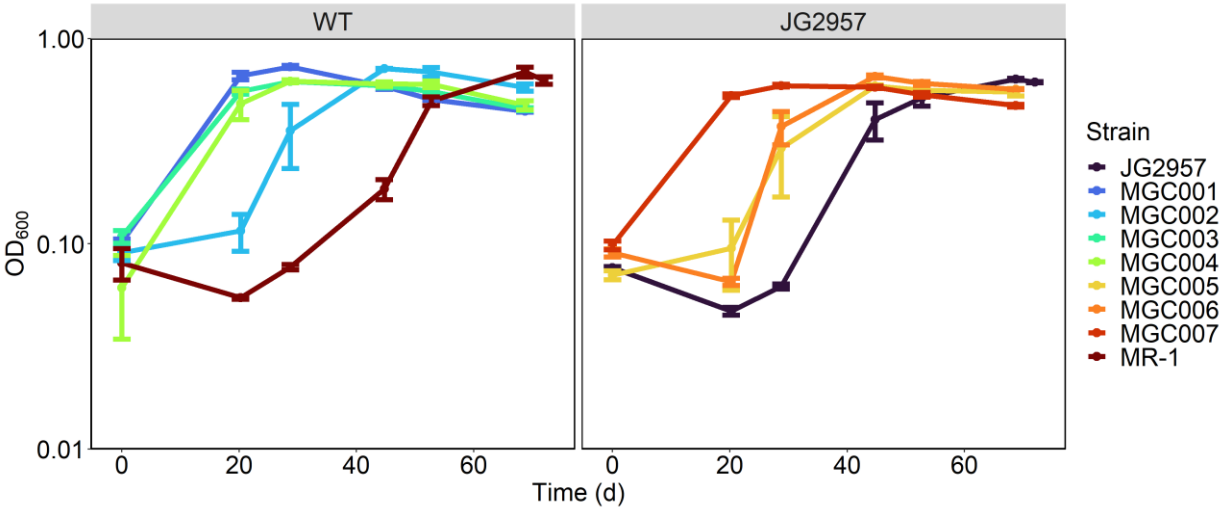

Figure 10. Growth curves of formate-tolerant strains cultivated in 50 ml minimal lactate medium with and 100 mM formate. All lactate is consumed and formate concentrations remain constant throughout the culturing period.

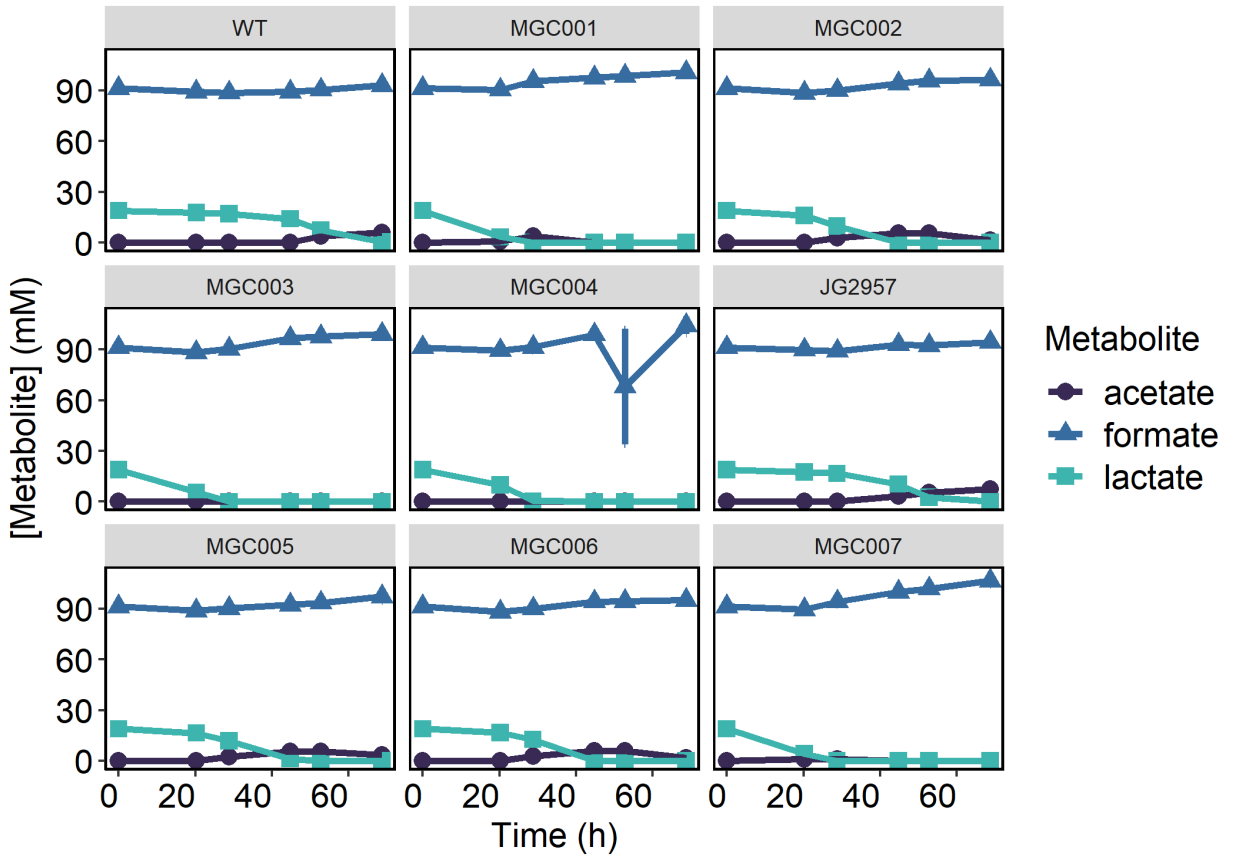

Figure 11. Metabolite concentrations of parent and formate-tolerant strains. Strains cultivated in 50 ml minimal medium with 20 mM lactate and 100 mM formate.

constant throughout cultivation of both the parent strains and the evolved formate tolerant strains, indicating that the evolved method of formate tolerance does not include formate oxidation or formate assimilation.

To determine the mutations that enabled increased formate tolerance, the genomes of the seven formate-tolerant strains and the two parent strains were sequenced. Raw sequencing reads were processed with porechop to remove sequencing adapters and breseq to align the reads to the reference sequences and identify mutations. Mutations that did not exist in the parent strain were flagged (**Table 4**). A transition mutation of G to A in SO_3758 (SO_RS17510), encoding a sodium-dependent bicarbonate transporter, occurred in three of the seven formate-tolerant strains (MGC002, MGC005, and MGC006),

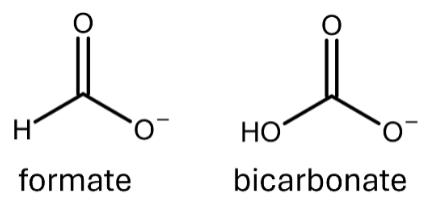

Figure 12. Chemical structures of formate and bicarbonate.

resulted in an amino acid sequence replacement A269T, changing a nonpolar, hydrophobic residue to a bulkier polar, hydrophilic residue. Considering that formate and bicarbonate have very similar structures (**Figure 12**), we hypothesized two potential effects of this mutation. First, the mutation could have provided greater specificity toward formate and provided the protein encoded by SO_3758 with formate efflux activity, preventing toxic intracellular accumulation. Second, the mutation may have decreased formate specificity and prevented the protein encoded by SO_3758 from importing toxic levels of formate.

In three of the remaining formate-tolerant strains (MGC003, MGC004, and MGC007), a mutation in SO_1320 (SO_RS06120), encoding a protein of unknown function, was observed. MGC007 had a G to A transition mutation resulting in a V106I amino acid sequence change and MGC003 and MGC004 had a G to T transversion mutation resulting in a V106F amino acid sequence change. We also carried out preliminary adaptive laboratory evolution on using *S. oneidensis* parent JG2955 which has two of the three formate dehydrogenases deleted (*fdhA1B1C1* and *fdhA2B2C2*). Interestingly, one strain (MGC008) isolated from this evolution also had a mutation in

Table 4. Mutations in formate-tolerant strains. Mutations that appeared in multiple strains are bolded and highlighted.

strain	seq id	position	mutation	annotation	gene	description
MGC001	NC_004347	2,782,334	T→C	intergenic (-97/-29)	*ppsA* ← / → *SO_RS12190*	phosphoenolpyruvate synthase/pyruvate, water dikinase regulatory protein
	NC_004347	3,258,800	Δ1 bp	intergenic (-86/+14)	*SO_RS14530* ← / ← *SO_RS14535*	tRNA-Glu/tRNA-Glu
	NC_004347	3,588,820	N→T	?94T (ACN→ACA)	*SO_RS16095* ←	IS256-like element ISSod4 family transposase
	NC_004347	3,928,289	G→T	R213L (CGC→CTC)	*SO_RS17595* →	DUF599 domain-containing protein
	NC_004349	138,980	Δ3 bp	coding (349-351/1041 nt)	*SO_RS22825* ←	IS481-like element ISSod13 family transposase
MGC002	NC_004347	3,258,789	N→T	intergenic (-75/+25)	*SO_RS14530* ← / ← *SO_RS14535*	tRNA-Glu/tRNA-Glu
	NC_004347	3,258,800	Δ1 bp	intergenic (-86/+14)	*SO_RS14530* ← / ← *SO_RS14535*	tRNA-Glu/tRNA-Glu
	NC_004347	**3,906,124**	**G→A**	**A269T (GCC→ACC)**	***SO_RS17510*** →	**sodium-dependent bicarbonate transport family permease**
MGC003	**NC_004347**	**1,374,567**	**C→A**	**V106F (GTC→TTC)**	***SO_RS06120*** ←	**DUF2721 domain-containing protein**
	NC_004347	2,143,924	$(CCATGA)_{10\rightarrow11}$	coding (686/1185 nt)	*SO_RS09420* →	cation diffusion facilitator family transporter
	NC_004347	3,258,800	Δ1 bp	intergenic (-86/+14)	*SO_RS14530* ← / ← *SO_RS14535*	tRNA-Glu/tRNA-Glu
	NC_004347	3,355,020	G→A	P74L (CCA→CTA)	*flhA* ←	flagellar biosynthesis protein FlhA
	NC_004347	4,740,503	G→A	W48* (TGG→TGA)	*SO_RS21100* →	alpha/beta hydrolase-fold protein
MGC004	**NC_004347**	**1,374,567**	**C→A**	**V106F (GTC→TTC)**	***SO_RS06120*** ←	**DUF2721 domain-containing protein**
	NC_004347	2,143,924	$(CCATGA)_{10\rightarrow11}$	coding (686/1185 nt)	*SO_RS09420* →	cation diffusion facilitator family transporter
	NC_004347	3,355,020	G→A	P74L (CCA→CTA)	*flhA* ←	flagellar biosynthesis protein FlhA
MGC005	NC_004347	2,353,953	C→T	D334N (GAT→AAT)	*ptsP* ←	phosphoenolpyruvate--protein phosphotransferase
	NC_004347	3,258,800	Δ1 bp	intergenic (-86/+14)	*SO_RS14530* ← / ← *SO_RS14535*	tRNA-Glu/tRNA-Glu
	NC_004347	**3,906,124**	**G→A**	**A269T (GCC→ACC)**	***SO_RS17510*** →	**sodium-dependent bicarbonate transport family permease**
MGC006	NC_004347	2,871,939	C→T	D23N (GAC→AAC)	*tolR* ←	protein TolR
	NC_004347	**3,906,124**	**G→A**	**A269T (GCC→ACC)**	***SO_RS17510*** →	**sodium-dependent bicarbonate transport family permease**
	NC_004349	138,980	Δ3 bp	coding (349-351/1041 nt)	*SO_RS22825* ←	IS481-like element ISSod13 family transposase
MGC007	**NC_004347**	**1,374,567**	**C→T**	**V106I (GTC→ATC)**	***SO_RS06120*** ←	**DUF2721 domain-containing protein**
	NC_004347	3,258,789	N→T	intergenic (-75/+25)	*SO_RS14530* ← / ← *SO_RS14535*	tRNA-Glu/tRNA-Glu
	NC_004347	3,258,800	Δ1 bp	intergenic (-86/+14)	*SO_RS14530* ← / ← *SO_RS14535*	tRNA-Glu/tRNA-Glu

SO_1320 affecting residue 52 where a serine was converted to an isoleucine. The two residue 106 alterations resulted in a bulkier amino acid in that position, and the S52I alteration replaced a polar, hydrophilic residue with a nonpolar, hydrophobic residue.

SO_1320 is upstream of SO_1319 (*yadS*) and SO_1318. To determine whether the mutations in SO_1320 affected the promoter sequence of downstream *yadS*, an 81 bp unmutated nucleotide sequence containing the end of SO_1320 and first eight nucleotides of *yadS* were analyzed by iPro54-PseKNC and Sigma70Pred to search for σ^{54} and σ^{70} promoters.[38,39] These analyses revealed no σ^{54} promoter in this location, but Sigma70Pred predicted the region contained a σ^{70} promoter. The same 81-nucleotide sequence including the G to A or G to T mutations resulting in V106 change to phenylalanine or isoleucine in the formate-tolerant strains were also analyzed by Sigma70Pred. In both cases, the sequence is still predicted to contain a σ^{70} promoter, suggesting that the mutations do not alter the transcription of downstream *yadS*. This finding, along with the observation that a mutation elsewhere in SO_1320 also results in formate tolerance, indicates that the mutations in SO_1320 alter this protein's activity in a way that helps the strains withstand greater formate concentrations.

To confirm that the SO_1320 mutations do not impact the transcription of *yadS*, two *S. oneidensis* CRISPRi knockdown strains were prepared, each targeting *yadS*. The *yadS* knockdown strains and the non-targeting control were cultivated in minimal lactate medium with 20 mM formate and varying levels of induction. The growth curves reveal that knockdown of *yadS* does not improve *S. oneidensis* formate tolerance over the non-targeting strain, confirming that the mutations in SO_1320 do not affect *yadS* expression (**Figure 13**).

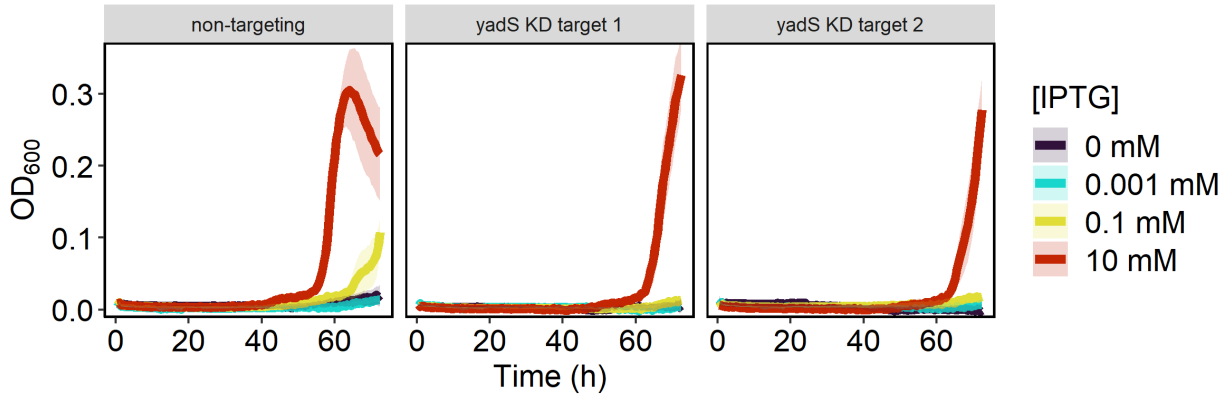

Figure 13. Growth curves of *yadS* CRISPRi knockdown (KD) strains and non-targeting control strain.

To confirm that mutations observed in SO_3758 and SO_1320 were responsible for enhanced formate tolerance, we attempted to confer formate tolerance to WT *S. oneidensis* by overexpressing the mutant sequences. Mutant genes were cloned from the formate-tolerant strains and placed on vector pRL814 under control of an IPTG-inducible promoter. The vectors carrying the mutants were transformed into *E. coli* and subsequently transferred to WT *S. oneidensis* via conjugation. The *S. oneidensis* strains harboring SO_3758, SO_3758_A269T, SO_1320, SO_1320_V106I, SO_1320_V106F, or SO_1320_S52I were cultivated in 200 µl of minimal lactate medium with varying formate concentrations and the WT or mutant gene was overexpressed with 100 µM IPTG (**Figure 14**). All strains, whether expressing WT or mutant versions of the genes were capable of growth without formate, showing that overexpression of these proteins was not toxic. The strains expressing the WT versions of SO_3758 and SO_1320 were only able to grow robustly in the no formate conditions. The strains expressing SO_3758_A269T, SO_1320_V106I, and SO_1320_S52I grew in elevated formate levels up to 40 mM with a final OD_{600} similar to that of cells grown in medium without formate. None of the strains tolerated 80 mM formate, indicating that other mutations accumulated during evolution of

the formate-tolerant strains could enhance their ability to withstand elevated levels of formate. The strain carrying the SO_1320_V106F mutant did not exhibit as significant growth benefits as the SO_1320_V106I strain. Even during cultivation with no formate it performed worse than the strain expressing SO_1320_WT. These complementation efforts confirmed that the identified mutations in SO_3758 and SO_1320 improved formate tolerance of WT *S. oneidensis*.

To predict the effect of the A269T substitution in the transporter encoded by SO_3758, we modeled the binding of bicarbonate and formate to the WT and mutant versions of the protein. To reveal the binding site for modeling substrate binding, the amino acid sequence of the *S. oneidensis* protein encoded by SO_3758 was aligned with the only sodium-dependent bicarbonate transporter with a solved structure, SbtA from

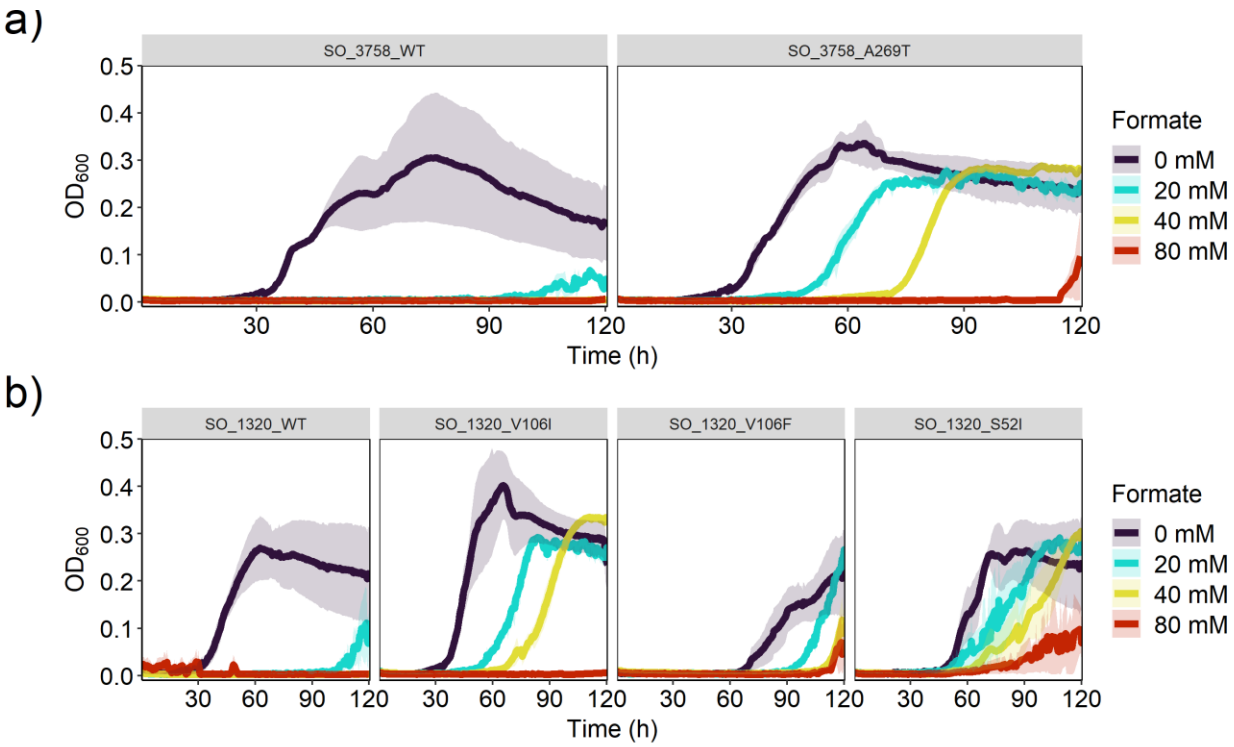

Figure 14. Growth curves of WT *S. oneidensis* harboring an IPTG-inducible expression vector containing WT or mutant versions of SO_3758 or SO_1320. Strains cultivated 200 µl minimal lactate medium with 100 µM IPTG and varying formate concentrations.

cyanobacteria, using the multiple sequence alignment (MSA) tool T-Coffee [40,49]. The alignment revealed that A269 in the protein encoded by SO_3758 corresponds to residue S323 in SbtA (**Figure 15**). While S323 has not been found to be directly involved in binding sodium or bicarbonate, it is the single residue that separates the two binding pockets, with S322 binding sodium and S324 binding bicarbonate [49,50]. These substrate-binding serines are conserved in the protein encoded by SO_3758, with SO_3758 S268 corresponding to SbtA S322 and SO_3758 S270 corresponding to SbtA S324 (**Figure 15**). The MSA revealed that the protein encoded by SO_3758 residues V99, S100, S270, and I272 are likely part of the bicarbonate binding pocket.

Protein models corresponding to the wild-type and mutated versions of SO_3758 were generated using AlphaFold,[43] and the binding of bicarbonate and formate were predicted with Autodock Vina.[44] The predicted local distance difference test (pLDDT) scores were calculated for each residue in the AlphaFold model, and are depicted in **Figure 16**. The binding pocket residues were predicted to have pLDDT scores of high (90> pLDDT > 70) to very high (pLDDT > 90) confidence. The docking grid was set to encompass residues predicted by MSA to be part of the binding pocket (V99, S100, S270, I272), A or T269, and nearby residues. The modeling of bicarbonate binding to the protein encoded by SO_3758_WT predicts that it forms polar interactions with V99, A101, Y271, I272, and A273 in the predicted native binding site, referred to here as site 1 (**Figure 17a**, **Figure 16b**, **Figure 16d**). Bicarbonate binding to site 1 has a predicted binding affinity of -3.2 kcal mol^{-1} (**Table 5**). Formate is also predicted to bind to site 1 in the protein encoded by SO_3758_WT, forming polar interactions with V99, S270, Y271, and I272 and having a weaker predicted binding affinity of -2.3 kcal mol^{-1} (**Figure 17b**).

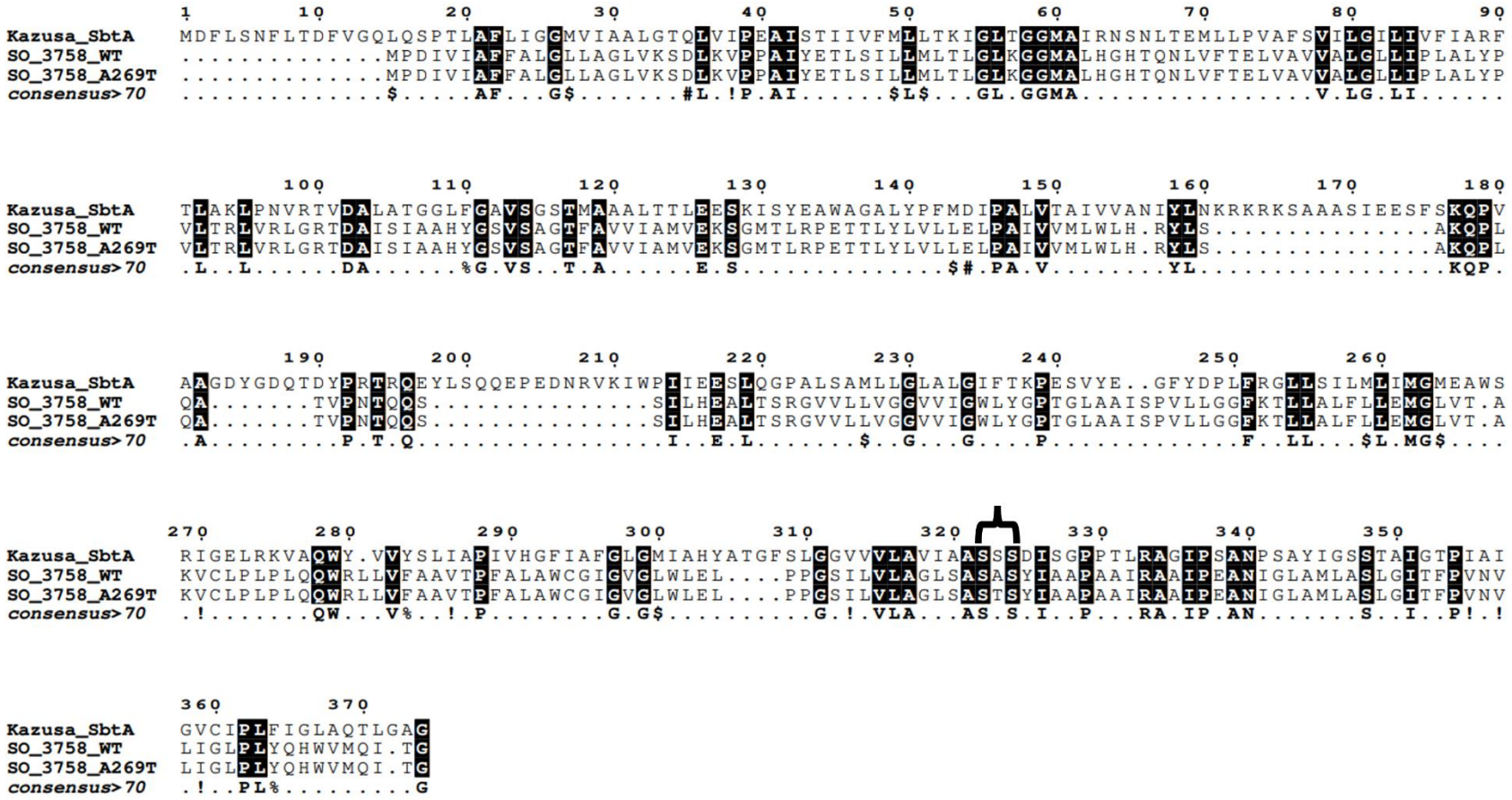

Figure 15. Multiple sequence alignment of cyanobacteria SbtA, and the proteins encoded by WT SO_3758 and SO_3758_A269T. Bracket highlights residues A269 from the protein encoded by WT SO_3758, T269 from the protein encoded by SO_3758_A269T, and corresponding cyanobacteria SbtA residue S323, as well as conserved flanking serine residues involved in the binding of bicarbonate and sodium.

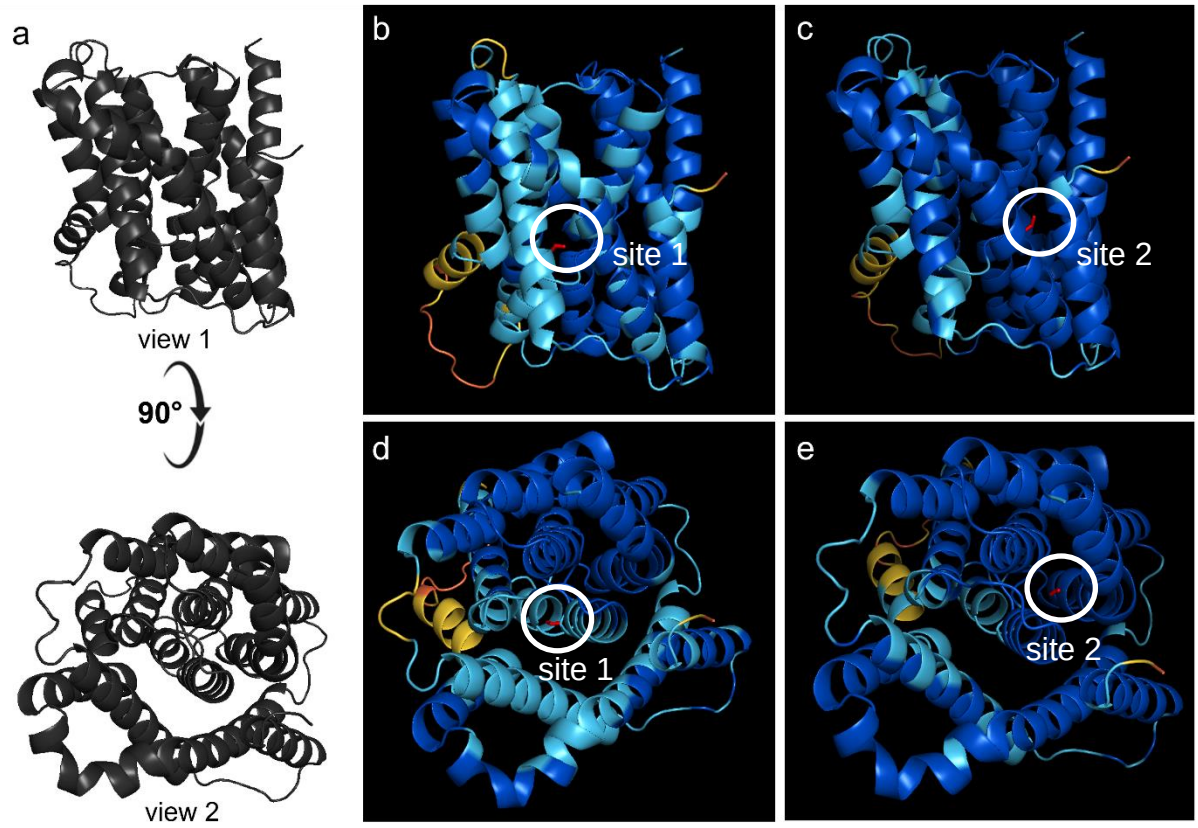

Figure 16. Representations of pLDDT scores from the protein sequence encoded by SO_3758 AlphaFold structural predictions. Residue color depicts pLDDT score. Dark blue represents a very high score (pLDDT > 90). Light blue represents a confident score (90 > pLDDT > 70). Yellow represents a low score (70 > pLDDT > 50). Orange represents a very low score (pLDDT < 50). a) General structure of SO_3758 shown at two angles. View 1 is shown in panels b and c. View 2 is shown in panels d and e. b) View 1 of the protein encoded by WT SO_3758. Formate is colored red and shown binding to site 1. c) View 1 of the protein encoded by SO_3758_A269T. Formate is colored red and shown binding to site 2. d) View 2 of the protein encoded by WT SO_3758. Formate is colored red and shown binding to site 1. c) View 2 of the protein encoded by SO_3758_A269T. Formate is colored red and shown binding to site 2.

Table 5. Predicted binding affinities of bicarbonate and formate to site 1 and site 2 of WT and mutant proteins encoded by SO_3758.

	Binding affinity to the protein encoded by SO_3758		Binding affinity to the protein encoded by SO_3758_A269T	
	Site 1 (kcal mol^{-1})	Site 2 (kcal mol^{-1})	Site 1 (kcal mol^{-1})	Site 2 (kcal mol^{-1})
Bicarbonate	-3.2	-2.9	-3.4	-3.7
Formate	-2.3	NA	-2.9	-3.1

When modeled with the protein encoded by SO_3758_A269T, bicarbonate is still predicted to bind to site 1 and form polar interactions with the same residues with a slightly stronger binding affinity of -3.4 kcal mol^{-1}. However, the greatest predicted binding affinity of -3.7 kcal mol^{-1} is in a binding pocket with the altered T269 residue, as well as residues T103 and N302, here referred to as site 2 (**Figure 17c**, **Figure 16c**, **Figure 16e**). This indicates that the A269T substitution altered the native bicarbonate binding site 1 slightly to promote tighter binding of the native substrate, even though residue 269 is not itself a part of site 1. More interestingly, it shows that the change in residue 269 alters site 2 to stronger affinity for the substrate. Finally, when formate binding is modeled with the protein encoded by SO_3758_A269T, the greatest predicted binding affinity (-3.1 kcal mol^{-1}) is also in site 2 with T103, N302, and the altered residue T269 (**Figure 17d**). This brings the predicted binding affinity of formate much closer to that of bicarbonate in site 1 of the native protein encoded by SO_3758 (-3.2 kcal mol^{-1}), suggesting that formate is a suitable substrate for this mutant. The predicted interaction of formate with threonine 269 in the protein encoded by SO_3758_A269T but not with alanine in the WT version also suggests that this alteration was beneficial in promoting formate binding.

The two binding sites in the protein encoded by SO_3758_A269T are predicted to bind both substrates, but formate is not predicted to bind to site 2 in the native protein (**Table 5**). Site 1 binds both bicarbonate and formate better than site 2. The opposite is true for the protein encoded by SO_3758_A269T where site 2 with residue threonine 269 binds both substrates better and increases the predicted binding affinity of formate to a similar level that is predicted for bicarbonate binding in the native protein. Based on this modeling, we anticipated that the A269T substitution in the protein encoded by SO_3758

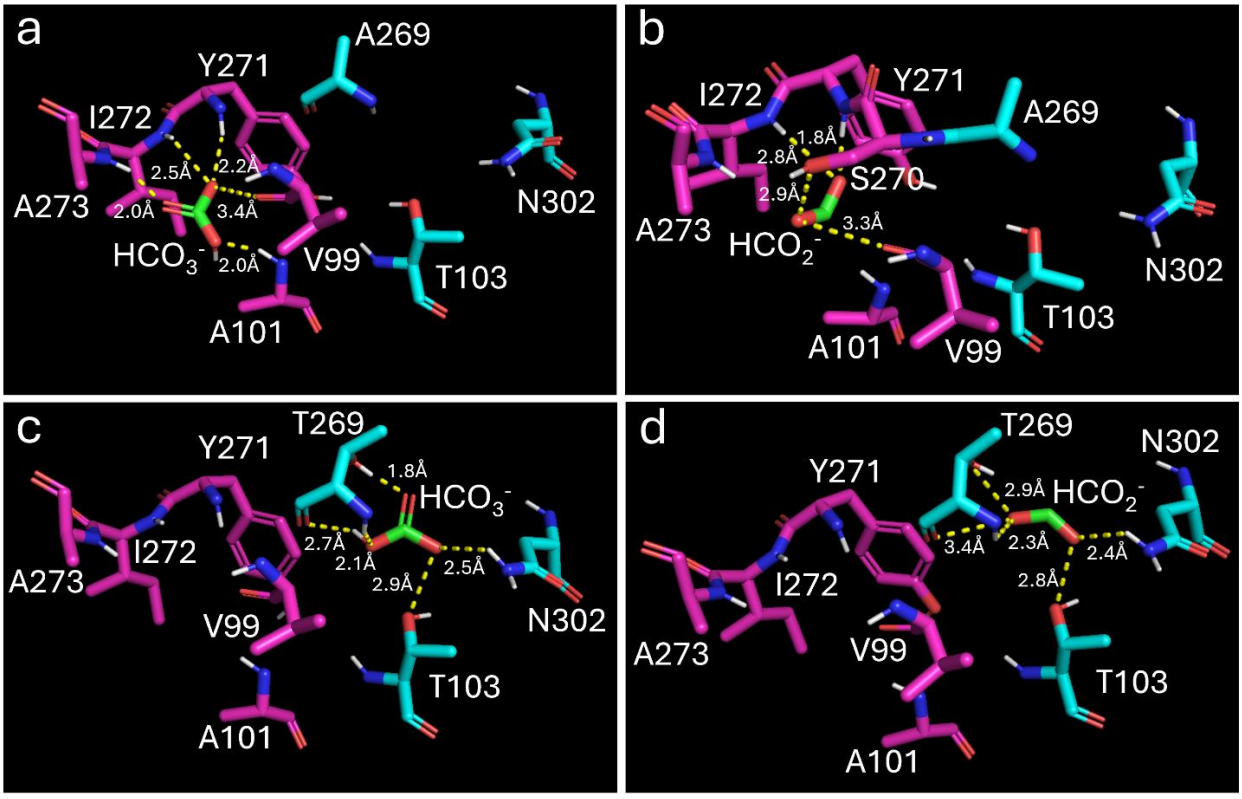

Figure 17. Ligand dock modeling of formate and bicarbonate to the proteins encoded by SO_3758_WT and SO_3758_A269T. Modeled binding of bicarbonate (HCO_3^-) to the proteins encoded by SO_3758_WT (a) and SO_3758_A269T (c) and of formate (HCO_2^-) to the proteins encoded by SO_3758_WT (b) and SO_3758_A269T (d). Residues in the native bicarbonate binding site (site 1) are shown in pink and residues in site 2 are shown in cyan. Formate and bicarbonate are shown in green. Nitrogen atoms are colored blue, oxygen atoms are colored red, and hydrogen atoms are colored white. Polar interactions between bicarbonate or formate and interacting residues are shown as yellow dotted lines and are labeled with the distance between the interacting atoms.

provided MGC002, MGC005, and MGC006 with greater formate efflux capacity to prevent the toxic accumulation of formate inside the cells.

The effects of mutations in DUF2721-containing protein encoded by SO_1320 are less clear and more difficult to ascertain. While the function of both DUF2721 and the protein encoded by SO_1320 are unknown, some clues exist to the protein's potential role. Both YadS and the protein encoded by SO_1328 expressed from the same operon as the protein encoded by SO_1320 are part of membrane protein families. YadS is annotated

as a trimeric intracellular cation (TRIC) channel and the protein encoded by SO_1318 is annotated as a nuclear transport factor 2-like (NTF2) protein.[51] The proximity of the protein encoded by SO_1320 to these membrane-bound transporter proteins could be an indicator that it shares a similar function.

In an attempt to elucidate the potential function of the protein encoded by SO_1320, the amino acid sequence was analyzed using DeepGO, a deep learning tool which predicts localization and function of a protein based on its sequence.[52] DeepGO predicted that the protein encoded by SO_1320 is localized to the cell membrane but was unable to predict its function, likely due to a lack of experimentally characterized homologs (**Table 6**). Further analysis of the amino acid sequence of the protein encoded by SO_1320 with DeepTMHMM,[53] a tool for predicting transmembrane proteins using deep neural networks, reiterates the protein's probable localization to the cell membrane, finding three transmembrane helices (**Figure 18**). These results suggest that the protein encoded by SO_1320 is associated with the cellular membrane, although it is still unclear what function it serves. Since the formate concentrations are constant throughout culturing of MGC003, MGC004, and MGC007 (formate tolerant strains with mutations in SO_1320), the evolved method of formate tolerance must not involve the oxidation or assimilation of formate. Potential formate tolerance mechanisms of SO_1320 mutants could include enhanced

Table 6. DeepGO predictions for the protein encoded by SO_1320.

Gene Ontology	Description	Prediction Score
Cellular Component		
GO:0110165	cellular anatomical entity	0.392872
GO:0016020	membrane	0.370649
Molecular Function		
Biological Process		

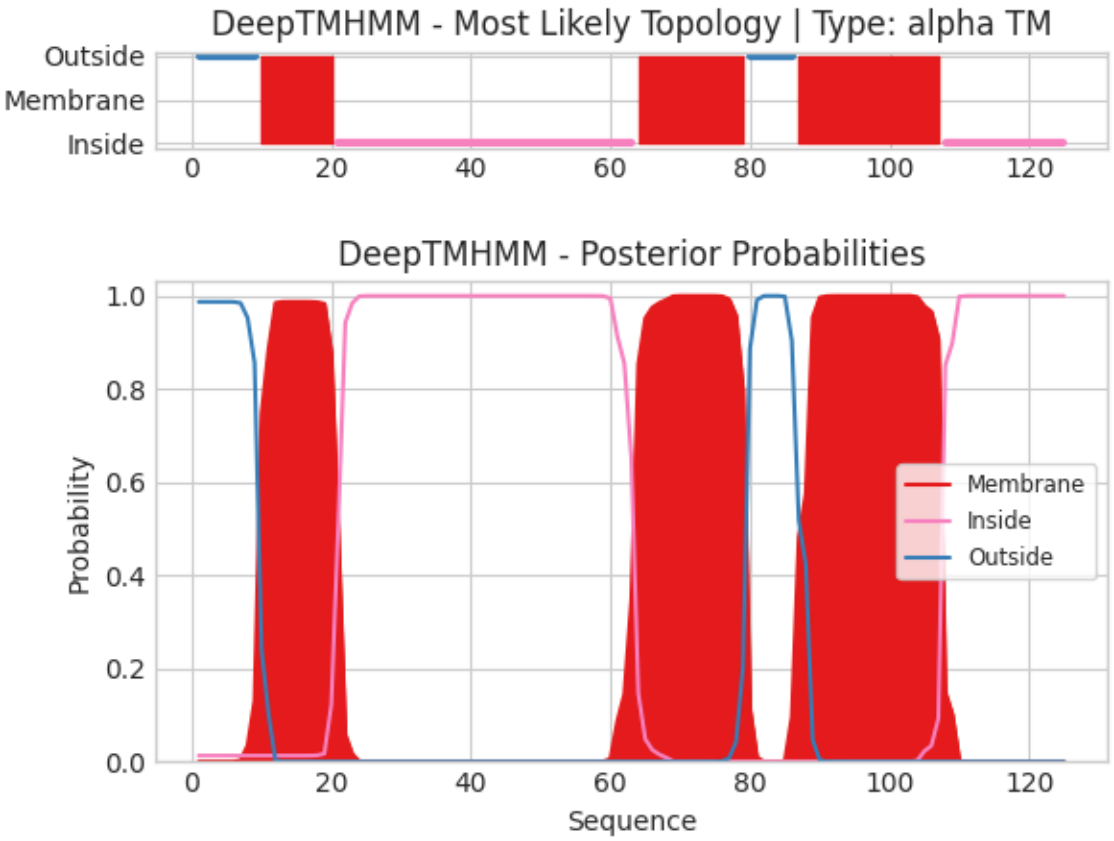

Figure 18. Structure prediction of the protein encoded by SO_1320 by DeepTMHMM.

active formate efflux, decreased active formate influx, or membrane stabilization preventing passive formate diffusion.

To determine if the protein encoded by SO_1320 could bind formate, the WT and mutated versions of this protein were modeled using AlphaFold[43] and formate binding was predicted with AutoDock Vina.[44] Modeling results colored with pLDDT scores are shown in **Figure 19**. The protein encoded by SO_1320 did not appear to have convincing formate binding activity, as the best predicted binding affinity was -2.1 kcal mol^{-1} at a site on the protein surface. Modeling of formate binding to the proteins encoded by SO_1320_V106I, SO_1320_V106F, and SO_1320_S52I calculated predicted binding affinities to formate of

-2.0 kcal mol^{-1}, -2.1 kcal mol^{-1}, and -2.1 kcal mol^{-1}, respectively. The low predicted binding affinity, the location of the predicted binding, and the lack of improvement to the predicted binding affinity in the mutants suggest that neither the WT or mutant version of the protein encoded by SO_1320 are acting as a formate transporter; however, it does not eliminate the possibility that it could be a formate channel or that it could form a multimeric complex with a formate transporter.

DISCUSSION

This work describes the evolution of seven formate-tolerant *S. oneidensis* strains for use in systems subjected to high formate concentrations. Two notable mutations arose during evolution of *S. oneidensis* for greater formate tolerance. The first is a substitution in alanine 269 to a threonine in the sodium-dependent bicarbonate transporter encoded by SO_3758. Every strain exhibiting this mutation in SO_3758 (MGC002, MGC005, and MGC006) shared the same A269T substitution in the encoded protein and was able to withstand greater formate concentrations than the parent strains. The second gene with mutations attributed to greater formate tolerance was SO_1320 encoding a protein of unknown function. Alterations occurred in residue 106, changing the native valine to either isoleucine (MGC007) or phenylalanine (MGC003 and MGC004), and in residue 52 (MGC008), changing the native serine to isoleucine. The evolved strains provided with the capacity to grow robustly on 100 mM formate in minimal lactate medium when the parent strains they are derived from were only capable of growth on 10-20 mM formate.

Strains harboring a substitution in V106 of the protein encoded by SO_1320 had a shorter lag phase than strains harboring the A269T substitution in the protein encoded by SO_3758, although all strains grew to a similar final OD_{600} (**Figure 10**). Therefore, the

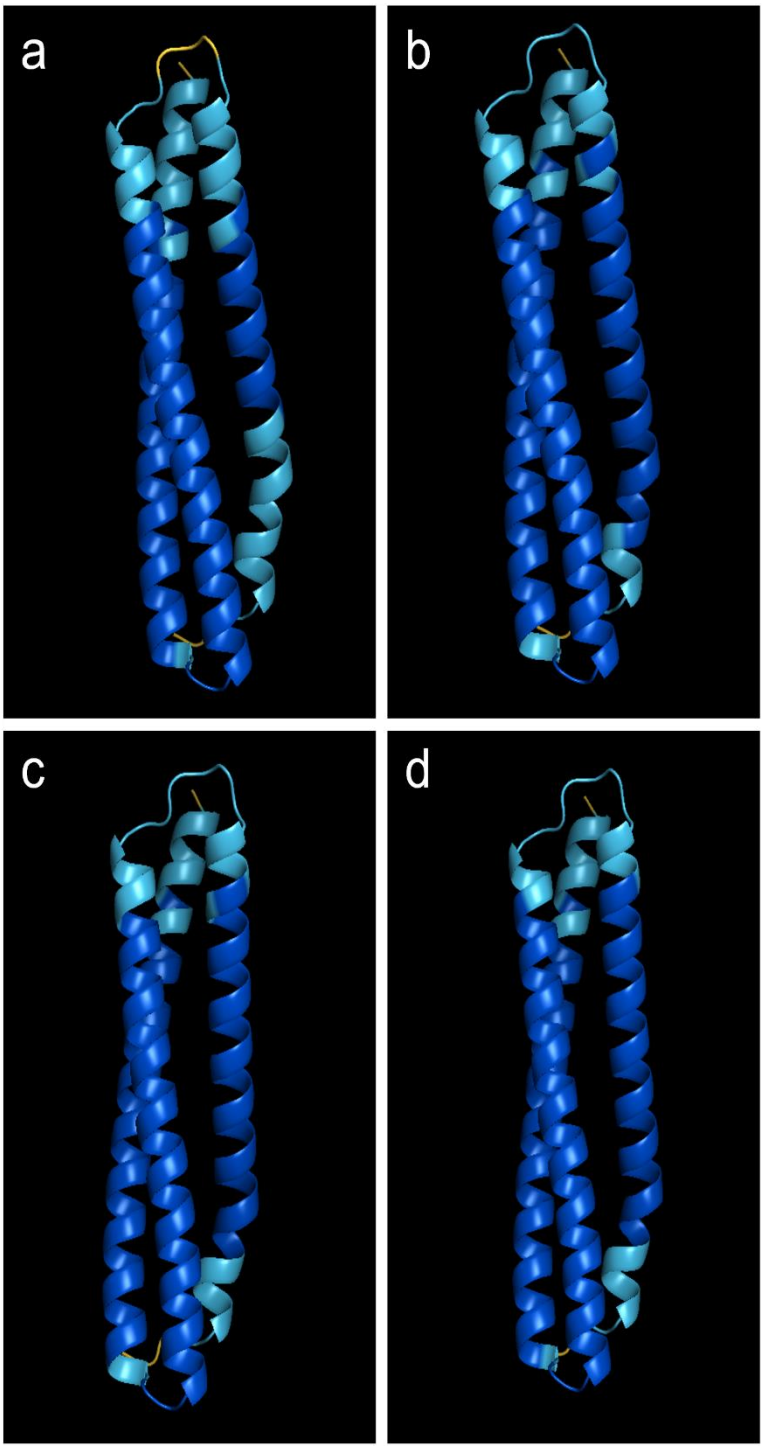

Figure 19. AlphaFold modeling of the proteins encoded by WT and mutant versions of SO_1320. Residue color depicts pLDDT score. Dark blue represents a very high score (pLDDT > 90). Light blue represents a confident score (90 > pLDDT > 70). Yellow represents a low score (70 > pLDDT > 50). Orange represents a very low score (pLDDT < 50). Models of proteins encoded by a) SO_1320, b) SO_1320_V106I, c) SO_1320_V106F, and d) SO_1320_S52I.

onset of formate tolerance benefits from the SO_1320 mutations are more instantaneous than the SO_3758_A269T mutation. The extra delay in growth of strains with the SO_3758_A269T mutation may be related to the mechanism by which it provides formate tolerance. Modeling of formate binding in the WT and mutant versions of the protein encoded by SO_3758 revealed that the conversion of alanine 269 to threonine increased the binding affinity of formate to a site deeper in the binding pocket. This site is predicted to bind bicarbonate in the native protein with a lower predicted binding affinity, indicating that the mutation did not create a new binding site, but rather strengthened an existing one. The predicted binding affinity of both bicarbonate and formate in the deeper binding site of the protein encoded by SO_3758_A269T is stronger than the binding of both substrates to both the native and deeper binding site in the unmutated protein. The mutation allows formate binding to a similar efficiency of the native bicarbonate binding, suggesting that the mutation has made formate a suitable substrate for the protein encoded by SO_3758_A269T. The ability to better bind formate suggests that the strains harboring this mutation had improved formate efflux capabilities over the WT. Without the benefit of being able to transport formate, the parent strains with WT SO_3758 could not prevent the toxic accumulation of formate in the cells. If the mechanism of formate tolerance in SO_3758 mutants is greater formate efflux rates, the delay in growth may be because formate continues to enter the cell, and the tolerance to the toxic compound only arises when SO_3758_A269T has cleared enough of it from the cytoplasm.

The role of changes in DUF2721-containing protein encoded by SO_1320 are less clear as neither this domain nor this protein have any known characterized homologues. SO_1320 is in an operon with genes encoding a membrane protein channel or membrane

transport protein (*yadS* and SO_1318), and sequence analysis tools predict three transmembrane helices. These clues suggest that the protein encoded by SO_1320 is also a membrane protein. Modeling of formate binding to WT and mutant versions of the protein encoded by SO_1320 indicate that the protein does not bind formate as a transporter might. While it is still unclear how SO_1320 mutants are providing cells with greater formate tolerance, our analysis does not rule out the possibilities that the protein of unknown function encoded by SO_1320 is involved in membrane stabilization or acts as a formate channel. Additionally, the protein encoded by SO_1320 could be one subunit in a multimeric formate transporter which binds formate in a different subunit.

Expression of these mutant genes in the *S. oneidensis* WT background on minimal lactate media increased formate tolerance two-fold. The ability to reconstruct the formate tolerant phenotype through expression of these altered proteins further confirms their role in the evolved strains. The simple point mutations which lead to these growth improvements provide two easily accessible methods for transferring formate tolerance to *S. oneidensis* and potentially other organisms. This could be a valuable tool in engineering biocatalysts that would benefit from reduced intracellular formate or bicarbonate levels, such as in organisms in which these compounds cease metabolic activity prematurely due to toxicity issues.

FUNDING SOURCES

This work was supported by a 2018 Beckman Young Investigator Award and a National Science Foundation CAREER Award (1750785) to MT.

ACKNOWLEDGEMENTS

We thank Dr. Jeffrey Gralnick for *S. oneidensis* strains JG2955 and JG2957. We also thank Drs. Nanye Long and Nicholas Panchy for their assistance with Breseq and AlphaFold.

REFERENCES

1. Dessì, P. *et al.* Microbial electrosynthesis: Towards sustainable biorefineries for production of green chemicals from CO_2 emissions. *Biotechnol Adv* **46**, 107675 (2021).

2. Jourdin, L. & Burdyny, T. Microbial Electrosynthesis: Where Do We Go from Here? *Trends Biotechnol* **39**, 359–369 (2021).

3. Jensen, H. M. *et al.* Engineering of a synthetic electron conduit in living cells. *PNAS* **107**, 19213–19218 (2010).

4. Schiel-Bengelsdorf, B. & Dürre, P. Pathway engineering and synthetic biology using acetogens. *FEBS Lett* **586**, 2191–2198 (2012).

5. Prévoteau, A., Carvajal-Arroyo, J. M., Ganigué, R. & Rabaey, K. Microbial electrosynthesis from CO_2: forever a promise? *Curr Opin Biotechnol* **62**, 48–57 (2020).

6. Rosenbaum, M. A. & Henrich, A. W. Engineering microbial electrocatalysis for chemical and fuel production. *Curr Opin Biotechnol* **29**, 93–98 (2014).

7. Katsyv, A. & Müller, V. Overcoming Energetic Barriers in Acetogenic C1 Conversion. *Front Bioeng Biotechnol* **8**, (2020).

8. Philips, J. Extracellular Electron Uptake by Acetogenic Bacteria: Does H_2 Consumption Favor the H_2 Evolution Reaction on a Cathode or Metallic Iron? *Front Microbiol* **10**, (2020).

9. Ganigué, R., Puig, S., Batlle-Vilanova, P., Balaguer, M. D. & Colprim, J. Microbial electrosynthesis of butyrate from carbon dioxide. *Chem Comm* **51**, 3235–3238 (2015).

10. Raes, S. M. T., Jourdin, L., Buisman, C. J. N. & Strik, D. P. B. T. B. Continuous Long-Term Bioelectrochemical Chain Elongation to Butyrate. *ChemElectroChem* **4**, 386–395 (2017).

11. Arends, J. B. A., Patil, S. A., Roume, H. & Rabaey, K. Continuous long-term electricity-driven bioproduction of carboxylates and isopropanol from CO_2 with a mixed microbial community. *J CO_2 Util* **20**, 141–149 (2017).

12. Harrington, T. D. *et al.* Neutral red-mediated microbial electrosynthesis by *Escherichia coli*, *Klebsiella pneumoniae*, and *Zymomonas mobilis*. *Bioresour Technol* **195**, 57–65 (2015).

13. Tefft, N. M. & Teravest, M. A. Reversing an Extracellular Electron Transfer Pathway for Electrode-Driven Acetoin Reduction. *ACS Synth Biol* **8**, 1590–1600 (2019).

14. Ross, D. E., Flynn, J. M., Baron, D. B., Gralnick, J. A. & Bond, D. R. Towards Electrosynthesis in *Shewanella*: Energetics of Reversing the Mtr Pathway for Reductive Metabolism. *PLoS One* **6**, e16649 (2011).

15. Rowe, A. R. *et al.* Tracking Electron Uptake from a Cathode into *Shewanella* Cells: Implications for Energy Acquisition from Solid-Substrate Electron Donors. *mBio* **9**, (2018).

16. Kouzuma, A. Molecular mechanisms regulating the catabolic and electrochemical activities of *Shewanella oneidensis* MR-1. *Biosci Biotechnol Biochem* **85**, 1572–1581 (2021).

17. Brutinel, E. D. & Gralnick, J. A. Shuttling happens: soluble flavin mediators of extracellular electron transfer in *Shewanella*. *Appl Microbiol Biotechnol* **93**, 41–48 (2012).

18. Richardson, D. J. *et al.* The 'porin–cytochrome' model for microbe-to-mineral electron transfer. *Mol Microbiol* **85**, 201–212 (2012).

19. Madsen, C. S. & TerAvest, M. A. NADH dehydrogenases Nuo and Nqr1 contribute to extracellular electron transfer by *Shewanella oneidensis* MR-1 in bioelectrochemical systems. *Sci Rep* **9**, 14959 (2019).

20. Beblawy, S. *et al.* Extracellular reduction of solid electron acceptors by *Shewanella oneidensis*. *Mol Microbiol* **109**, 571–583 (2018).

21. Kane, A. L. *et al.* Formate Metabolism in *Shewanella oneidensis* Generates Proton Motive Force and Prevents Growth without an Electron Acceptor. *J Bacteriol* **198**, 1337–1346 (2016).

22. Marritt, S. J. *et al.* A functional description of CymA, an electron-transfer hub supporting anaerobic respiratory flexibility in *Shewanella*. *Biochem J* **444**, 465–474 (2012).

23. Myers, C. R. & Myers, J. M. Cloning and sequence of cymA, a gene encoding a tetraheme cytochrome *c* required for reduction of iron(III), fumarate, and nitrate by *Shewanella putrefaciens* MR-1. *J Bacteriol* **179**, 1143–1152 (1997).

24. Sturm, G. *et al.* A dynamic periplasmic electron transfer network enables respiratory flexibility beyond a thermodynamic regulatory regime. *ISME J* **9**, 1802–1811 (2015).

25. Coursolle, D. & Gralnick, J. A. Reconstruction of Extracellular Respiratory Pathways for Iron(III) Reduction in *Shewanella oneidensis* Strain MR-1. *Front Microbiol* **3**, (2012).

26. Coursolle, D., Baron, D. B., Bond, D. R. & Gralnick, J. A. The Mtr Respiratory Pathway Is Essential for Reducing Flavins and Electrodes in *Shewanella oneidensis*. *J Bacteriol* **192**, 467–474 (2010).

27. Cotton, C. A., Edlich-Muth, C. & Bar-Even, A. Reinforcing carbon fixation: CO_2 reduction replacing and supporting carboxylation. *Curr Opin Biotechnol* **49**, 49–56 (2018).

28. François, J. M., Lachaux, C. & Morin, N. Synthetic Biology Applied to Carbon Conservative and Carbon Dioxide Recycling Pathways. *Front Bioeng Biotechnol* **7**, (2020).

29. Bar-Even, A., Noor, E. & Milo, R. A survey of carbon fixation pathways through a quantitative lens. *J Exp Bot* **63**, 2325–2342 (2012).

30. Calzadiaz-Ramirez, L. & Meyer, A. S. Formate dehydrogenases for CO_2 utilization. *Curr Opin Biotechnol* **73**, 95–100 (2022).

31. Amao, Y. Formate dehydrogenase for CO_2 utilization and its application. *J CO_2 Util* **26**, 623–641 (2018).

32. Bar-Even, A. Formate Assimilation: The Metabolic Architecture of Natural and Synthetic Pathways. *Biochemistry* **55**, 3851–3863 (2016).

33. Reda, T., Plugge, C. M., Abram, N. J. & Hirst, J. Reversible interconversion of carbon dioxide and formate by an electroactive enzyme. *PNAS* **105**, 10654–10658 (2008).

34. Ghosh, I. N. *et al.* OptSSeq explores enzyme expression and function landscapes to maximize isobutanol production rate. *Metab Eng* **52**, 324–340 (2019).

35. Peters, J. M. *et al.* Enabling genetic analysis of diverse bacteria with Mobile-CRISPRi. *Nat Microbiol 2019 4:2* **4**, 244–250 (2019).

36. Ford, K. C., Kaste, J. A. M., Shachar-Hill, Y. & Teravest, M. A. Flux-Balance Analysis and Mobile CRISPRi-Guided Deletion of a Conditionally Essential Gene in Shewanella oneidensis MR-1. *ACS Synth Biol* **11**, 3405–3413 (2022).

37. Deatherage, D. E. & Barrick, J. E. Identification of Mutations in Laboratory-Evolved Microbes from Next-Generation Sequencing Data Using breseq. *Methods Mol Biol* **1151**, 165–188 (2014).

38. Lin, H., Deng, E.-Z., Ding, H., Chen, W. & Chou, K.-C. iPro54-PseKNC: a sequence-based predictor for identifying sigma-54 promoters in prokaryote with pseudo k-tuple nucleotide composition. *Nucleic Acids Res* **42**, 12961–12972 (2014).

39. Patiyal, S., Singh, N., Ali, M. Z., Pundir, D. S. & Raghava, G. P. S. Sigma70Pred: A highly accurate method for predicting sigma70 promoter in *Escherichia coli* K-12 strains. *Front Microbiol* **13**, (2022).

40. Notredame, C., Higgins, D. G. & Heringa, J. T-coffee: a novel method for fast and accurate multiple sequence alignment. *J Mol Biol* **302**, 205–217 (2000).

41. Kulmanov, M., Khan, M. A. & Hoehndorf, R. DeepGO: predicting protein functions from sequence and interactions using a deep ontology-aware classifier. *Bioinformatics* **34**, 660–668 (2018).

42. Hallgren, J. *et al.* DeepTMHMM predicts alpha and beta transmembrane proteins using deep neural networks. *bioRxiv* (2022).

43. Jumper, J. *et al.* Highly accurate protein structure prediction with AlphaFold. *Nature* **596**, 583–589 (2021).

44. Trott, O. & Olson, A. J. AutoDock Vina: Improving the speed and accuracy of docking with a new scoring function, efficient optimization, and multithreading. *J Comput Chem* **31**, 455–461 (2010).

45. Schrödinger LLC. *The PyMOL Molecular Graphics System, Version~2.5.8*. https://pymol.org/2/ (2015).

46. Nicholls, P. Formate as an inhibitor of cytochrome *c* oxidase. *Biochem Biophys Res Commun* **67**, 610–616 (1975).

47. Warnecke, T. & Gill, R. T. Organic acid toxicity, tolerance, and production in *Escherichia coli* biorefining applications. *Microb Cell Fact* **4**, 25 (2005).

48. Cotton, C. A., Claassens, N. J., Benito-Vaquerizo, S. & Bar-Even, A. Renewable methanol and formate as microbial feedstocks. *Curr Opin Biotechnol* **62**, 168–180 (2020).

49. Liu, X.-Y. *et al.* Structures of cyanobacterial bicarbonate transporter SbtA and its complex with PII-like SbtB. *Cell Discov* **7**, 63 (2021).

50. Fang, S. *et al.* Molecular mechanism underlying transport and allosteric inhibition of bicarbonate transporter SbtA. *PNAS* **118**, (2021).

51. Heidelberg, J. F. *et al.* Genome sequence of the dissimilatory metal ion–reducing bacterium *Shewanella oneidensis*. *Nat Biotechnol* **20**, 1118–1123 (2002).

52. Kulmanov, M., Khan, M. A. & Hoehndorf, R. DeepGO: predicting protein functions from sequence and interactions using a deep ontology-aware classifier. *Bioinformatics* **34**, 660–668 (2018).

53. Hallgren, J. *et al.* DeepTMHMM predicts alpha and beta transmembrane proteins using deep neural networks. *bioRxiv* (2022) doi:10.1101/2022.04.08.487609.

CHAPTER 3:

RNF COMPLEX GENERATES REDUCED FERREDOXIN FOR IRON-SULFUR CLUSTER FORMATION IN *SHEWANELLA ONEIDENSIS* MR-1

PREFACE

Early on in my PhD program, my main research focus was engineering-based applied science. I intended to create an electroautotrophic strain of *S. oneidensis* for use in MES. While that remained the goal throughout my time here, it was a risky endeavor. Although I had two approaches to make this strain, there was no guarantee it would work, and especially no guarantee it would work in the time available to me. So, I added a more exploratory project to my repertoire – elucidating the role of Rnf in *S. oneidensis*.

Originally, Rnf was interesting to us as a prospective source of low potential electrons for carbon fixation. Rnf connects the NADH and ferredoxin pools by ion motive force and has been shown to operate in either the ferredoxin-reducing and ferredoxin-oxidizing direction. Characterization of this enzyme complex in *S. oneidensis* was expected to give us insight into its catalytic activity and the fate of the ferredoxin. I was able to determine the direction of the activity (it has ferredoxin-reducing activity like we were hoping), but the fate of the reduced ferredoxin surprised us.

We were able to confirm our hypothesis through a collaboration with Daniel Amador-Noguez's lab at University of Wisconsin, Madison. A graduate student of his, Julio Rivera Vazquez, ran LC-MS metabolomics on metabolite extracts that I prepared from our knockdown strains. The data we got from this collaboration was instrumental in confirming the Rnf model that we proposed.

This project was a great example of following the data where it leads you, because the model we ultimately proposed for Rnf function in *S. oneidensis* was not at all on our radar when the project began. It was a helpful exercise for me in combatting confirmation bias and being open-minded about all the potential explanations for an observation.

Ultimately, I believe what we discovered has greater impact than our original hypothesis, and I'm excited to see where future research into this topic leads.

This chapter describes the experimentation of Rnf in *S. oneidensis* and presents a new model for Rnf activity across species.

ABSTRACT

Rnf (***R****hodobacter* **n**itrogen **f**ixation) is a membrane protein complex found in diverse bacteria that connects the NADH pool to ferredoxins and couples its redox reaction to ion translocation across the membrane. In the ion motive force-generating direction, Rnf oxidized ferredoxins for NADH production. Alternatively, in the ion motive force-consuming direction, Rnf generates reduced ferredoxins from NADH. This activity has been implicated in a range of pathways, including nitrogen fixation and SoxR reduction. In this work, we characterize the role of the Rnf complex in *Shewanella oneidensis*, an organism without nitrogen fixation or a Sox system. Insights into the role of Rnf in this host give rise to a comprehensive model for Rnf function across species. We propose the Rnf function is two-pronged. The first is that Rnf generates reduced ferredoxins for enzymes requiring them as cofactors. The second is that one of the most impactful enzymes that uses Rnf-derived ferredoxins is cysteine desulfurase, which transfers elemental sulfur from cysteine to an iron-sulfur cluster during iron-sulfur cluster biosynthesis and repair. The dual functionality of Rnf activity emphasizes its significance in maintaining cellular redox balance and facilitating vital metabolic processes in bacteria. Understanding the mechanisms by which Rnf contributes to iron-sulfur cluster biosynthesis and enzyme activity can provide insights into bacterial physiology.

The Rnf complex was first described in *Rhodobacter capsulatus* for its involvement in nitrogen fixation, leading to its moniker Rnf (***R****hodobacter* **n**itrogen **f**ixation).[1,2] In *R. capsulatus*, the Rnf complex generates reduced ferredoxin from NADH powered by ion motive force.[1,3] The low potential reduced ferredoxin ($E^{0'}$ = -500 to -420 mV) and ATP are used by nitrogenase (Nif) to reduce nitrogen to ammonia (**Figure 20a**).[1] Since its discovery in *R. capsulatus*, Rnf has been found in many other bacteria and some archaea, including organisms that do not fix nitrogen.[3] For example, Rnf in *Escherichia coli* does not contribute to nitrogen fixation, but rather returns the oxygen-sensing transcription factor SoxR to its inactivated state by reducing its iron-sulfur cluster (ISC).[4] Rnf also operates as a sodium pump driven by ferredoxin oxidation, such as in *Acetobacterium woodii*, where the first characterization connected Rnf activity to caffeate reduction (**Figure 20b**).[5]

Many studies attempt to classify the direction of Rnf activity in a particular organism.[1,2,5,6] While useful for identifying certain pathways Rnf participates in, evidence

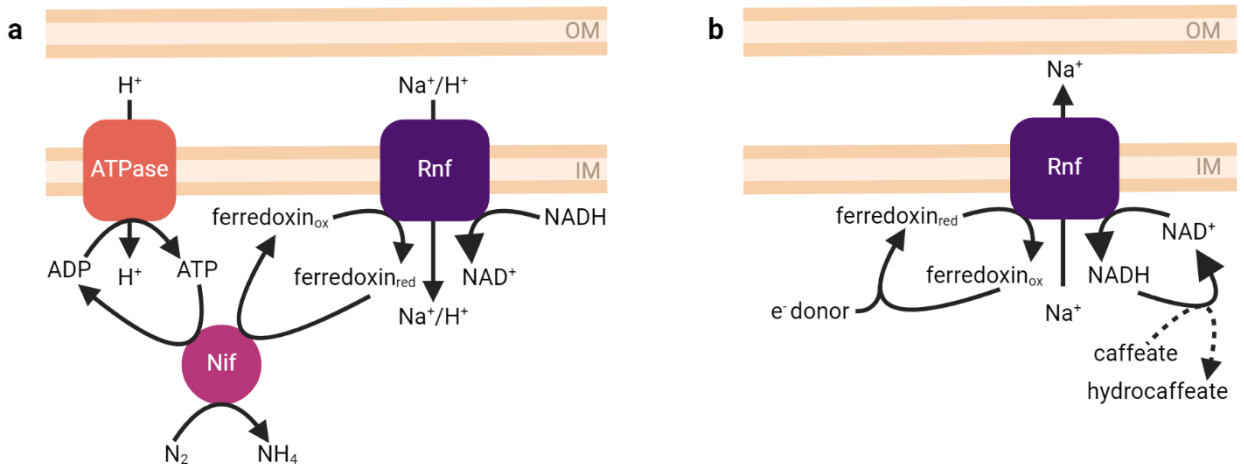

Figure 20. Rnf activities in the ferredoxin-reducing and ferredoxin-oxidizing directions. a) In *R. capsulatus*, Rnf generates reduced ferredoxin from NADH using sodium or proton motive force. Reduced ferredoxins are used along with ATP to power nitrogen fixation. b) In *A. woodii*, Rnf oxidizes reduced ferredoxin to pump sodium across the inner membrane. This activity is part of caffeate reduction.

suggests Rnf can operate bidirectionally depending on the ferredoxin:NADH ratio. For example, the *A. woodii* Rnf was originally characterized as operating in the sodium-pumping direction driven by ferredoxin oxidation.[5] However, a more recent study found that the complex can also catalyze ferredoxin reduction when NADH levels are greater than that of ferredoxin, such as when the organism is cultivated with low-energy substrates.[7] This points to a broader role of Rnf connecting the ferredoxin and NADH pools depending on cellular needs. Additionally, the variety of pathways found to include Rnf activity also suggests an unidentified link connecting Rnf to these diverse processes.

Rnf operons have some variation in structure depending on the species.[3] *R. capsulatus* has an operon structure of *rnfABCDGEH*.[2] A common variation on this structure which is shared by organisms such as *E. coli* and *Shewanella oneidensis* is the substitution of *rnfH* with *nth*, a gene encoding endonuclease III.[8,9] While the inclusion of *nth* in the *rnf* operon is not uncommon, no link between Rnf and Nth has been established to date.

R. capsulatus rnf operon was suggested to be negatively controlled by ferric-uptake regulator (Fur), with less Rnf expression under iron-limiting conditions.[2] Decreased Rnf expression under iron-limiting conditions as regulated by Fur was also found in *C. difficile*.[10] Regulation of Rnf by iron availability suggests some connection between Rnf and iron metabolism, although the functional link has yet to be established.

Shewanella oneidensis is a heterotrophic, facultative anaerobe, with the capability to respire extracellular electron acceptors using a process called extracellular electron transfer.[11–13] This organism can respire a diverse set of terminal electron acceptors such as nitrate, nitrite, dimethyl sulfoxide, vanadate, and iron oxides.[14–17] Its respiratory flexibility

is the result of a branched electron transfer chain which has been the subject of many studies.[18–21] As such, the electron transfer pathways of *S. oneidensis* are well understood, which makes it a good host to study the wider role of Rnf in electron transfer. Additionally, *S. oneidensis* does not have a SoxRS system, cannot fix nitrogen, and cannot respire caffeate, so its Rnf likely does not have any of the previously proposed functions. This poises *S. oneidensis* as a promising host to elucidate the broader role that Rnf plays.

The connection of NADH and ferredoxin pools is an important aspect for bioengineering in cases such as carbon dioxide or nitrogen fixation. The reduction potentials of carbon dioxide to carbon monoxide and formate is $E^{0'}$ = -520 and $E^{0'}$ = -610 mV, respectively.[22] These reduction reactions are especially important in the bioengineering of microbial hosts for conversion of carbon dioxide into value-added products via microbial electrosynthesis. However, they are difficult to achieve because they require electron donors with low potentials. Driving electrons uphill can be a powerful tool in making these reactions more attainable. Previously, we have shown that proton motive force could be used to drive NADH dehydrogenase in reverse in a bioengineered strain of *S. oneidensis*, moving electrons from the quinone pool to lower potential NADH.[23] The ability to drive electrons to an even lower potential (i.e. ferredoxin) would be an important step toward developing more robust hosts for microbial electrosynthesis. In this work, we examine the function of Rnf in *S. oneidensis* and propose a model which may explain its effect in previously studied systems.

METHODS

Strains and plasmids

Strains and plasmids used in this study are listed in **Table 7** and **Table 8**, respectively. sgRNA in CRISPRi knockdown vector pJMP2846, also carrying dCas9, were prepared to target *rnfA*, *iscS*, or *nth* using previously described methods.[24,25] Assembled CRISPRi vectors were inserted into *S. oneidensis* MR-1 using a Tn7-based triparental conjugation method.[25] The donor strains were 2,6-diaminopimelic acid (DAP)-auxotroph *E. coli* WM3064 carrying the assembled CRISPRi vector and DAP-auxotroph *E. coli* WM3064 pJMP2644 carrying a transposase. After a mating period of 8 hours on LB agar plates supplemented with 0.3 mM DAP, counter-selection was performed on LB agar plates supplemented with 50 μg ml^{-1} kanamycin in the absence of DAP. *S. oneidensis* colonies were screened for correct sgRNA construction with the sgRNA_check and appropriate sgRNA reverse primers (**Table 9**).

Table 7. Strains described in Chapter 3.

Strain	Description	Reference
S. oneidensis MR-1	WT *S. oneidensis*	Lab stock
Non-targeting	WT *S. oneidensis* harboring pJMP2846	This study
rnf knockdown	WT *S. oneidensis* harboring pJMP2846-rnf-88	This study
iscS knockdown	WT *S. oneidensis* harboring pJMP2846-iscS-111	This study
nth knockdown	WT *S. oneidensis* harboring pJMP2846-nth-141	This study
E. coli WM3064	Conjugal transfer donor strain, DAP auxotroph	Lab stock

Table 8. Plasmids described in Chapter 3.

Plasmid	Description	Reference
pJMP2846	Non-targeting CRISPRi vector with dCas9 and sgRNA under control of an IPTG-inducible promoter, kanamycin resistance	25
pJMP2846-rnf-88	pJMP2846 with non-targeting sgRNA replaced with *rnfA*-targeting sgRNA, kanamycin resistance	This study
pJMP2846-iscS-111	pJMP2846 with non-targeting sgRNA replaced with *iscS*-targeting sgRNA, kanamycin resistance	This study
pJMP2846-nth-141	pJMP2846 with non-targeting sgRNA replaced with *nth*-targeting sgRNA, kanamycin resistance	This study
pJMP2644	Contains transposase for triparental conjugation, ampicillin resistance	25

Table 9. Primers described in Chapter 3.

Primer	Sequence (5'->3')	Description
MG_087	TAGTTTGCTGGAGACCCCCATAAA	*rnfA* sgRNA forward
MG_088	AAACTTTATGGGGGTCTCCAGCAA	*rnfA* sgRNA reverse
MG_110	TAGTCGAGTCGCGGAAAAAATGTT	*iscS* sgRNA forward
MG_111	AAACAACATTTTTTCCGCGACTCG	*iscS* sgRNA reverse
MG_140	TAGTTTCAGCTCGGTCTGTGGTTT	*nth* sgRNA forward
MG_141	AAACAAACCACAGACCGAGCTGAA	*nth* sgRNA reverse
sg_RNA check	GGTCCTTGAGCCCCATTATC	sgRNA forward

Culturing

Knockdown strains were precultured in 2 ml LB supplemented with 50 µg ml^{-1} kanamycin overnight at 30 °C with shaking at 250 rpm. The pre-cultures were washed three times and resuspended in basal M5 media (1.29 mM K_2HPO_4, 1.65 mM KH_2PO_4, 7.87 mM NaCl, 1.70 mM NH_4SO_4, 475 µM $MgSO_4 \cdot 7H_2O$, 0.1 g L^{-1} casamino acids, 10 mM HEPES, pH 7.2). Washed cells were used to inoculate minimal medium cultures to an initial OD_{600} of 0.02 unless otherwise specified. Minimal lactate medium was comprised of M5 basal medium supplemented with Wolfe's mineral solution, Wolfe's vitamin solution without riboflavin, and 20 mM D,L-lactate. Inducer isopropyl β-D-1-thiogalactopyranoside (IPTG) was added to cultures at the specified concentrations. Where specified, thioflavin T (ThT), carbonyl cyanide m-chlorophenyl hydrazone (CCCP), and ETH2120 were added to cultures at working concentrations of 10 µM. Culture volumes are specified for each experiment and were conducted at 30 °C with shaking at 250 - 275 rpm. ThT was excited at 412 nm and fluorescence was monitored at 490 nm. Fluorescence intensity is reported as the ThT fluorescence normalized to the OD_{600}.

Colony forming units

Cell viability was determined by plating 3 µl spots of washed and serially diluted pre-cultures (prepared as described above) onto LB agar plates supplemented with 50 µg ml^{-1} kanamycin and the specified amount of IPTG. Plates were incubated at 30 °C for ~16 hours. Colonies were counted from dilutions that produced single colonies.

LC-MS Metabolomics

The *rnf*, *iscS*, and non-targeting knockdown strains were pre-cultured as described above and inoculated into 50 ml minimal lactate medium supplemented with 50 µg ml^{-1}

kanamycin to an initial OD_{600} of 0.035. The cultures were incubated at 30 °C with shaking at 250 rpm for 12 hours. Inoculation of cultures were staggered over the course of an hour, and metabolites were extracted after 12 h of culturing in the same order the cultures were inoculated. This staggering of inoculation and extraction ensured metabolites were extracted as close to the same total cultivation time for each sample as possible. Extraction was performed as previously described.[26] Briefly, 5 ml of each culture was harvested via vacuum filtration onto a 0.2 µm nylon membrane filter, and cells were resuspended in ice-cold HPLC-grade extraction solvent (20:20:10 acetonitrile:methanol:H_2O). Samples were centrifuged at 16,100 rpm for 10 minutes, and 180 µl of supernatant was dried under a nitrogen stream. LC-MS and metabolomics data analysis was performed as previously described.[26]

Data analysis

Data were analyzed using R version 4.3.1 and packages ggplot2 3.4.2, dplyr 1.1.2, viridis 0.6.4, grid 4.3.1, and gridExtra 2.3.[27–32]

RESULTS

To guide our investigation into the role of Rnf and its link to diverse pathways, we first attempted to establish a link between Rnf and Nth through ferredoxin. Nth does not require ferredoxin for its activity; however, the ISC biosynthesis and repair protein cysteine desulfurase (IscS) does require reduced ferredoxin as an electron donor for ISC assembly.[33,34] As an ISC protein, Nth is repaired by IscS in *E. coli*.[35] The potential link between Rnf and IscS was promising not only as a means of connecting Rnf and Nth activity, but also for explaining the regulation of the Rnf operon by Fur in some organisms.

To investigate this model further experimentally, we hoped to characterize the phenotype of an *rnf* deletion strain. Deletion of *rnf* from the *S. oneidensis* genome was attempted multiple times using a homologous recombination method commonly used for this organism but was never successful. The inability to delete this gene suggested that Rnf is essential in *S. oneidensis*. To study the role of Rnf in *S. oneidensis* without a knockout and to test essentiality, we created IPTG-inducible CRISPRi knockdown strains using Mobile-CRISPRi.[25] We generated a strain to knock down the entire *rnf* operon including *nth*, a second to knock down only *nth*, and a third to knock down *iscS*. To determine if these genes were essential, we plated the knockdown strains and controls onto LB agar plates supplemented with kanamycin and a range of IPTG concentrations. The controls included a non-targeting negative control, an essential gene control (*rpoC*), and a non-essential gene control (*ccmF*). Colony forming units were calculated to determine cell viability for each condition. The *rnf* and *iscS* knockdowns displayed similar decreases in cell viability as the essential gene control with increased IPTG concentrations, whereas IPTG had no effect on the *nth*-only (the last gene in the *rnf* operon) knockdown and negative controls (**Figure 21**). This result confirmed that Rnf is essential in *S. oneidensis*, providing explanation for our inability to generate a knockout. Additionally, IscS also appears to be essential, whereas Nth does not. The knockdown effect is also observed in minimal lactate medium liquid cultures (**Figure 22**). The knockdown of *nth* displays only a slight growth deficit compared the non-targeting control, with a 18% decrease in carrying capacity (final OD_{600}); whereas the knockdown of *rnf* and *iscS* show substantial growth deficits with a 66% and 79% decrease in carrying capacity, respectively (**Table 10**). The low impact of the *nth* knockdown on cell viability suggests

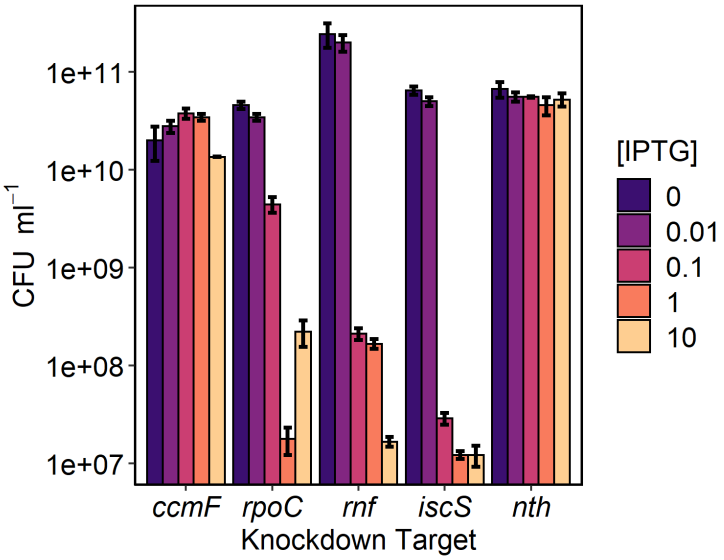

Figure 21. Colony forming units (CFU) of knockdown strains plated into LB with increasing concentrations of knockdown inducer IPTG. IPTG concentrations are in mM.

that Nth is not essential in *S. oneidensis*. This was confirmed by the ability to delete *nth* from the *S. oneidensis* genome, and the observation that the deletion had little impact on growth (**Figure 23**). Since the CRISPRi system interferes with transcription, protein levels only begin to drop once the system is induced and the existing protein is diluted out by cell division. This means that the severity of the knockdown effect is dependent on the number of doublings that occur in the culture. Therefore, inoculation to a lower OD_{600} results in a greater knockdown effect because more doublings occur (**Figure 24**). In 50 ml minimal lactate medium, the induced *rnf* knockdown strain displays a 69%, 38%, and 9% decrease in carrying capacity compared to the uninduced controls when inoculated to an initial OD_{600} of 0.005, 0.02, and 0.05, respectively (**Table 11**). Due to this observation, the knockdown strains were routinely cultivated by inoculating to an initial OD_{600} of 0.02 to ensure an adequate balance between phenotype effect and biomass production.

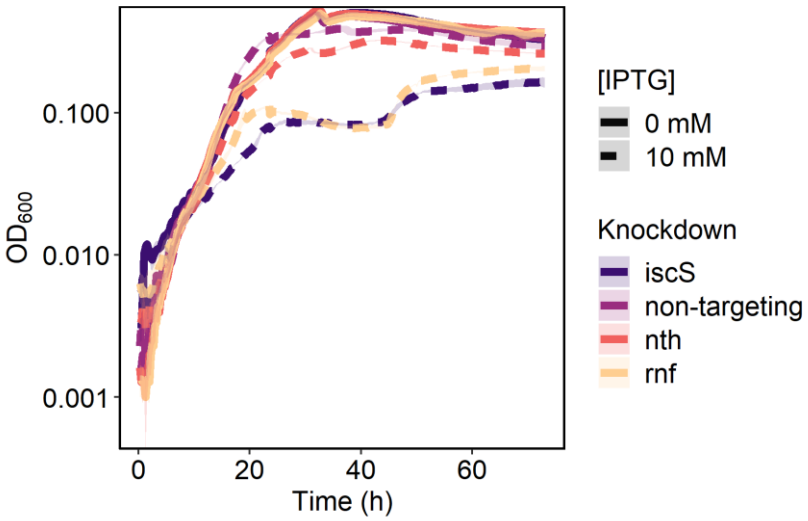

Figure 22. Growth curves of the induced and uninduced non-targeting, *rnf*, *iscS*, and *nth* knockdown strains in 200 µl of minimal lactate medium.

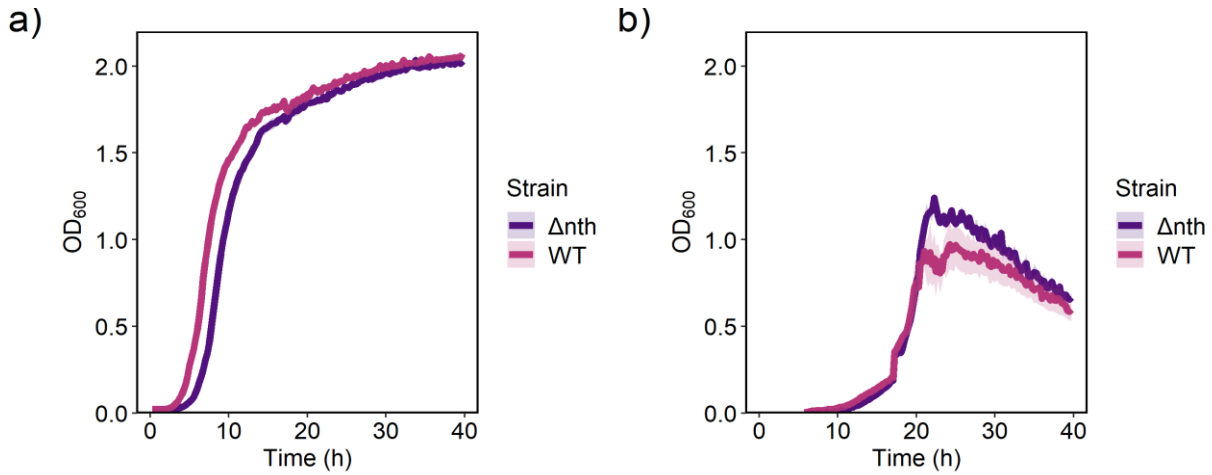

Figure 23. Growth curves of WT *S. oneidensis* and Δ*nth*. a) Cultivation of the strains in LB. b) Cultivation of the strains in minimal lactate medium.

Table 10. Carrying capacity, growth rates, and their percent differences from the non-targeting strain of knockdowns cultivated in 200 µl of minimal lactate medium.

Knockdown strain	0 mM IPTG			
	Carrying Capacity (OD_{600})	Growth Rate (h^{-1})	Carrying Capacity % difference from non-targeting	Growth Rate % difference from non-targeting
Non-targeting	0.409 ± 0.003	0.303 ± 0.019	NA	NA
rnf knockdown	0.421 ± 0.0003	0.274 ± 0.015	2.9%	18.5%
iscS knockdown	0.425 ± 0.004	0.327 ± 0.025	3.9%	7.9%
nth knockdown	0.434 ± 0.003	0.298 ± 0.018	6.1%	1.7%

Knockdown strain	10 mM IPTG			
	Carrying Capacity (OD_{600})	Growth Rate (h^{-1})	Carrying Capacity % difference from non-targeting	Growth Rate % difference from non-targeting
Non-targeting	0.351 ± 0.002	0.428 ± 0.022	NA	NA
rnf knockdown	0.118 ± 0.001	0.448 ± 0.002	66.4%	4.7%
iscS knockdown	0.073 ± 0.004	0.376 ± 0.020	79.2%	12.1%
nth knockdown	0.287 ± 0.001	0.249 ± 0.008	18.2%	41.8%

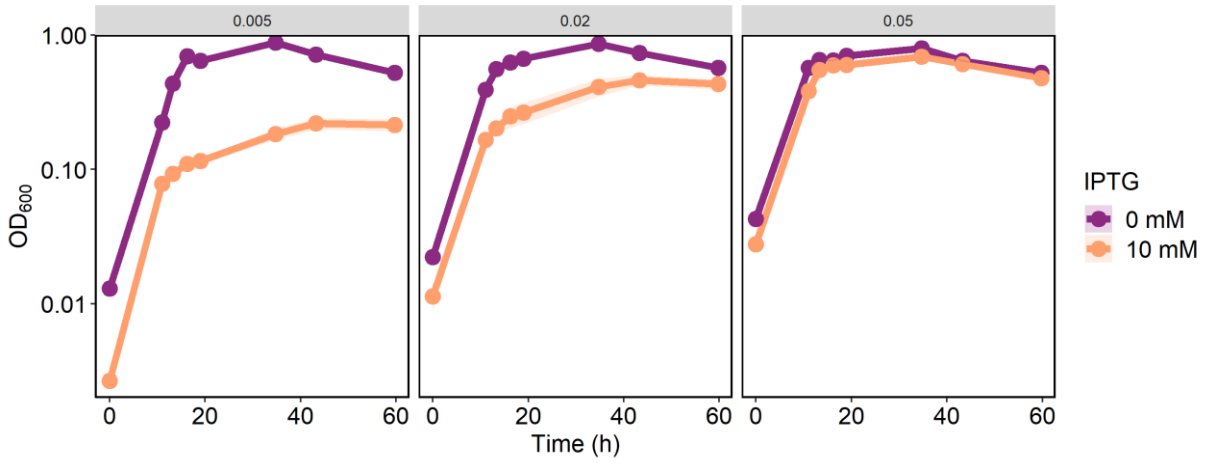

Figure 24. Growth curves of the induced and uninduced non-targeting, *rnf*, and *iscS* knockdown strains in 50 ml minimal lactate medium.

Table 11. Carrying capacity, growth rates, and percent differences from the uninduced conditions of the *rnf* knockdown strain in 50 ml minimal lactate medium inoculated to different initial OD_{600} ($OD_{600\ i}$).

$OD_{600\ i}$	0 mM IPTG	
	Carrying Capacity (OD_{600})	Growth Rate (h^{-1})
0.005	0.685 ± 0.059	0.659 ± 0.415
0.02	0.694 ± 0.051	0.367 ± 0.231
0.05	0.620 ± 0.041	0.912 ± 3.204

$OD_{600\ i}$	10 mM IPTG			
	Carrying Capacity (OD_{600})	Growth Rate (h^{-1})	Carrying Capacity % difference from uninduced	Growth Rate % difference from uninduced
0.005	0.212 ± 0.011	0.131 ± 0.031	69.1%	80.1%
0.02	0.430 ± 0.016	0.160 ± 0.032	38.0%	56.4%
0.05	0.566 ± 0.032	0.870 ± 0.831	8.7%	4.6%

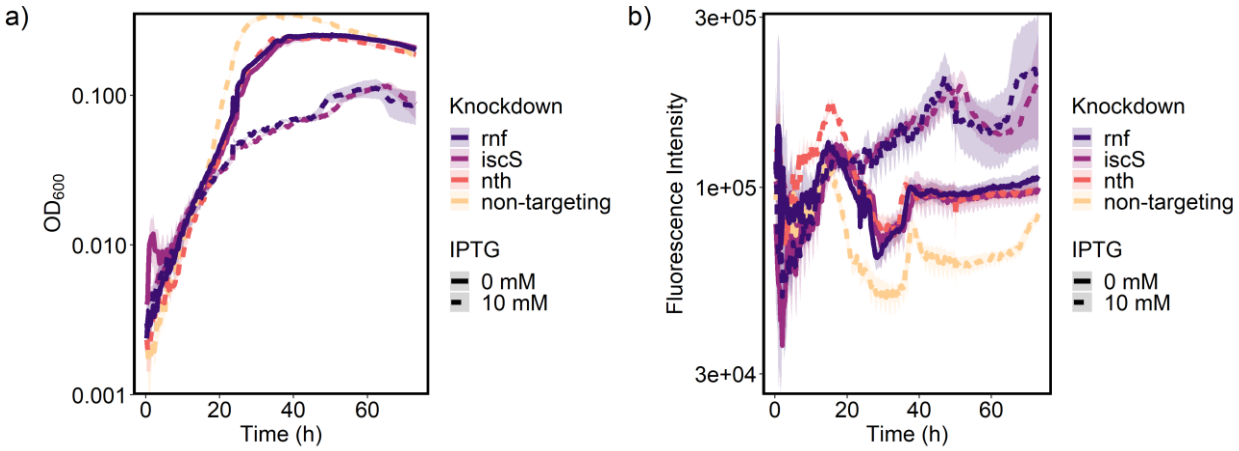

Figure 25. a) Growth curves and b) OD-corrected ThT fluorescence of uninduced and induced non-targeting, *rnf*, and *iscS* knockdown strains. Strains cultivated in 200 µl of minimal lactate medium with 10 µM ThT.

To determine the direction of Rnf activity under standard culturing conditions, we cultivated the uninduced and induced knockdown strains in minimal lactate medium with ThT, a cationic dye indicator which has been shown to have an inverse correlation to membrane potential in *S. oneidensis*.[36] Since Rnf either contributes to or depletes ion motive force depending on the reaction direction (**Figure 20**), membrane potential is an indicator of which reaction Rnf was catalyzing under the tested conditions. The induced *rnf* and *iscS* knockdown strains displayed greater ThT fluorescence intensity than the *rnf* and *iscS* uninduced controls and the induced non-targeting control (**Figure 25**). These results indicate that the knockdown strain has less depletion of ion motive force, suggesting that Rnf uses ion motive force to power ferredoxin reduction under these conditions. The similar effect observed in the *iscS* knockdown suggests that Rnf and IscS are associated with the same pathway because IscS on its own does not utilize ion motive force. Because Nth activity also does not interface with ion motive force, the fact similar ThT fluorescence between the induced *nth* knockdown and the uninduced *rnf* and *iscS* knockdowns suggest that Nth is not directly associated with Rnf.

Our results suggest that Rnf in *S. oneidensis* uses ion motive force to generate reduced ferredoxins. To confirm whether this was the case, metabolomic analysis was conducted on the induced and uninduced non-targeting, *rnf*, and *iscS* knockdown strains. The metabolomics approach for elucidating the role of Rnf was previously described for *Zymomonas mobilis* and was the basis for this experiment.[26] Pathways involving reduced ferredoxin as a cofactor, such as the methylerythritol phosphate (MEP) pathway, were expected to show accumulated metabolites if the Rnf knockdown was, in fact, producing reduced ferredoxins under the conditions tested. The induced and uninduced knockdown strains were inoculated to an initial OD_{600} of 0.035 in 50 ml of minimal lactate medium supplemented with kanamycin and grown to mid-exponential phase. A higher initial OD_{600} in this experiment than others was used to generate enough knockdown strain biomass for metabolites to be detected. The metabolites were extracted after 12 hours of growth and were analyzed by LC-MS (**Figure 26** and **27**). This analysis revealed that the most accumulated metabolite in both the induced *rnf* and *iscS* knockdown strains compared to the uninduced control was 2-*C*-methyl-D-erythritol-2,4-cyclophosphate (cMEPP). The induced *rnf* and *iscS* knockdowns displayed a 91.2-fold and 84.4-fold increase in cMEPP over the uninduced control, respectively. This metabolite is part of the MEP pathway and is the substrate for 4-hydroxy-3-methyl-butenyl-1-diphosphate synthase (IspG). Notably, IspG requires reduced ferredoxin as a cofactor in the reduction of cMEPP, as does IspH which catalyzes the next step in the pathway (**Figure 28**). In addition, four other MEP pathway metabolites before IspG were also accumulated. CDP-MEP accumulated 2.3-fold in the *rnf* knockdown and 1.9-fold in the *iscS* knockdown; CDP-ME accumulated 1.8-fold in the *rnf* knockdown and 1.4-fold in the *iscS* knockdown; and both IPP and DMAPP

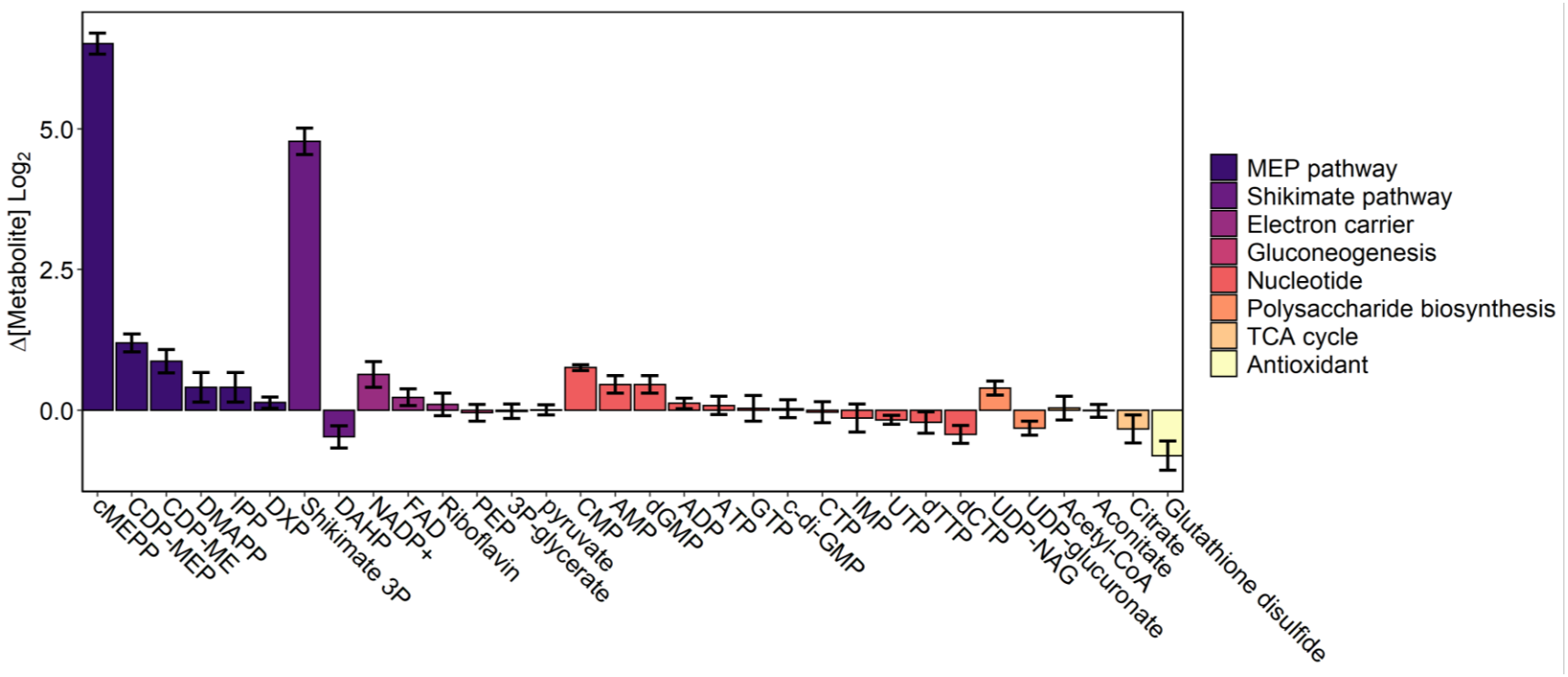

Figure 26. Change in metabolite concentrations on a $\log_2$ scale from induced *rnf* knockdown cultures. Values normalized to metabolite concentrations from the induced non-targeting control. More positive numbers indicate more of that metabolite in the *rnf* knockdown strain than in the induced non-targeting control.

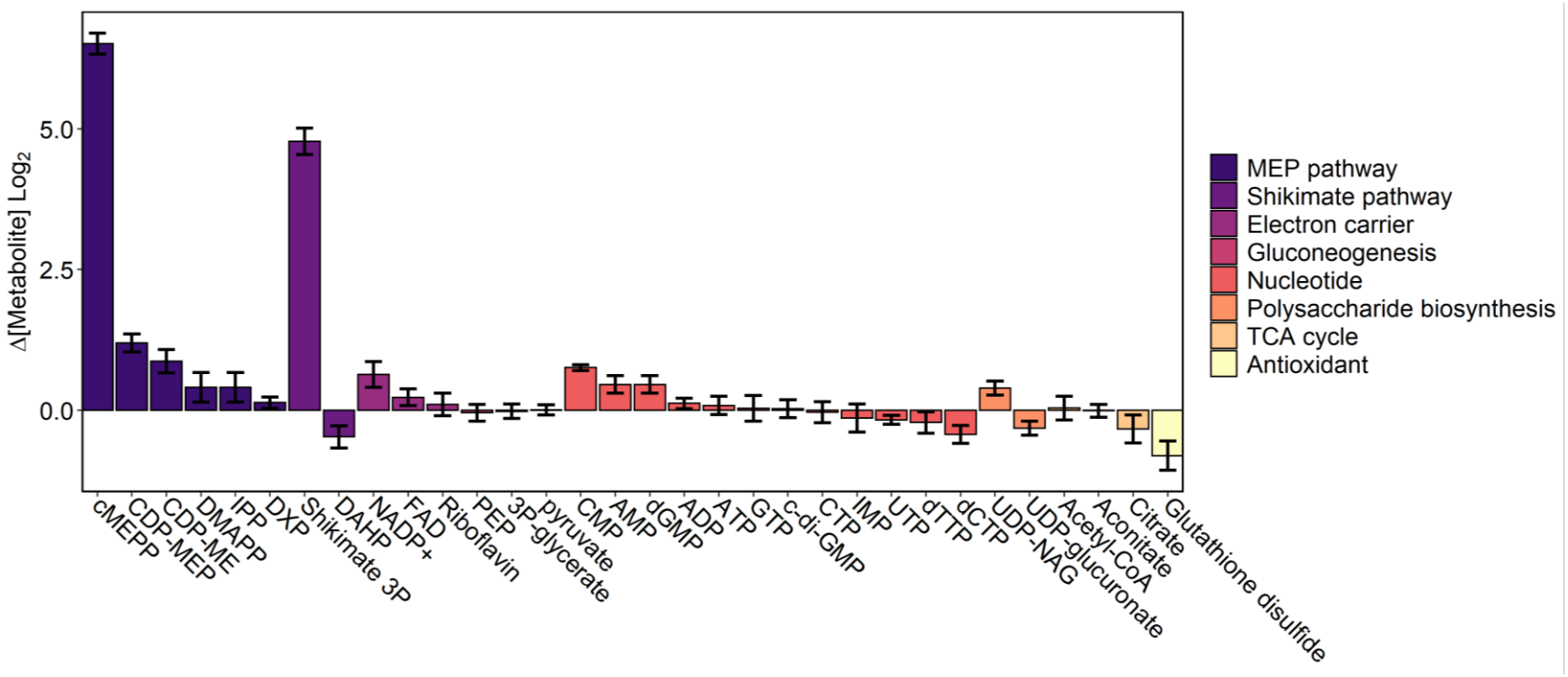

Figure 27. Change in metabolite concentrations on a log_2 scale from induced *iscS* knockdown cultures. Values normalized to metabolite concentrations from the induced non-targeting control. More positive numbers indicate more of that metabolite in the *iscS* knockdown strain than in the induced non-targeting control.

accumulated 1.3-fold in the *rnf* knockdown and 1.0-fold in the *iscS* knockdown. Accumulation of MEP pathway metabolites in both the *rnf* knockdown and the *iscS* knockdown strains strongly suggest that Rnf is producingreduced ferredoxins during *S. oneidensis* cultivation on minimal lactate media, and that those ferredoxins are utilized by IscS for ISC biosynthesis and repair.

Other notable changes in the metabolomic profiles include decreased levels of TCA cycle metabolites citrate and aconitate. Citrate levels decreased 0.8-fold (i.e. 20% decrease) in the *rnf* knockdown and 0.7-fold in the *iscS* knockdown. Aconitate levels decreased 0.9-fold in both the *rnf* and *iscS* knockdowns. The oxidized form of antioxidant glutathione (glutathione disulfide) was decreased 0.6-fold in both the *rnf* and the *iscS*

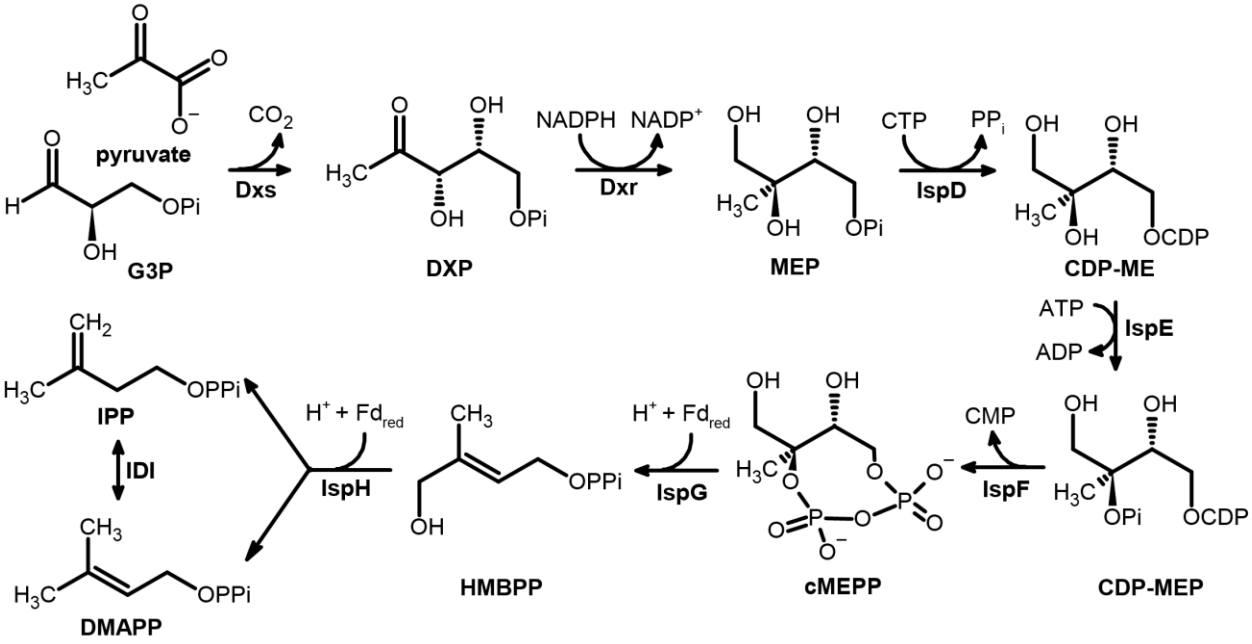

Figure 28. The MEP pathway for biosynthesis of isoprenoid precursors. Isoprenoid precursors isopentyl diphosphate (IPP) and dimethylallyl diphosphate (DMAPP) are synthesized from pyruvate and glycerol-3-phosphate (G3P). Abbreviations: DXP, 1-deoxy-D-xylylose-5-phosphate; MEP, 2-*C*-methyl-D-erythritol-4-phosphate; CDP-ME, methylerythritol cytidyl diphosphate; CDP-MEP, 4-diphosphocytidyl-2-*C*-methyl-D-erythritol-2-phosphate; cMEPP, 2-*C*-methyl-D-erythritol-2,4-cyclodiphosphate; HMBPP, 4-hydroxy-3-methyl-butenyl-1-diphosphate; CTP, cytidine triphosphate; CDP, cytidine 5'-diphosphate; CMP, cytidine monophosphate; PPi, diphosphate; Fd_{red}, reduced ferredoxin.

knockdown strains. Finally, shikimate pathway metabolites shikimate 3-phosphate was increased 27.4-fold and 28.5-fold in the *rnf* knockdown and the *iscS* knockdown strain, respectively; and 3-deoxy-D-arabinoheptulosonate 7-phosphate (DAHP) was decreased 0.7-fold in both strains.

DISCUSSION

In this work, we explored the function of Rnf in *S. oneidensis*, an organism without pathways Rnf has been proposed to be part of (e.g., nitrogen fixation, SoxR reduction), to elucidate the additional functions of this complex. In *S. oneidensis* grown on minimal lactate medium, Rnf uses ion motive force to drive ferredoxin reduction from NADH. We found that the *rnf* knockdown phenotype resembled the *iscS* knockdown phenotype, and that their metabolomic profiles were similar.

Based on these data, we propose a comprehensive model for Rnf that can account for the diverse and seemingly unrelated functions proposed across different species. In our model, Rnf serves as a crucial source of reduced ferredoxins using ion motive force and NADH. The link between Rnf activity and pathways such as nitrogen fixation, SoxR reduction, and isoprenoid precursor biosynthesis is two-pronged. First, as a low potential electron carrier, ferredoxin serves as a necessary cofactor for many cellular reactions, including nitrogen fixation, SoxR reduction, H_2 evolution, Fpr activity, ISC formation and repair, and isoprenoid precursor biosynthesis.[37–43] This positions Rnf as a vital source of reduced ferredoxins for essential cellular processes (**Figure 29**). Secondly, since reduced ferredoxins are also an important cofactor in ISC biosynthesis and repair,[33,38] the influence of Rnf activity reaches even further than the first tier of directly supplying an essential cofactor. Since many important reactions are catalyzed by ISC proteins which rely on the

Isc system for creation of their ISCs, the availability of reduced ferredoxins for cysteine desulfurase activity becomes essential for the activation and maintenance of ISC proteins (**Figure 29**). This includes many of the enzymes which use reduced ferredoxin as a co-factor in the first tier (e.g. Nif, SoxR, IspG). However, it also connects pathways with ISC enzymes which do not use reduced ferredoxin as a cofactor to Rnf, such as DNA repair, the TCA cycle, the pentose phosphate pathway, nitrate respiration, and NADH dehydrogenase.[44–48] In addition to its role in ISC assembly, IscS has also been shown to directly repair oxidized ISCs in ISC proteins, such as Nth, using reduced ferredoxin as an electron donor.[33,35,38] Notably, the accumulation of MEP pathway metabolites was also observed via metabolomic analysis of a *Z. mobilis rnfE* knockdown strain, suggesting that extending this model to include other species is rational.[26]

Interestingly, Rnf is not an essential protein in *E. coli*, as determined by the ability to insert transposons into *rnf* genes and generate *rnf* knockouts in this organism.[4,49,50] This difference in essentiality of Rnf between *E. coli* and *S. oneidensis* may be due to the presence of another ISC assembly system in *E. coli* – the sulfur mobilization (SUF) system. While the Isc proteins are primarily responsible for ISC biosynthesis, the SUF system also participates in this activity, especially under conditions of iron limitation or oxidative stress.[51] One important difference between the SUF and Isc systems is the electron donor for iron reduction. The Isc system requires reduced ferredoxin while the SUF system uses $FADH_2$.[33,34,52,53] Therefore, the non-essentiality of Rnf in *E. coli* could be due to a ferredoxin-independent ISC biosynthesis alternative which is not present in *S. oneidensis*.

This is corroborated by the observation that deletion of only the Isc system or only

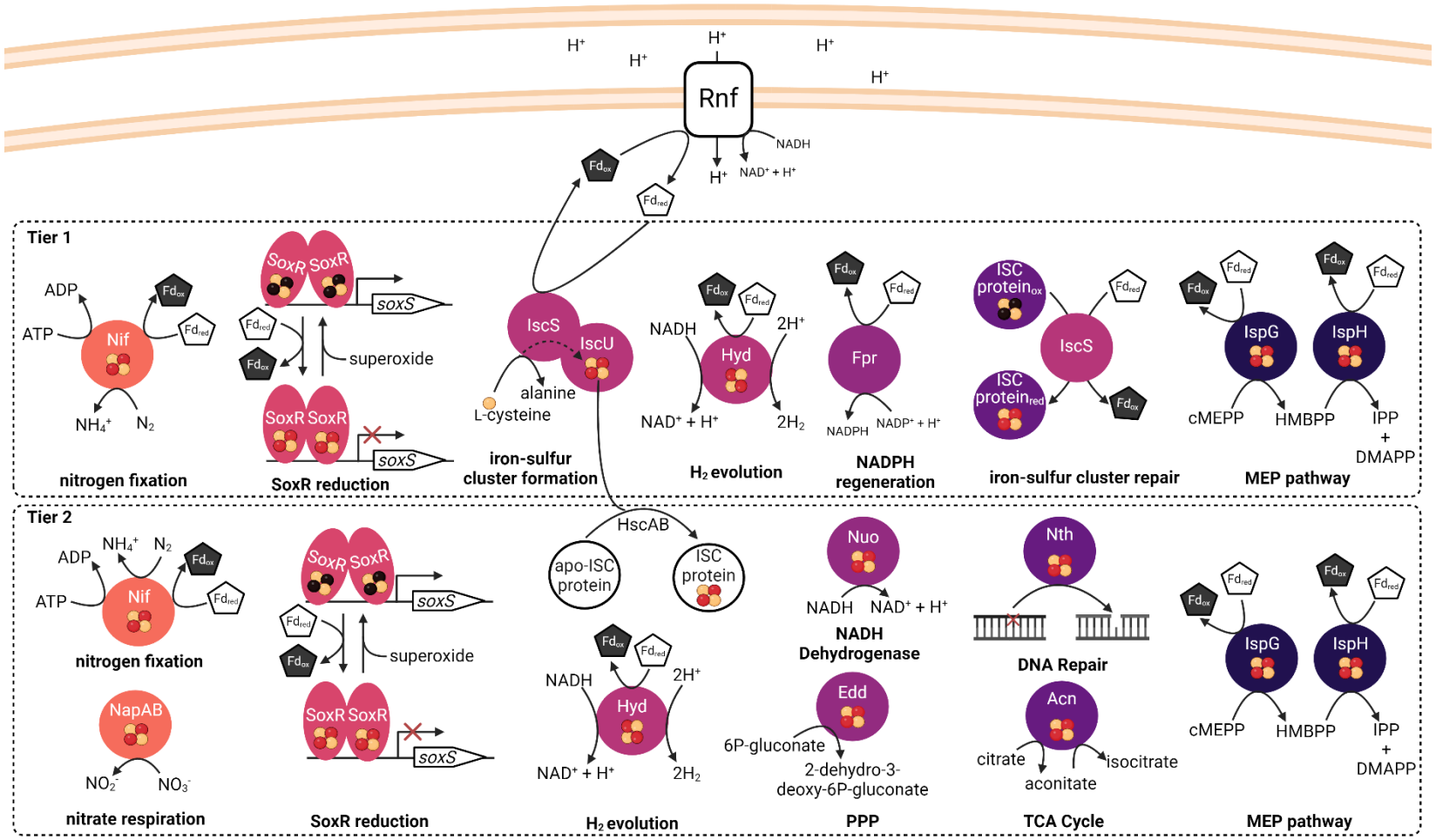

Figure 29. Proposed comprehensive model for Rnf function. Rnf generates reduced ferredoxins from NADH powered by ion motive force. Tier 1: reduced ferredoxins are used as essential cofactors in many cellular processes, including those previously though to include Rnf in their associated pathways (e.g. nitrogen fixation, SoxR reduction). Tier 2: reduced ferredoxins are essential for assembly of iron sulfur cluster (ISC)-containing proteins. Enzymatic reactions catalyzed by ISC proteins require ferredoxin for preparation of their iron-sulfur clusters, even if the proteins themselves do not use reduced ferredoxin as a cofactor. Iron-sulfur clusters are represented by two iron (red sphere) and two sulfur (yellow sphere) atoms.

the SUF system in *E. coli* allows ISC formation and viable cells.[54,55] However, deletion of both the Isc and SUF systems results in a strain which is incapable of ISC biosynthesis.[56] Interestingly, IspG and IspH of the MEP pathway appear to be the main restrictor of growth without ISCs.[57,58] Expression of an alternative ISC-free isoprenoid precursor biosynthesis pathway restores growth of *E. coli* without the Isc and SUF systems.[57] The absence of a SUF system in *S. oneidensis* further points to the relationship between Rnf and ISC biosynthesis and repair.

Application of this model to observations collected in previous Rnf studies can connect seemingly unrelated functions through shared requirements for reduced ferredoxin or ISC proteins. For example, *E. coli* Rnf was previously shown to be involved in the reduction of the SoxR ISC cluster.[4] The link between SoxR and Rnf was most heavily influenced by RnfC, which oxidizes NADH and stabilizes the ferredoxin-reducing domain RnfB. Yet, another study proposed that Fpr, a NADPH: ferredoxin oxidoreductase, was responsible for the reduction of SoxR.[42] The overlapping activities of Rnf and Fpr in ferredoxin reduction allows ferredoxin to be connected to both the NADH pool via Rnf and the NADPH pool via Fpr. Our model suggests that the link between Rnf and SoxR is that ferredoxin is required for SoxR reduction. A still-unidentified mediator for SoxR reduction using reduced ferredoxin is likely required, as reduced ferredoxin alone was shown to be insufficient for reducing SoxR.[59]

While Rnf and Fpr do have some overlapping functions, their activities cannot always complement one another. It was demonstrated that Fpr has no influence over re-activation of oxidized aconitase, 6-phosphogluconate dehydratase, or dihydroxy acid dehydratase.[60] This lack of complementation could be observed in the metabolomic

analysis of our knockdown strains, where citrate and aconitate were decreased by 0.8-fold and 1.0-fold, respectively in the induced *rnf* knockdown strain and by 0.7-fold and 0.9-fold, respectively in the *iscS* knockdown strain (**Figure 26** and **27**). Citrate and aconitate are substrates for aconitase, the second step in the TCA cycle. Aconitase is an ISC protein, which is likely impacted by decreased Rnf and IscS activity. A decrease in these metabolites rather than an accumulation such as the observed backup in the MEP pathway may be due to the greater complexity in regulation of the TCA cycle.

NADPH was not detected in any sample, suggesting that it was oxidized during the extraction process. Therefore, the higher levels of $NADP^+$ may suggest an overall increase in the NADP(H) pool size in the induced knockdown strains. The inhibition of Rnf activity in combination with the downstream inhibition of other ISC proteins or ferredoxin-dependent proteins which use NAD(P)H as a cofactor may lead to an decrease in the NAD(P)H:$NAD(P)^+$ ratio. The increase in NADP(H) pool size could be an attempt to balance the decreasing NAD(P)H:$NAD(P)^+$ ratio resulting from decreased Rnf and IscS activities. Additionally, the NAD^+ and $NADP^+$ pools are connected by NAD^+ kinase, which may explain the observation of greater NADP(H) pool size even though NAD(H) was not detected. The lower NADPH/$NADP^+$ ratio suggests a more oxidized cellular environment. A shift in the cellular redox balance can alter metabolic pathways and signaling, which can have serious impacts on cellular health.[61] Rnf appears to be integral to maintaining redox homeostasis by providing necessary low potential electron carriers. As such, the severe growth impact of the induced *rnf* knockdown is the culmination of the disruption of redox balance and essential metabolic pathways.

Further evidence for a disruption to the cellular redox balance was observed with

the decreased levels of glutathione disulfide in both the *rnf* and *iscS* knockdown strains. Glutathione disulfide is the oxidized form of antioxidant glutathione, which is an important contributor to maintaining cellular redox balance.[62,63] Glutathione reacts with free radicals to form a glutathione radical, which can react with a second glutathione radical to produce glutathione disulfide.[63] Altered glutathione disulfide levels indicate a shift in the cellular redox balance, which may have additional impacts on disulfide bonds.[64]

The second-most accumulated metabolite in both the induced *rnf* and *iscS* knockdown strains was shikimate 3-phosphate. This metabolite is part of the shikimate pathway for aromatic amino acid precursor biosynthesis.[65] This pathway is not comprised of ISC enzymes nor enzymes using ferredoxin as a cofactor. While the mechanism for a backup in the shikimate pathway as a result of decreased Rnf or IscS activity is not immediately clear, the observation highlights the reach of Rnf activity. Likely, regulatory changes occur due to decreased ferredoxin availability and/or decreased ISC biosynthesis and repair which interfere with essential pathways such as aromatic amino acid biosynthesis.

This novel, comprehensive model for Rnf function connects previous explanations of its activity to the broad impact that Rnf has across many cellular functions. Reduced ferredoxins generated by Rnf go on to power essential pathways like isoprenoid precursor biosynthesis and ISC assembly and repair. Disruption of ISC assembly exponentially interferes with other essential processes requiring ISC proteins like those involved in DNA repair, the TCA cycle, and the pentose phosphate pathway. The broad impacts of Rnf activity are central to its classification as an essential protein and explain its effect on reactions such as nitrogen fixation and SoxR reduction.

REFERENCES

1. Schmehl, M. *et al.* Identification of a new class of nitrogen fixation genes in *Rhodobacter capsalatus*: a putative membrane complex involved in electron transport to nitrogenase. *Mol Gen Genet* **241–241**, 602–615 (1993).

2. Jouanneau, Y., Jeong, H., Hugo, N., Meyer, C. & Willison, J. C. Overexpression in *Escherichia coli* of the *rnf* genes from *Rhodobacter capsulatus*. *Eur J Biochem* **251**, 54–64 (1998).

3. Biegel, E., Schmidt, S., González, J. M. & Müller, V. Biochemistry, evolution and physiological function of the Rnf complex, a novel ion-motive electron transport complex in prokaryotes. *CMLS* **68**, 613–634 (2011).

4. Koo, M. S. *et al.* A reducing system of the superoxide sensor SoxR in *Escherichia coli*. *EMBO J* **22**, 2614–2622 (2003).

5. Müller, V., Imkamp, F., Biegel, E., Schmidt, S. & Dilling, S. Discovery of a Ferredoxin:NAD $^{+}$ -Oxidoreductase (Rnf) in *Acetobacterium woodii*. *Ann N Y Acad Sci* **1125**, 137–146 (2008).

6. Kuhns, M., Trifunović, D., Huber, H. & Müller, V. The Rnf complex is a Na^{+} coupled respiratory enzyme in a fermenting bacterium, *Thermotoga maritima*. *Commun Biol* **3**, 431 (2020).

7. Westphal, L., Wiechmann, A., Baker, J., Minton, N. P. & Müller, V. The Rnf Complex Is an Energy-Coupled Transhydrogenase Essential To Reversibly Link Cellular NADH and Ferredoxin Pools in the Acetogen *Acetobacterium woodii*. *J Bacteriol* **200**, (2018).

8. Hayashi, K. *et al.* Highly accurate genome sequences of *Escherichia coli* K-12 strains MG1655 and W3110. *Mol Syst Biol* **2**, (2006).

9. Heidelberg, J. F. *et al.* Genome sequence of the dissimilatory metal ion–reducing bacterium *Shewanella oneidensis*. *Nat Biotechnol* **20**, 1118–1123 (2002).

10. Berges, M. *et al.* Iron Regulation in *Clostridioides difficile*. *Front Microbiol* **9**, (2018).

11. Hernandez, M. E. & Newman, D. K. Extracellular electron transfer. *CMLS* **58**, 1562–1571 (2001).

12. Beblawy, S. *et al.* Extracellular reduction of solid electron acceptors by *Shewanella oneidensis*. *Mol Microbiol* **109**, 571–583 (2018).

13. Shi, L., Squier, T. C., Zachara, J. M. & Fredrickson, J. K. Respiration of metal (hydr)oxides by *Shewanella* and *Geobacter*: a key role for multihaem *c* -type cytochromes. *Mol Microbiol* **65**, 12–20 (2007).

14. Gralnick, J. A., Vali, H., Lies, D. P. & Newman, D. K. Extracellular respiration of dimethyl sulfoxide by *Shewanella oneidensis* strain MR-1. *PNAS* **103**, 4669–4674 (2006).

15. Carpentier, W., De Smet, L., Van Beeumen, J. & Brigé, A. Respiration and Growth of *Shewanella oneidensis* MR-1 Using Vanadate as the Sole Electron Acceptor. *J Bacteriol* **187**, 3293–3301 (2005).

16. Chen, Y. & Wang, F. Insights on nitrate respiration by *Shewanella*. *Front Mar Sci* **1**, (2015).

17. Shi, L. *et al.* Molecular Underpinnings of Fe(III) Oxide Reduction by *Shewanella oneidensis* MR-1. *Front Microbiol* **3**, (2012).

18. Madsen, C. S. & TerAvest, M. A. NADH dehydrogenases Nuo and Nqr1 contribute to extracellular electron transfer by *Shewanella oneidensis* MR-1 in bioelectrochemical systems. *Sci Rep* **9**, 14959 (2019).

19. Marritt, S. J. *et al.* The roles of CymA in support of the respiratory flexibility of *Shewanella oneidensis* MR-1. *Biochem Soc Trans* **40**, 1217–1221 (2012).

20. Coursolle, D. & Gralnick, J. A. Modularity of the Mtr respiratory pathway of *Shewanella oneidensis* strain MR-1. *Mol Microbiol* **77**, 995–1008 (2010).

21. Tiedje, J. M. Shewanella—the environmentally versatile genome. *Nat Biotechnol* **20**, 1093–1094 (2002).

22. Zhu, D. D., Liu, J. L. & Qiao, S. Z. Recent Advances in Inorganic Heterogeneous Electrocatalysts for Reduction of Carbon Dioxide. *Adv Mater* **28**, 3423–3452 (2016).

23. Tefft, N. M. & Teravest, M. A. Reversing an Extracellular Electron Transfer Pathway for Electrode-Driven Acetoin Reduction. *ACS Synth Biol* **8**, 1590–1600 (2019).

24. Ford, K. C., Kaste, J. A. M., Shachar-Hill, Y. & Teravest, M. A. Flux-Balance Analysis and Mobile CRISPRi-Guided Deletion of a Conditionally Essential Gene in *Shewanella oneidensis* MR-1. *ACS Synth Biol* **11**, 3405–3413 (2022).

25. Peters, J. M. *et al.* Enabling genetic analysis of diverse bacteria with Mobile-CRISPRi. *Nat Microbiol 2019 4:2* **4**, 244–250 (2019).

26. Enright, A. L. *et al.* The genetics of aerotolerant growth in an alphaproteobacterium with a naturally reduced genome. *mBio* **14**, (2023).

27. R Core Team. R: A language and environment for statistical computing. *R Foundation for Statistical Computing* Preprint at https://www.R-project.org/ (2021).

28. H. Wickham. ggplot2: Elegant Graphics for Data Analysis. Preprint at (2016).

29. Hadley Wickham, Romain François, Lionel Henry & Kirill Müller. dplyr: A Grammar of Data Manipulation. *R package version 1.0.9* Preprint at https://CRAN.R-project.org/package=dplyr (2022).

30. Garnier, S. *et al.* viridis(Lite) - Colorblind-Friendly Color Maps for R. (2023).

31. Ulrich, J. TTR: Technical Trading Rules. (2021).

32. Auguie, B. gridExtra: Miscellaneous Functions for “Grid” Graphics. Preprint at (2017).

33. Kim, J. H., Frederick, R. O., Reinen, N. M., Troupis, A. T. & Markley, J. L. [2Fe-2S]-Ferredoxin Binds Directly to Cysteine Desulfurase and Supplies an Electron for Iron–Sulfur Cluster Assembly but Is Displaced by the Scaffold Protein or Bacterial Frataxin. *J Am Chem Soc* **135**, 8117–8120 (2013).

34. Takahashi, Y. & Nakamura, M. Functional Assignment of the ORF2-iscS-iscU-iscA-hscB-hscA-fdx-0RF3 Gene Cluster Involved in the Assembly of Fe-S Clusters in *Escherichia coli*. *J Biochem* **126**, 917–926 (1999).

35. Rogers, P. A., Eide, L., Klungland, A. & Ding, H. Reversible inactivation of *E. coli* endonuclease III via modification of its [4Fe-4S] cluster by nitric oxide. *DNA Repair (Amst)* **2**, 809–817 (2003).

36. Pirbadian, S., Chavez, M. S. & El-Naggar, M. Y. Spatiotemporal mapping of bacterial membrane potential responses to extracellular electron transfer. *PNAS* **117**, 20171–20179 (2020).

37. Addison, H., Glatter, T., K. A. Hochberg, G. & Rebelein, J. G. Two distinct ferredoxins are essential for nitrogen fixation by the iron nitrogenase in *Rhodobacter capsulatus*. *mBio* (2024) doi:10.1128/mbio.03314-23.

38. Yan, R. *et al.* Ferredoxin Competes with Bacterial Frataxin in Binding to the Desulfurase IscS*. *J Biol Chem* **288**, 24777–24787 (2013).

39. Srour, B., Gervason, S., Monfort, B. & D’Autréaux, B. Mechanism of Iron–Sulfur Cluster Assembly: In the Intimacy of Iron and Sulfur Encounter. *Inorganics (Basel)* **8**, 55 (2020).

40. Zhou, J., Yang, L., Wang, C., Choi, E.-S. & Kim, S.-W. Enhanced performance of the methylerythritol phosphate pathway by manipulation of redox reactions relevant to IspC, IspG, and IspH. *J Biotechnol* **248**, 1–8 (2017).

41. Buckel, W. & Thauer, R. K. Flavin-Based Electron Bifurcation, Ferredoxin, Flavodoxin, and Anaerobic Respiration With Protons (Ech) or NAD+ (Rnf) as Electron Acceptors: A Historical Review. *Front Microbiol* **9**, (2018).

42. Liochev, S. I., Hausladen, A., Beyer, W. F. & Fridovich, I. NADPH: ferredoxin oxidoreductase acts as a paraquatdiaphorase and is a member of the soxRS regulon. *PNAS* **91**, 1328–1331 (1994).

43. Carrillo, N. & Ceccarelli, E. A. Open questions in ferredoxin-NADP $^{+}$ reductase catalytic mechanism. *Eur J Biochem* **270**, 1900–1915 (2003).

44. Simpson, P. J. L., Richardson, D. J. & Codd, R. The periplasmic nitrate reductase in *Shewanella*: the resolution, distribution and functional implications of two NAP isoforms, NapEDABC and NapDAGHB. *Microbiology (N Y)* **156**, 302–312 (2010).

45. Sled', V. D. *et al.* Bacterial NADH-quinone oxidoreductases: Iron-sulfur clusters and related problems. *J Bioenerg Biomembr* **25**, 347–356 (1993).

46. Gardner, P. R. & Fridovich, I. Superoxide sensitivity of the *Escherichia coli* 6-phosphogluconate dehydratase. *J Biol Chem* **266**, 1478–1483 (1991).

47. Kennedy, M. C. & Stout, C. D. Aconitase: An Iron—Sulfur Enzyme. *Prog Inorg Chem* **38**, 323–339 (1992).

48. Fu, W., O'Handley, S., Cunningham, R. P. & Johnson, M. K. The role of the iron-sulfur cluster in *Escherichia coli* endonuclease III. A resonance Raman study. *J Biol Chem* **267**, 16135–16137 (1992).

49. Baba, T. *et al.* Construction of *Escherichia coli* K-12 in-frame, single-gene knockout mutants: the Keio collection. *Mol Syst Biol* **2**, (2006).

50. Goodall, E. C. A. *et al.* The Essential Genome of *Escherichia coli* K-12. *mBio* **9**, (2018).

51. Pérard, J. & Ollagnier de Choudens, S. Iron–sulfur clusters biogenesis by the SUF machinery: close to the molecular mechanism understanding. *J Biol Inorg Chem* **23**, 581–596 (2018).

52. Wollers, S. *et al.* Iron-Sulfur (Fe-S) Cluster Assembly. *J Biol Chem* **285**, 23331–23341 (2010).

53. Saini, A., Mapolelo, D. T., Chahal, H. K., Johnson, M. K. & Outten, F. W. SufD and SufC ATPase Activity Are Required for Iron Acquisition during in Vivo Fe-S Cluster Formation on SufB. *Biochemistry* **49**, 9402–9412 (2010).

54. Tokumoto, U. & Takahashi, Y. Genetic Analysis of the isc Operon *in Escherichia coli* Involved in the Biogenesis of Cellular Iron-Sulfur Proteins. *J Biochem* **130**, 63–71 (2001).

55. Outten, F. W., Djaman, O. & Storz, G. A *suf* operon requirement for Fe–S cluster assembly during iron starvation in *Escherichia coli*. *Mol Microbiol* **52**, 861–872 (2004).

56. Tokumoto, U. Interchangeability and Distinct Properties of Bacterial Fe-S Cluster Assembly Systems: Functional Replacement of the isc and suf Operons in *Escherichia coli* with the nifSU-Like Operon from *Helicobacter pylori*. *J Biochem* **136**, 199–209 (2004).

57. Tanaka, N. *et al.* Novel features of the ISC machinery revealed by characterization of *Escherichia coli* mutants that survive without iron–sulfur clusters. *Mol Microbiol* **99**, 835–848 (2016).

58. Esquilin-Lebron, K., Dubrac, S., Barras, F. & Boyd, J. M. Bacterial Approaches for Assembling Iron-Sulfur Proteins. *mBio* **12**, (2021).

59. Gaudu, P. & Weiss, B. SoxR, a [2Fe-2S] transcription factor, is active only in its oxidized form. *PNAS* **93**, 10094–10098 (1996).

60. Krapp, A. R. *et al.* The Flavoenzyme Ferredoxin (Flavodoxin)-NADP(H) Reductase Modulates NADP(H) Homeostasis during the *soxRS* Response of *Escherichia coli*. *J Bacteriol* **184**, 1474–1480 (2002).

61. Sporer, A. J., Kahl, L. J., Price-Whelan, A. & Dietrich, L. E. P. Redox-Based Regulation of Bacterial Development and Behavior. *Annu Rev Biochem* **86**, 777–797 (2017).

62. Knoke, L. R. *et al.* The role of glutathione in periplasmic redox homeostasis and oxidative protein folding in *Escherichia coli*. *Redox Biol* **64**, 102800 (2023).

63. Smirnova, G. V. & Oktyabrsky, O. N. Glutathione in Bacteria. *Biochemistry (Moscow)* **70**, 1199–1211 (2005).

64. Vašková, J., Kočan, L., Vaško, L. & Perjési, P. Glutathione-Related Enzymes and Proteins: A Review. *Molecules* **28**, 1447 (2023).

65. Herrmann, K. M. & Weaver, L. M. The Shikimate Pathway. *Annu Rev Plant Physiol Plant Mol Biol* **50**, 473–503 (1999).

CHAPTER 4:

A COMMON INDUCER MOLECULE ENHANCES SUGAR UTILIZATION BY *SHEWANELLA ONEIDENSIS* MR-1

This chapter is adapted from a publication in The Journal of Industrial Microbiology & Biotechnology.[1]

PREFACE

As part of my investigation into the role of Rnf in *S. oneidensis*, I had attempted to find culturing conditions in which I could generate knockouts of the *rnf* operon and *iscS*. During this process I discovered that cultivating the *rnf* and *iscS* knockdown strains on sugar substrate N-acetylglucosamine improved their carrying capacity over cultivation on lactate. While at first this result was exciting (maybe I could use this condition for generating the difficult knockouts), it quickly became concerning when the non-targeting control also showed improved growth on the substrate. Was the dCas9 or the sgRNA somehow improving the fitness of cells growing on N-acetylglucosamine?

The CRISPRi components turned out to play no part in the phenotype, because we soon discovered that wild-type *S. oneidensis* also displayed enhanced growth on N-acetylglucosamine when cultivated with the same concentration of IPTG used for induction of the CRIPSRi system. This was an unexpected observation that we were interested in exploring further – leading to this study on the effect of IPTG on *S. oneidensis* growth on N-acetylglucosamine.

This work was published in August 2023 in *The Journal of Industrial Microbiology and Biotechnology* in the special issue on “Frontiers of Industrial Microbiology and Biotechnology”.[1]

ABSTRACT

Shewanella oneidensis MR-1 is an electroactive bacterium that is a promising host for bioelectrochemical technologies, which makes it a common target for genetic engineering, including gene deletions and expression of heterologous pathways. Expression of heterologous genes and gene knockdown via CRISPRi in *S. oneidensis* are

both frequently induced by isopropyl β-D-1-thiogalactopyranoside (IPTG), a commonly used inducer molecule across many model organisms. Here, we report and characterize an unexpected phenotype; IPTG enhances the growth of wild-type *S. oneidensis* MR-1 on the sugar substrate N-acetylglucosamine. IPTG improves the carrying capacity of *S. oneidensis* growing on N-acetylglucosamine while the growth rate remains similar to cultures without the inducer. Extracellular acetate accumulates faster and to a higher concentration in cultures without IPTG than those with it. IPTG appears to improve acetate metabolism which combats the negative effect that acetate accumulation has on the growth of *S. oneidensis* with N-acetylglucosamine. We recommend using extensive experimental controls and careful data interpretation when using both N-acetylglucosamine and IPTG in *S. oneidensis* cultures.

INTRODUCTION

Shewanella oneidensis MR-1 is a facultatively anaerobic bacterium with great potential as a host for bioelectrochemical technologies due to its well characterized extracellular electron transfer pathway and diverse genetic toolbox.[2,3] Some of these technologies include using *S. oneidensis* as a biosensor for arsenic or toxic water[4,5] and for electricity generation from waste.[6,7] However, *S. oneidensis* natively has limited options for carbon substrates and does not naturally accumulate high-value compounds.[8] These limitations make pathway engineering a crucial component of this organism's expanded utility in bioelectrochemical systems.

Sugar metabolism is particularly limited in *S. oneidensis*, with several essential genes for sugar utilization missing or nonfunctional. For sugar transport, the *S. oneidensis* MR-1 genome encodes one set of phosphotransferase system genes for an unknown

substrate, but phosphoenolpyruvate is not sufficiently produced to sustain the energy requirements for the system to function.[9,10] Additionally, the genome does not encode an annotated glucose permease, glucose kinase, or the important glycolysis enzyme 6-phosphofructokinase, which prevents *S. oneidensis* from utilizing most six carbon sugars.[10,11] N-acetylglucosamine (NAG) is a rare exception to this rule, as *S. oneidensis* MR-1 converts NAG to fructose 6-phosphate with a NAG permease, NAG kinase, NAG 6-phosphate deacetylase, and glucosamine 6-phosphate deaminase.[12] With a limited pool of compounds which can be utilized for carbon and energy, *S. oneidensis* and its engineered strains are typically grown using lactate, pyruvate, acetate, or NAG as substrates.

Another prominent feature of *S. oneidensis* metabolism is acetate accumulation. Under anoxic conditions, *S. oneidensis* MR-1 excretes high levels of acetate because of limited TCA cycle activity.[13] Under oxic conditions, acetate accumulation and subsequent uptake are also observed in *S. oneidensis* cultures growing on NAG or lactate.[14,15] Acetate is a common product of overflow metabolism, and *S. oneidensis* begins to use the excreted acetate as a secondary substrate via the glyoxylate shunt when the main substrate is depleted.[15] The accumulation of acetate is usually accompanied with a drop in medium pH which can affect the health of the cells.[16] In *S. oneidensis*, acetate is produced from acetyl-CoA and vice versa by the combined, reversible activities of acetate kinase and phosphate acetyltransferase; additionally, acetyl-CoA can be produced from acetate *via* acetyl-coenzyme A synthetase.[17]

To improve *S. oneidensis* as a host for use in bioelectrochemical systems, expansion of substrate utilization and product scope are critical. Gene expression under

the control of an inducible promoter is one of the most common methods for experimenting with both native and non-native pathways *in vivo*. One tool that uses IPTG-inducible expression for studying gene function and for pathway engineering in *S. oneidensis* is the Mobile CRISPRi knockdown system.[18] Promoters inducible by IPTG are utilized for both protein synthesis via common *S. oneidensis*-compatible vectors and CRISPRi knockdown systems. For example, Ford *et al*. deleted a gene previously thought to be essential in *S. oneidensis* (*gpmA*) by uncovering optimal knockout conditions using an IPTG-inducible CRISPRi system.[19] *S. oneidensis* has been engineered to utilize substrates such as xylose and glucose via IPTG-inducible systems.[20,21] Improved extracellular electron transfer in *S. oneidensis* has been achieved through various IPTG-inducible methods including using two types of transcriptional logic gates to fine-tune expression of extracellular electron transfer genes,[22] expression of NAD^+ biosynthesis genes for increased intracellular NAD(H) levels,[23] expression of a synthetic flavin pathway from *Bacillus subtilis* to increase secreted flavins,[24] and expression of diguanylate cyclase from *Escherichia coli* for enhanced *S. oneidensis* biofilm formation.[25] IPTG-inducible systems have also been used for production of 5-aminolevulinic acid[26] and *n*-butanol[27] in *S. oneidensis*, increasing the organism's potential product scope.

The use of IPTG for induction of heterologous genes is widespread due to the efficiency and simplicity of the system. The synthetic inducer is used to regulate the lac repressor (LacI) which regulates the *lac* operon in *E. coli*. Natively, the *lac* operon is expressed when lactose is present to produce lactose metabolic genes β-galactosidase, lactose permease, and a transacetylase.[28,29] Lactose is detected indirectly by its isomer allolactose which can bind to LacI.[28] LacI binds to the *lac* operator when allolactose

concentrations are low, which physically blocks transcription of the *lac* operon. Allolactose induces transcription of the *lac* operon by binding to LacI and releasing it from the DNA.[30] IPTG can be used as a replacement for allolactose since it isn't hydrolyzed by cells, making it a gratuitous inducer whose concentration does not change during the course of the experiment.[29] When used in the context of heterologous gene expression, IPTG induces expression of a synthetic operon which is regulated by LacI. IPTG is an indispensable tool for genetic engineering of many organisms, *S. oneidensis* included. In this work, we characterize the unexpected phenotype of wild-type *S. oneidensis* MR-1 in which growth on the sugar substrate NAG is enhanced by the presence of IPTG and advise circumspection when using NAG and IPTG together in evaluation of engineered *S. oneidensis* strains.

RESULTS

IPTG-enhanced growth of wild-type *S. oneidensis* was discovered during experimentation with CRISPRi knockdown strains. With this system, a small guide RNA is engineered to target a gene of interest. The small guide RNA forms a complex with a catalytically inactive Cas9 which binds to the target gene and blocks its transcription.[18] We observed that when grown on NAG, inducing the non-targeting control plasmid (pJMP2846) of the CRISPRi system with IPTG improved growth. To determine if this was due to the induction of the non-targeting control, we cultured wild-type *S. oneidensis* harboring pJMP2846 on 20 mM NAG with and without 10 mM IPTG and compared it to wild-type *S. oneidensis* without the plasmid under the same conditions (**Figure 30**). We found that the improvement to growth was not exclusive to the CRISPRi non-targeting strain and explored the phenotype further in wild-type *S. oneidensis* carrying no heterologous plasmid.

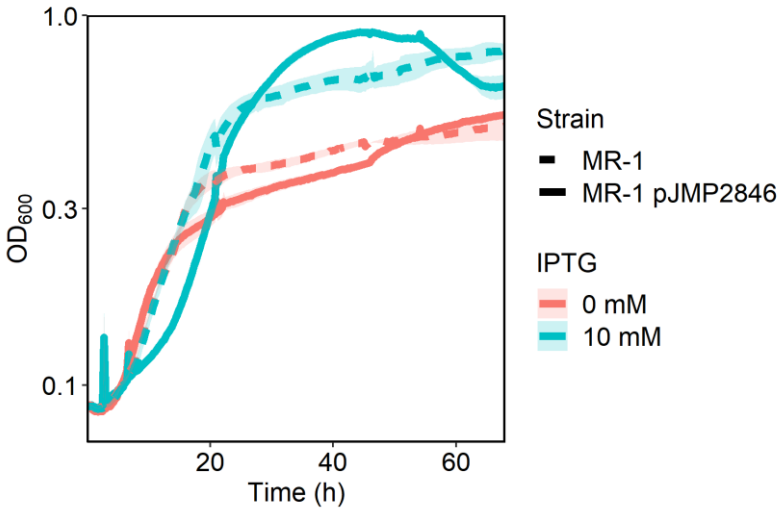

Figure 30. Growth of wild-type *S. oneidensis* and *S. oneidensis* CRISPRi non-targeting strain (MR-1 pJMP2846). Strains cultivated in 200 µl minimal medium with 20 mM NAG with or without 10 mM IPTG. Y-axis is on a logarithmic scale. Lines represent the average of three biological replicates and transparent ribbons represent standard error.

To determine if IPTG influenced *S. oneidensis* growth on various substrates, the wild-type strain was cultivated with 20 mM of NAG, lactate, or acetate with and without 10 mM IPTG in 96-well plates (**Figure 31a**). When *S. oneidensis* was grown on 20 mM NAG, the carrying capacity (final OD_{600}) nearly doubled from 0.372 ± 0.002 without IPTG to 0.648 ± 0.004 with IPTG while the growth rate remained similar at 0.181 ± 0.005 h^{-1} without IPTG and 0.168 ± 0.005 h^{-1} with IPTG (**Figure 31a**, **Table 12**). IPTG slightly decreased the carrying capacity during growth on lactate but did not significantly affect the growth rate of MR-1 on either lactate or acetate (**Table 12**).

To determine whether the carrying capacity increased because *S. oneidensis* can consume IPTG as a carbon substrate, the wild-type strain was cultivated with 10 mM IPTG as the only available carbon source. *S. oneidensis* was incapable of growth on IPTG alone. Additionally, *S. oneidensis* cultivated on 30 mM NAG did not share the same growth phenotype as when cultivated with 20 mM NAG and 10 mM IPTG (**Figure 31b**), indicating

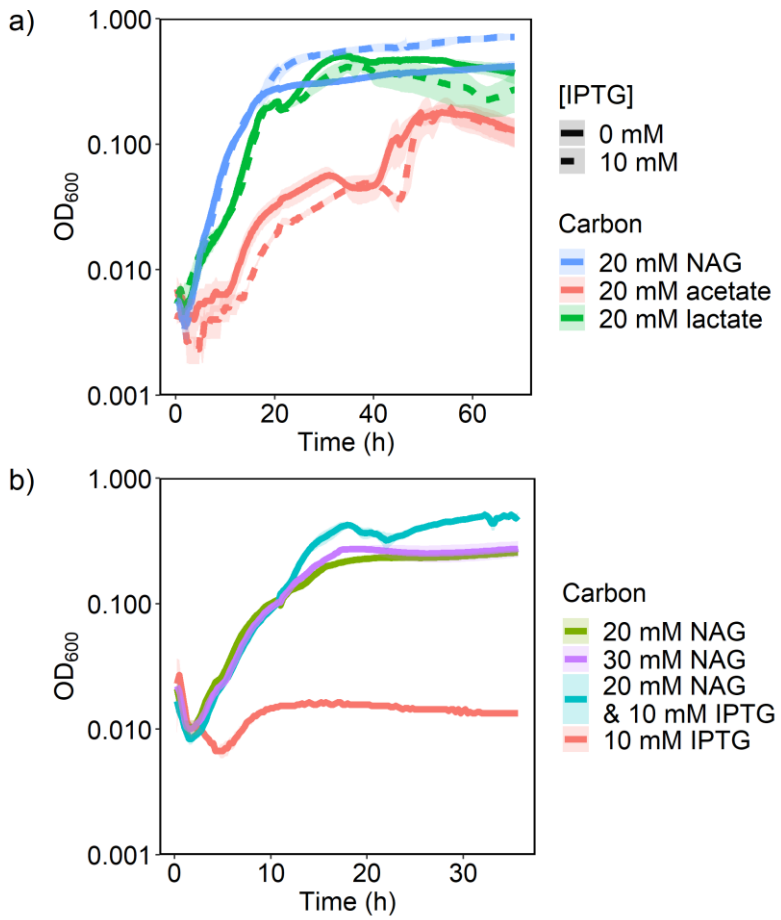

Figure 31. Growth of wild-type *S. oneidensis* in various conditions. (a) Growth of *S. oneidensis* MR-1 cultivated on 20 mM of different carbon substrates with or without 10 mM IPTG in 200 µl M5 minimal medium in 96-well plates. (b) *S. oneidensis* MR-1 cultivated on NAG and/or IPTG in 200 µl M5 minimal medium. Y-axis is on a logarithmic scale. Lines represent the average of three biological replicates and transparent ribbons represent standard error.

Table 12. Growth rate and carrying capacity of *S. oneidensis* strains depicted in Figure 31a.

Substrate	Growth Rate (h^{-1})		Carrying capacity (OD_{600})	
	- IPTG	+ IPTG	- IPTG	+ IPTG
NAG	0.181 ± 0.005	0.168 ± 0.005	0.372 ± 0.002	0.648 ± 0.004
Lactate	0.250 ± 0.01	0.266 ± 0.028	0.447 ± 0.003	0.322 ± 0.005
Acetate	0.120 ± 0.008	0.193 ± 0.017	0.175 ± 0.005	0.165 ± 0.004

that changes in osmotic pressure were not responsible for the increased carrying capacity. This observation also indicates that IPTG does not act as a secondary substrate, demonstrated by the lack of carrying capacity increase by 30 mM NAG as compared to the increase in carrying capacity of 20 mM NAG and 10 mM IPTG.

We next investigated whether IPTG influenced metabolic product formation in *S. oneidensis* grown on NAG. *S. oneidensis* was cultivated in 50 ml of minimal medium in 250-ml flasks with 20 mM NAG either with or without 10 mM IPTG (**Figure 32a**). We observed a similar increase in carrying capacity in the presence of IPTG, although the effect was diminished in flasks versus in 96-well plates. We confirmed by microscopy that cell size was the same in both conditions, indicating that the difference in OD_{600} reflects a difference in cell density (**Figure 33**). Samples from these cultures were analyzed via HPLC to detect changes in metabolic products. In cultures with IPTG, acetate accumulation was minimal and was quickly consumed (**Figure 32a**). NAG and IPTG co-eluted in our HPLC method and their peaks could not be resolved. However, no NAG/IPTG peak was detected after 18 hours in the no IPTG condition, and the peak area was equal to that of 10 mM IPTG in the IPTG-containing cultures after 16 hours. Further, we did not detect IPTG degradation as measured by galactose levels in the media. This indicates complete utilization of NAG both with and without IPTG. The pH trends of these cultures were consistent with the observed acetate concentrations, with the pH dropping when acetate concentrations were high (**Figure 32a**). We also investigated the effect of IPTG on cultures grown with 40 mM D,L-lactate and found that IPTG had no effect (**Figure 34**).

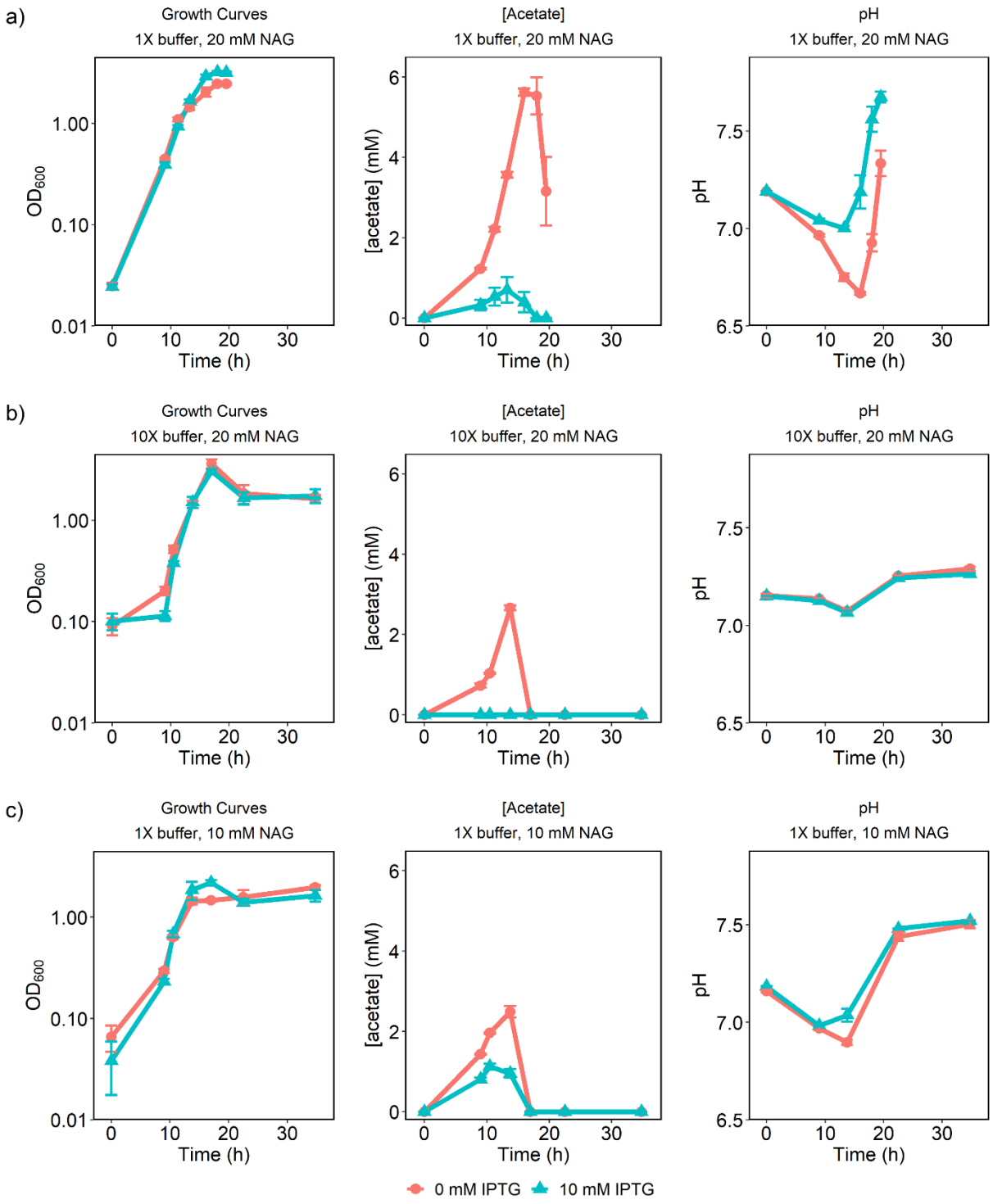

Figure 32. MR-1 cultures in 50 ml M5 minimal medium with and without 10 mM IPTG in varying conditions. a) 20 mM NAG growth curves, acetate concentrations, and pH. b) 20 mM NAG + 10X buffer growth curves, acetate concentrations, and pH. c) 10 mM NAG growth curves, acetate concentrations, and pH. Lines represent the average of three biological replicates and error bars represent standard error. Y-axis of growth curves are on a logarithmic scale.

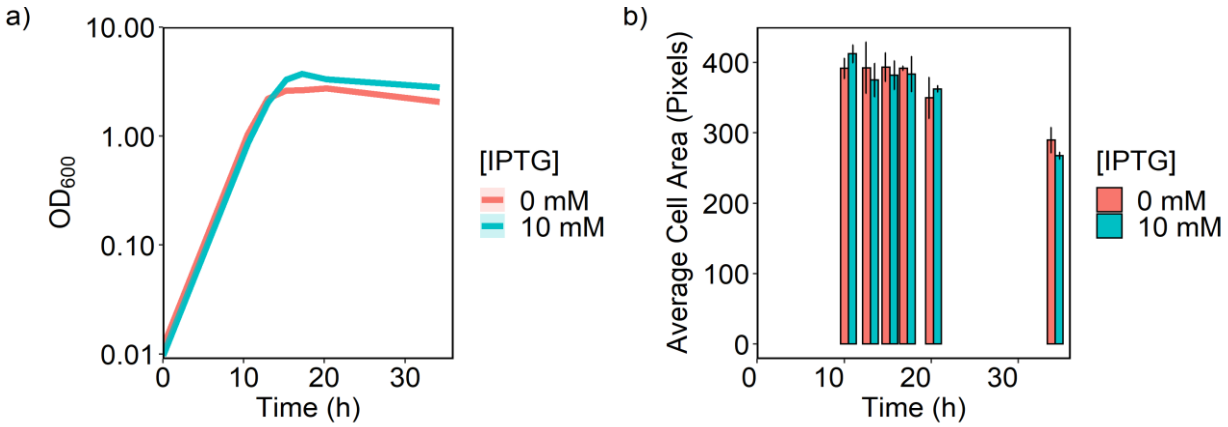

Figure 33. Comparison of *S. oneidensis* MR-1 cell size during NAG cultivation with or without IPTG. a) Growth curve of *S. oneidensis* MR-1 in 20 mM NAG with or without 10 mM IPTG in 50 ml cultures. b) Average cell area of *S. oneidensis* MR-1 at various times during the growth curve. +/- IPTG values at each timepoint are not significantly different (t-test, $p > 0.05$).

The acidification of the cultures and accumulation of acetate could be prevented when *S. oneidensis* was cultivated in the same conditions except with a 10X buffering capacity (**Figure 32b**) or with half the original concentration of NAG (**Figure 32c**). The difference in carrying capacity between +/- IPTG conditions was reduced with higher buffering capacity or lower starting NAG concentrations (**Table 13**), although acetate accumulation remained lower in the cultures with IPTG. This observation indicates that IPTG still significantly alters metabolism of *S. oneidensis* even when the growth appears unaffected. NAG was also completely utilized in cultures with either 10 mM NAG or with 10X buffering capacity, and no IPTG was detected. Taken together, the trends of growth, acetate accumulation, and culture pH suggest that acetate accumulation stalls growth of *S. oneidensis* and that IPTG counteracts the negative effects of acetate accumulation in the cultures.

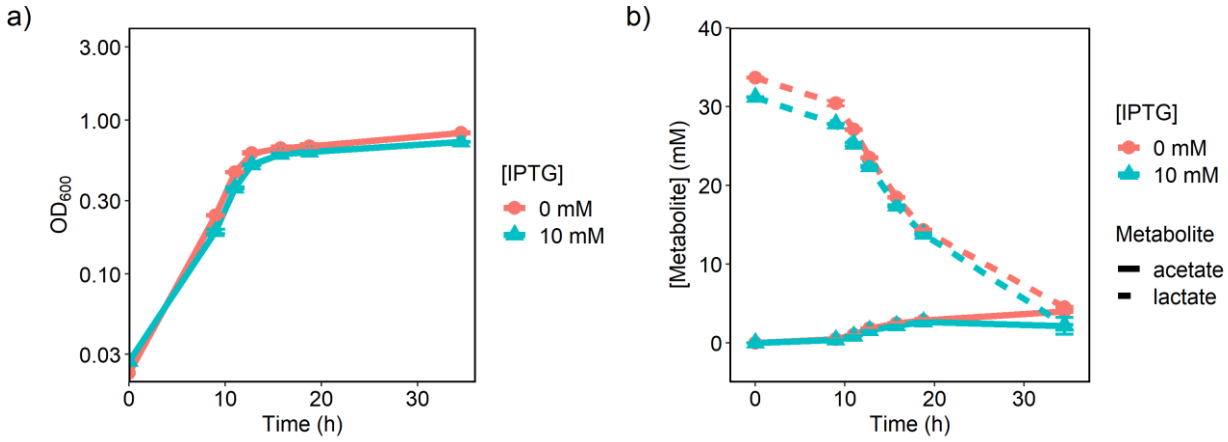

Figure 34. 50 ml a) growth curves and b) metabolite analysis of *S. oneidensis* MR-1 on 40 mM D,L-lactate with or without 10 mM IPTG.

Table 13. Growth rate and carrying capacity of *S. oneidensis* growth depicted in Figure 34. Strains cultivated in 50 mL M5 minimal medium. Values were calculated from the growth curves using the R package "growthCurver" using default values.

Conditions	Growth Rate (h^{-1})		Carrying Capacity (OD_{600})	
	-IPTG	+IPTG	-IPTG	+IPTG
20 mM NAG 1X buffering capacity **(Figure 34a)**	0.393 ± 0.062	0.560 ± 0.045	2.644 ± 0.162	3.345 ± 0.082
20 mM NAG 10X buffering capacity **(Figure 34b)**	0.956 ± 0.663	1.034 ± 0.553	2.257 ± 0.255	2.072 ± 0.183
20 mM NAG 1X buffering capacity **(Figure 34c)**	1.658 ± 0.085	1.759 ± 0.11	0.633 ± 0.163	1.326 ± 0.978

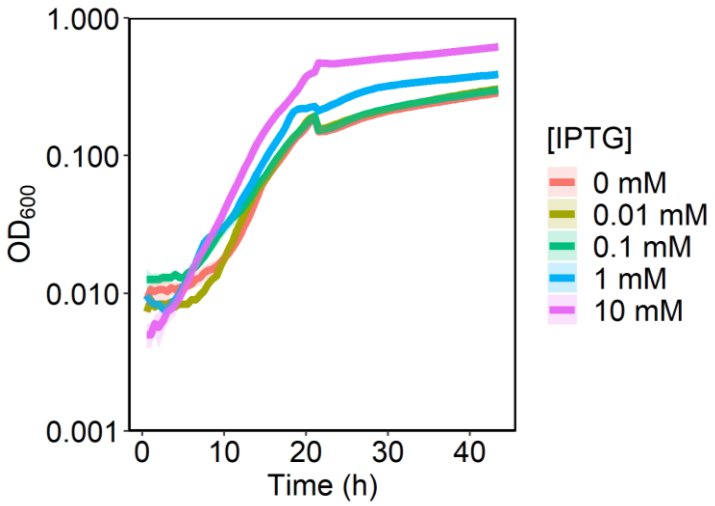

Figure 35. MR-1 growth curves in 200 µl M5 minimal medium with 20 mM NAG and varying IPTG concentrations. Y-axis is on a logarithmic scale. Lines represent the average of three biological replicates and transparent ribbons represent standard error.

IPTG at concentrations of 1.0 and 10 mM significantly increased the carrying capacity ($p \leq 0.05$) for cultures with 20 mM NAG in 200 µl cultures in a 96-well plate (**Figure 35**). However, IPTG concentrations of 1 mM or less did not enhance MR-1 growth on 20 mM NAG in 50-ml cultures (**Figure 36**).

Since IPTG is similar in structure to NAG (**Figure 37a**), we hypothesized that IPTG induced expression of NAG metabolic genes. The key genes involved in metabolism of NAG are controlled by the NagR repressor, which is released from the operator site in the presence of NAG.[31] Deletion of *nagR* in *S. oneidensis* results in a strain that is capable of growth on glucose due to the unregulated, constitutive expression of NAG permease and NAG kinase which can perform the functions of the missing glucose permease and kinase to some degree.[11] To determine whether IPTG induced the NagR regulon, we cultivated *S. oneidensis* in minimal medium with 20 mM D-glucose and varying concentrations of IPTG. Our results show that higher IPTG concentrations diminish the ability for *S. oneidensis* to grow on glucose, suggesting that IPTG did not induce the NagR regulon

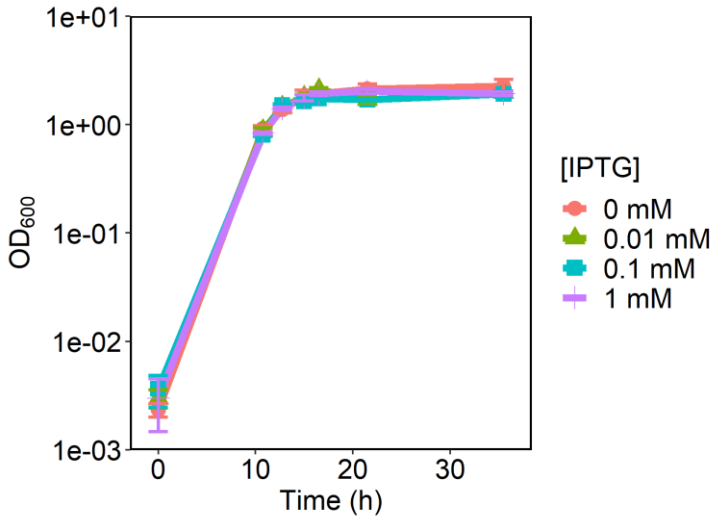

Figure 36. S. oneidensis growth curves in 50 ml M5 minimal medium with 20 mM NAG and varying IPTG concentrations. Y-axis is on a logarithmic scale. Lines represent the average of three biological replicates and error bars represent standard error.

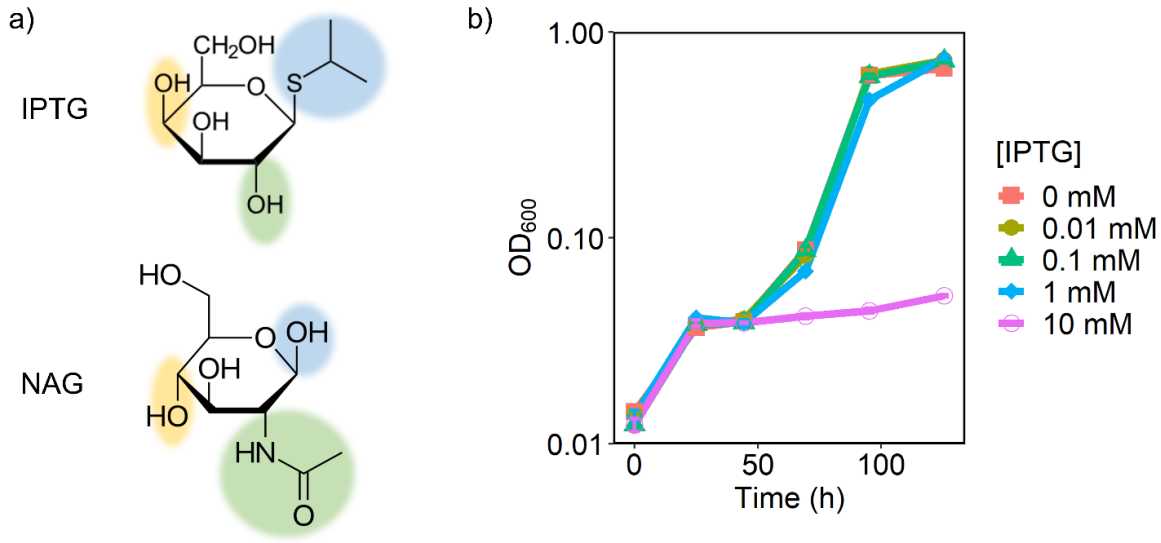

Figure 37. (a) The chemical structures of IPTG and NAG. Their structures differ in the highlighted regions. (b) Growth curves of *S. oneidensis* growth on 20 mM glucose with varying concentrations of IPTG. Y-axis is on a logarithmic scale. Lines represent the average of three biological replicates and error bars represent standard error.

(**Figure 37b**). *S. oneidensis* cannot natively grow on glucose; however, the ability to utilize glucose evolves quickly because only a single mutation is required for the phenotype to arise.[11] This accounts for the growth observed on glucose after prolonged culturing.

DISCUSSION

Our results indicate that IPTG reduced acetate accumulation by MR-1 during growth on NAG. Rapid accumulation of acetate in the absence of IPTG was accompanied by a drop in culture pH. Acetate accumulation in *E. coli* cultures inhibits growth by causing decreased expression of TCA cycle and glyoxylate shunt genes.[16] Acetate accumulation also appears to impact growth of *S. oneidensis* in our experiments, although it is not known whether acetate decreases expression of TCA cycle genes in this organism. Higher buffering capacity and lower NAG concentrations both reduced acetate accumulation to a rate that did not inhibit growth. With more buffering capacity, the pH presumably did not inhibit the expression of TCA cycle or glyoxylate shunt genes to the same extent as in cultures with the standard buffering capacity, thus allowing acetate to be more quickly metabolized. Lower NAG concentrations similarly prevent such a notable drop in pH; however, in this case it is due to less accumulation of acetate. The presence of IPTG in both cases displayed a compounding effect in which the acetate accumulation was even lower. These data point to a role of IPTG in improving acetate metabolism in *S. oneidensis* MR-1, perhaps through the induction of TCA cycle and/or glyoxylate shunt genes. Although we initially hypothesized that IPTG may interact with the native NagR regulator, another possibility is that it induces the HexR regulon, which includes genes of the glyoxylate shunt. Since the glyoxylate shunt is responsible for assimilating acetate as a carbon and energy source, its upregulation could increase the rate of acetate

assimilation.[15] Although outside the scope of this study, future work could explore the influence of IPTG on the HexR regulon and interaction with the HexR protein.

High-throughput experimentation with induction of heterologous genes in a 96-well plate is a common practice. Using this culturing method, we found that as little as 1 mM IPTG can cause a significant effect on growth. Higher IPTG concentrations of 10 mM were required for the effect to be seen in 250-ml shake flasks. While this is a high concentration of the inducer, it remains within the standard working range. The difference in required IPTG to observe the enhanced growth between these two culturing methods may be caused by oxygen availability. Larger cultures with more shaking are more efficiently aerated,[32] and in *S. oneidensis* a higher availability of oxygen leads to a decrease in acetate production and higher carbon flux toward the TCA cycle.[33] The differences in *S. oneidensis* metabolism caused by oxygen levels suggest that in the smaller cultures, acetate accumulates to an even greater level than we report from the shake flasks, potentially explaining the greater impact that IPTG has on growth in these conditions.

Unexpectedly, we found that at the 200 µl scale, *S. oneidensis* grown on 20 mM NAG and or on 20 mM lactate without IPTG have similar final cell density, despite the greater size of the NAG molecule. We speculate that this was due to incomplete NAG utilization under this condition, although we could not measure NAG because of the small culture size. As culture size decreases, aeration and oxygen availability also decrease.[32] Oxygen limitation reduces the substrate utilization of *S. oneidensis.*[38] At the 50 ml scale, we observe the expected growth yield difference between *S. oneidensis* growth on NAG vs D,L-lactate (**Figure 34**).

To our knowledge, the phenotype of wild-type *S. oneidensis* displaying enhanced growth on NAG with IPTG has not been reported in the scientific literature. The enhanced growth of wild-type *S. oneidensis* on NAG when cultivated with IPTG is an important observation to be mindful of when testing inducible systems in this organism because of this inducer's capability of altering *S. oneidensis* metabolism. The impact of this was showcased by our discovery of the phenotype during experimentation with *S. oneidensis* CRISPRi control strains. This observation may also be buried in the literature and could raise questions regarding results without thorough controls. For example, Jeon *et al.* report optimal *n*-butanol production by an engineered strain of *S. oneidensis* on 2% NAG, 0.3% butyrate and 0.1 mM IPTG under microaerobic conditions.[27] This strain overexpresses recombinant proteins CoA transferase, acetyl-CoA synthase, and alcohol dehydrogenase from an IPTG-inducible promoter. Since the carbon source was NAG, it is unclear whether the IPTG aided in *n*-butanol production because of expression of these proteins, or if it was decreasing acetate accumulation in the media. The *n*-butanol-producing strain generated the highest titers under microaerobic conditions. Our data suggest less aeration (therefore lower oxygen concentrations) exacerbates the effect of IPTG on NAG-cultivated *S. oneidensis*. So, one could speculate that this effect is responsible for the higher production of *n*-butanol under microaerobic conditions. We encourage researchers working with *S. oneidensis* to be mindful of these observations during their efforts to engineer this organism so that false positive correlations can be avoided.

METHODS

Bacterial strains and culturing conditions

Wild-type *Shewanella oneidensis* MR-1 was used for all experiments in this study. Plasmid pJMP2846 was used as the CRISPRi non-targeting control.[18] *S. oneidensis* was grown at 30 °C with shaking in M5 minimal medium (1.29 mM K_2HPO_4, 1.65 mM KH_2PO_4, 7.87 mM NaCl, 1.70 mM NH_4SO_4, 475 µM $MgSO_4 \cdot 7H_2O$, 10 mM HEPES, 0.01% (w/v) casamino acids, 1× Wolfe's mineral solution, and 1× Wolfe's vitamin solution without riboflavin, pH 7.2). For cultures with 10X buffering capacity, HEPES concentration was increased to 100 mM. M5 was supplemented with either sodium D,L-lactate, NAG, or sodium acetate to final concentrations of 20 mM unless otherwise stated. IPTG was added to cultures at the specified concentrations. Growth experiments were conducted in either 96-well plates containing 200 µl of media or 250-ml shake flasks containing 50 ml of media. Culture volumes are specified for each experiment.

OD_{600} and pH Measurement

OD_{600} was measured every 15-30 minutes using an H1M BioTek Plate Reader for 200 µl cultures. OD_{600} of 50-ml cultures were measured on an Eppendorf BioSpectrometer using a 1 ml culture sample in a disposable cuvette with a 1-cm pathlength (diluted 1:10 when OD_{600} was above 1.0).

A 2-ml culture sample was taken from 50-ml cultures for pH measurement. The sample was centrifuged at 8,000 rpm for 5 minutes to remove cells from the media. The pH of the supernatant was measured using a Mettler Toledo FiveEasy Plus FP20 pH meter.

HPLC Analysis

HPLC samples were prepared by centrifuging 1 ml aliquots from 50 ml cultures at 16,100 rpm for 10 minutes in a Minispin Plus Eppendorf microcentrifuge. 700 µl of the supernatant was transferred to a 2 ml glass HPLC vial. Sodium acetate standards were prepared at concentrations of 30, 20, 15, 7, and 3 mM in Milli-Q water. Samples were refrigerated at 10 °C in the HPLC autosampler during the run.

HPLC analysis was performed on a Shimadzu 20A HPLC using an Aminex HPX-87H column (BioRad, Hercules, CA) with a Microguard Cation H^+ guard column (BioRad, Hercules, CA) at 50 °C. Analysis was conducted at a 0.6 ml min^{-1} flow rate in 5 mM sulfuric acid and a 30-minute run time. HPLC eluent was prepared by diluting 98% HPLC-grade sulfuric acid solution in Milli-Q water. The eluent was degassed at 37 °C for 3 to 5 days prior to use. Acetate was detected by refractive index (RID-20A). NAG concentration could not be measured due to co-elution with IPTG.

Data analysis

Growth and HPLC data were analyzed using RStudio using packages ggplot2, dplyr, grid, and gridExtra.[34–36] *Carrying capacity and growth rates of S. oneidensis cultures were determined using the R package "growthCurver" using default values.*[37]

Microscopy

Samples (2 µl) of 50 ml growth curves were periodically imaged on a Leica DM 1000 LED microscope and images were taken from a Leica ICC50 W camera and Leica app. Average cell areas were calculated with Image J.[39]

ACKNOWLEDGEMENTS

We thank Drs. Jason Peters and Amy Banta for Mobile-CRISPRi materials and consultation, Nicholas Tefft for assistance with HPLC measurements, and Shaylynn Miller for assistance with Image J.

FUNDING SOURCES

This material is based upon work supported by a 2018 Beckman Young Investigator Award to MT.

REFERENCES

1. Gruenberg, M. C. & TerAvest, M. A. A common inducer molecule enhances sugar utilization by *Shewanella oneidensis* MR-1. *J Ind Microbiol Biotechnol* **50**, (2023).

2. Kouzuma, A. Molecular mechanisms regulating the catabolic and electrochemical activities of *Shewanella oneidensis* MR-1. *Biosci Biotechnol Biochem* **85**, 1572–1581 (2021).

3. Zou, L., Huang, Y. Hong, Long, Z. er & Qiao, Y. On-going applications of Shewanella species in microbial electrochemical system for bioenergy, bioremediation and biosensing. *World J Microbiol Biotechnol* **35**, 1–9 (2019).

4. Webster, D. P. *et al.* An arsenic-specific biosensor with genetically engineered *Shewanella oneidensis* in a bioelectrochemical system. *Biosens Bioelectron* **62**, 320–324 (2014).

5. Zang, Y. *et al.* A bio-electrochemical sensor based on suspended *Shewanella oneidensis* MR-1 for the sensitive assessment of water biotoxicity. *Sens Actuators B Chem* **341**, 130004 (2021).

6. Lin, T. *et al.* Synthetic *Saccharomyces cerevisiae-Shewanella oneidensis* consortium enables glucose-fed high-performance microbial fuel cell. *AIChE Journal* **63**, 1830–1838 (2017).

7. Min, D. *et al.* Enhancing Extracellular Electron Transfer of *Shewanella oneidensis* MR-1 through Coupling Improved Flavin Synthesis and Metal-Reducing Conduit for Pollutant Degradation. *Environ Sci Technol* **51**, 5082–5089 (2017).

8. Venkateswaran, K. *et al.* Polyphasic taxonomy of the genus *Shewanella* and description of *Shewanella oneidensis* sp. nov. *Int J Syst Bacteriol* **49**, 705–724 (1999).

9. Serres, M. H. & Riley, M. Genomic Analysis of Carbon Source Metabolism of *Shewanella oneidensis* MR-1: Predictions versus Experiments. *J Bacteriol* **188**, 4601 (2006).

10. Rodionov, D. A. *et al.* Genomic encyclopedia of sugar utilization pathways in the *Shewanella* genus. *BMC Genomics* **11**, 494 (2010).

11. Chubiz, L. M. & Marx, C. J. Growth Trade-Offs Accompany the Emergence of Glycolytic Metabolism in *Shewanella oneidensis* MR-1. *J Bacteriol* **199**, (2017).

12. Yang, C. *et al.* Comparative Genomics and Experimental Characterization of N-Acetylglucosamine Utilization Pathway of *Shewanella oneidensis*. *J Biol Chem* **281**, 29872–29885 (2006).

13. Brutinel, E. D. & Gralnick, J. A. Anomalies of the anaerobic tricarboxylic acid cycle in *Shewanella oneidensis* revealed by Tn-seq. *Mol Microbiol* **86**, 273–283 (2012).

14. Duhl, K. L., Tefft, N. M. & TerAvest, M. A. *Shewanella oneidensis* MR-1 Utilizes both Sodium- and Proton-Pumping NADH Dehydrogenases during Aerobic Growth. *Appl Environ Microbiol* **84**, (2018).

15. Feng, X., Xu, Y., Chen, Y. & Tang, Y. J. Integrating Flux Balance Analysis into Kinetic Models to Decipher the Dynamic Metabolism of *Shewanella oneidensis* MR-1. *PLoS Comput Biol* **8**, e1002376 (2012).

16. Orr, J. S., Christensen, D. G., Wolfe, A. J. & Rao, C. V. Extracellular acidic pH inhibits acetate consumption by decreasing gene transcription of the tricarboxylic acid cycle and the glyoxylate shunt. *J Bacteriol* **201**, 410–428 (2019).

17. Flynn, C. M., Hunt, K. A., Gralnick, J. A. & Srienc, F. Construction and elementary mode analysis of a metabolic model for *Shewanella oneidensis* MR-1. *Biosystems* **107**, 120–128 (2012).

18. Peters, J. M. *et al.* Enabling genetic analysis of diverse bacteria with Mobile-CRISPRi. *Nat Microbiol 2019 4:2* **4**, 244–250 (2019).

19. Ford, K. C., Kaste, J. A. M., Shachar-Hill, Y. & TerAvest, M. A. Flux-Balance Analysis and Mobile CRISPRi-Guided Deletion of a Conditionally Essential Gene in *Shewanella oneidensis* MR-1. *ACS Synth Biol* **11**, 3405–3413 (2022).

20. Li, F. *et al.* Engineering *Shewanella oneidensis* enables xylose-fed microbial fuel cell. *Biotechnol Biofuels* **10**, 1–10 (2017).

21. Cheng, L. *et al.* Developing a base-editing system to expand the carbon source utilization spectra of *Shewanella oneidensis* MR-1 for enhanced pollutant degradation. *Biotechnol Bioeng* **117**, 2389–2400 (2020).

22. Dundas, C. M., Walker, D. J. F. & Keitz, B. K. Tuning Extracellular Electron Transfer by *Shewanella oneidensis* Using Transcriptional Logic Gates. *ACS Synth Biol* **9**, 2301–2315 (2020).

23. Li, F. *et al.* Modular engineering to increase intracellular NAD(H/+) promotes rate of extracellular electron transfer of *Shewanella oneidensis*. *Nat Comm 2018 9:1* **9**, 1–13 (2018).

24. Yang, Y. *et al.* Enhancing Bidirectional Electron Transfer of *Shewanella oneidensis* by a Synthetic Flavin Pathway. *ACS Synth Biol* **4**, 815–823 (2015).

25. Liu, T. *et al.* Enhanced Shewanella biofilm promotes bioelectricity generation. *Biotechnol Bioeng* **112**, 2051–2059 (2015).

26. Yi, Y.-C. & Ng, I.-S. Redirection of metabolic flux in *Shewanella oneidensis* MR-1 by CRISPRi and modular design for 5-aminolevulinic acid production. *Bioresour Bioprocess 2021 8:1* **8**, 1–11 (2021).

27. Jeon, J. M. *et al.* Butyrate-based n-butanol production from an engineered *Shewanella oneidensis* MR-1. *Bioprocess Biosyst Eng* **41**, 1195–1204 (2018).

28. Lewis, M. A tale of two repressors – a historical perspective. *J Mol Biol* **409**, 14 (2011).

29. Wilson, C. J., Zhan, H., Swint-Kruse, L. & Matthews, K. S. The lactose repressor system: Paradigms for regulation, allosteric behavior and protein folding. *CMLS* **64**, 3–16 (2007).

30. Jobe, A. & Bourgeois, S. lac repressor-operator interaction: VI. The natural inducer of the lac operon. *J Mol Biol* **69**, 397–408 (1972).

31. Novichkov, P. S. *et al.* RegPrecise 3.0 – A resource for genome-scale exploration of transcriptional regulation in bacteria. *BMC Genomics* **14**, 745 (2013).

32. Somerville, G. A. & Proctor, R. A. Cultivation conditions and the diffusion of oxygen into culture media: The rationale for the flask-to-medium ratio in microbiology. *BMC Microbiol* **13**, 9 (2013).

33. Tang, Y. J., Hwang, J. S., Wemmer, D. E. & Keasling, J. D. *Shewanella oneidensis* MR-1 Fluxome under Various Oxygen Conditions. *Appl Environ Microbiol* **73**, 718–729 (2007).

34. R Core Team. R: A language and environment for statistical computing. *R Foundation for Statistical Computing* Preprint at https://www.R-project.org/ (2021).

35. H. Wickham. ggplot2: Elegant Graphics for Data Analysis. Preprint at (2016).

36. Hadley Wickham, Romain François, Lionel Henry & Kirill Müller. dplyr: A Grammar of Data Manipulation. *R package version 1.0.9* Preprint at https://CRAN.R-project.org/package=dplyr (2022).

37. Sprouffske, K. & Wagner, A. Growthcurver: An R package for obtaining interpretable metrics from microbial growth curves. *BMC Bioinformatics* **17**, 1–4 (2016).

38. Pinchuk, G. E., Hill, E. A., Geydebrekht, O. v., de Ingeniis, J., Zhang, X., Osterman, A., Scott, J. H., Reed, S. B., Romine, M. F., Konopka, A. E., Beliaev, A. S., Fredrickson, J. K., & Reed, J. L. Constraint-Based Model of Shewanella oneidensis MR-1 Metabolism: A Tool for Data Analysis and Hypothesis Generation. *PLoS Comput Biol*, *6*(6), e1000822 (2010).

39. Schneider, C. A., Rasband, W. S., & Eliceiri, K. W. NIH Image to ImageJ: 25 years of image analysis. *Nat Methods*, *9*(7), 671–675 (2012).

CHAPTER 5:

ELECTRO-FERMENTATION INFLUENCES FERMENTATION PRODUCTS IN ENGINEERED *ESCHERICHIA COLI*

PREFACE

This investigation began as summer projects for two undergraduate students: Carrie Gregg and Andrew Scheil. The goal of the project was to determine whether an electroactive strain of *E. coli* developed by my advisor's postdoc lab could participate in EET with a fermentable substrate. The previous studies with the organism used the non-fermentable substrate lactate in order to study the EET pathway. Now, with confirmation that EET does occur, we were interested in exploring the biotechnological potential of the strain by using the fermentable substrate glucose.

The project began with Carrie and I experimenting with solid and soluble iron as the terminal electron acceptor while Andrew and his graduate student mentor, Shay Miller, were experimenting with an anode as the terminal electron acceptor. Over the course of the summer, it became clear that we were seeing the same results in both cases – the fermentation product ratios were shifting toward more oxidized products when the electroactive *E. coli* was participating in EET. We had some promising preliminary data showing there was an interesting story here, but the summer was ending. Carrie returned to her home institution and Andrew started on a different project.

I took over primary ownership of this project and repeated experiments both with iron and an anode as the terminal electron acceptor. I was also able to take this project a step further by reversing the EET pathway using a cathode as an electron source and demonstrated the opposite shift in fermentation product ratios. I performed some additional analysis of the electron and carbon flow through the system which allowed us to make some further conclusions about the efficiency of the system and areas which could be improved upon. This is by far one of the most collaborative projects I had the

pleasure of working on during my PhD, and I really enjoyed having multiple hands and minds contributing toward the same goal. While I do enjoy independent work, this project was a nice change of pace from some of the others which were solely my responsibility from their inception.

This chapter describes the work that was done on investigating anodic and cathodic electro-fermentation with an electroactive strain of *E. coli*.

ABSTRACT

Escherichia coli is a popular host for fermentative biosynthesis of small molecule products due to its well understood metabolism and large genetic toolbox. A major limitation to product scope and yield using fermentation is the requirement that oxidation and reduction reactions be balanced. In this work, we demonstrate unbalanced electro-fermentation using an electroactive strain of *E. coli* expressing the Mtr pathway from *Shewanella oneidensis*. The Mtr pathway could act as an electron sink by transporting intracellular electrons derived from substrate oxidation to an extracellular electron acceptor, thus favoring production of oxidized fermentation products. We also show that the Mtr pathway is reversible in *E. coli* and could alternatively act as an electron source by importing electrons from a cathode, therefore favoring reduced fermentation products. This proof-of-concept suggests that electro-fermentation could be a useful tool for improving fermentations that are currently restrained by redox balance.

INTRODUCTION

Fermentation is the metabolic process of balancing substrate oxidation and reduction reactions in the absence of oxygen or other electron acceptors, which many organisms can use to conserve energy.[1] During this process, a substrate is oxidized to

generate an intermediate and reducing equivalents (e.g., NADH, $FADH_2$).[1,2] For a balanced reaction, the intermediate must be subsequently reduced for the regeneration of the oxidized cofactor (i.e. NAD^+, FAD).[1,2] These balanced redox reactions enable ATP generation via substrate level phosphorylation.[1] For example, *Escherichia coli* produces ethanol, lactate, succinate, formate, and acetate as major fermentation products from glucose (**Figure 38**), and cellular redox balance is maintained by generating different ratios of these products.[3]

Metabolic engineering techniques have been harnessed for production of value-added chemicals, nutritional supplements, pharmaceuticals, and proteins via fermentation.[4–9] Major constraints of fermentation processes include limited product scopes and low product yields, which arise from the requirement for redox equivalents to be balanced between substrates and products during fermentation.[10,11] Electro-

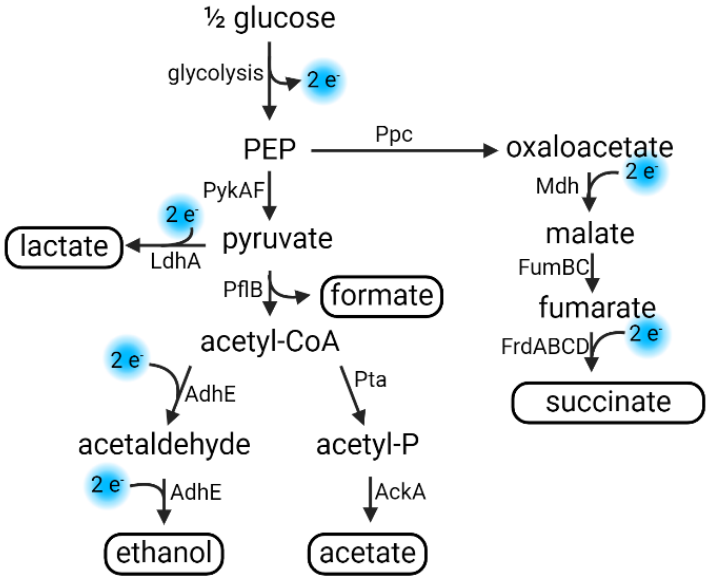

Figure 38. Major fermentation pathways in *E. coli*. Boxed metabolites indicate common fermentation products. Abbreviations: PEP, phosphoenolpyruvate; *ppc*, PEP carboxylase; *pykAF*, pyruvate kinase; *ldhA*, lactate dehydrogenase; *pflB*, pyruvate formate lyase; *adhE*, aldehyde dehydrogenase, *pta*, phosphate acetyl transferase; *ackA*, acetate kinase; *mdh*, malate dehydrogenase; *fumBC*, fumarate hydratase; *frdABCD*, fumarate reductase; e^-, electron. Created with Biorender.com.

fermentation is an emerging technology in which an electrode can act as an electron source or sink, allowing unbalanced fermentation by alleviating the constraint of redox balance.[12] Electro-fermentation is possible with microorganisms capable of extracellular electron transfer (EET), which allows electron transport across the cellular membrane to or from an electrode. Electroactive microorganisms can participate in EET through direct or mediated electron transfer.[13–18] Direct EET requires direct contact between the cell and the extracellular electron acceptor.[16–18] Indirect EET involves electron shuttling from the cell surface to the extracellular electron acceptor by an electron carrier.[13–15]

Mixed microbial cultures are used as the biocatalyst in most electro-fermentation systems; however, they are limited in their potential for improvement of substrate scope and product yield, purity, and scope due to their intrinsic unknown composition.[12] As an alternative, electro-fermentation could be engineered using well-studied strains with large synthetic biology toolboxes. For example, *E. coli* is a well-understood model organism with many synthetic biology tools available for strain improvement, making it an appealing host for engineering electroactivity.[19] To take advantage of the benefits that come with using *E. coli* as a host, electroactive *E. coli* strains have been engineered to reduce extracellular electron acceptors. Some strains utilize synthetic electron conduits for extracellular electron transfer such as modified carbon nanoparticles which are added to wild-type *E. coli* and traverse the cell membrane.[20] Other strains express membrane cytochromes from the Mtr pathway in *Shewanella oneidensis*, which are products of work pioneered by research groups led by Seward, Spormann, Gescher, and Ajo-Franklin.[21–24]

The *S. oneidensis* Mtr pathway is composed of CymA and MtrCAB. CymA is an inner membrane tetraheme cytochrome *c* which transfers electrons from the inner

membrane quinone pool to MtrCAB.[25,26] The MtrCAB complex is composed of MtrC, an outer membrane cytochrome *c*; MtrA, a periplasmic cytochrome *c*; and MtrB, a β-barrel protein which spans the outer membrane and houses MtrA and MtrC.[27,28] The native function of the Mtr pathway in *S. oneidensis* is to transfer intracellular electrons to extracellular electron acceptors; however, this pathway can also operate in reverse and power intracellular reduction reactions.[29–32]

Seward and Gescher conducted initial work exploring the heterologous expression of *S. oneidensis* cytochromes in *E. coli*.[21–23] The first of these studies showed that MtrA could be matured by the native *E. coli* cytochrome *c* maturation pathway (Ccm) and could reduce soluble iron.[21] *E. coli* expressing MtrA alone could not reduce solid iron, which was an indicator that there was no native *E. coli* mechanism which could transport electrons to the cell surface.[21,33] Gescher *et al.* showed that expressing CymA alone or CymA and MtrA together both allowed *E. coli* to reduce chelated iron; however, these strains also were incapable of reducing solid electron acceptors.[22,23,33] The electroactive *E. coli* MFe444 developed by Ajo-Franklin and colleagues expresses CymA and MtrCAB from *S. oneidensis* and the native *E. coli* cytochrome maturation system.[24] In this strain, the Mtr pathway allows electrons derived from substrate oxidation by quinone-linked oxidoreductases (e.g., lactate dehydrogenase) to be passed to the outer surface of the cell via the Mtr pathway. Electron transfer from the cell surface to a solid electron acceptor in this system is largely dependent on flavins as electron shuttles, as observed in *S. oneidensis* (**Figure 39**). MFe444 reduces Fe^{3+} with or without riboflavin when provided lactate as the electron donor; however, riboflavin improves electron transfer to solid iron minerals by 2.5-fold.[24] MFe444 also generates a higher current in bioelectrochemical

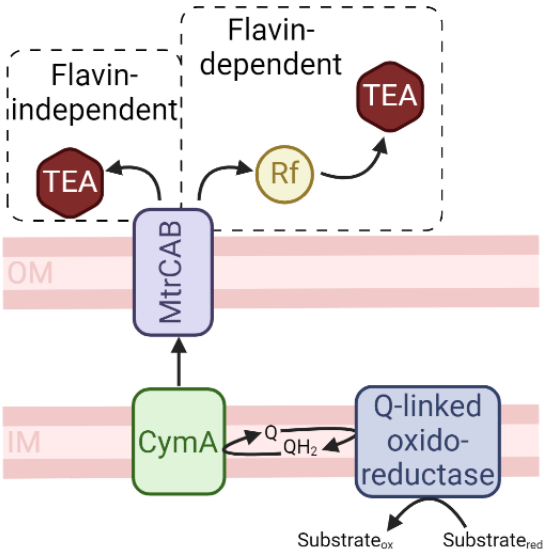

Figure 39. Mtr pathway from *S. oneidensis* expressed in MFe444. CymA and MtrCAB from *S. oneidensis* are expressed from an IPTG-inducible plasmid. Electrons from substrate oxidation by a quinone-linked (Q-linked) oxidoreductase are passed through the inner membrane quinone pool to CymA, then transported across the outer membrane via MtrCAB. During flavin-independent EET, electrons are deposited directly into the terminal electron acceptor (TEA). In flavin-dependent EET, riboflavin (Rf) shuttles electrons to the TEA. Created with Biorender.com.

systems than a control strain expressing only the cytochrome maturation genes.[24,34,35] When connected to the electrode during lactate metabolism, the spectrum of metabolites generated by MFe444 is shifted toward more oxidized products, such as acetate, and away from reduced products, such as ethanol. However, less than 20% of available lactate was consumed under this condition because the current electron transfer rates were not sufficient to enable growth via respiration.

These findings indicate the functional expression of the Mtr pathway; however, *E. coli* does not ferment lactate. MFe444 can also use the Mtr pathway for inward electron transfer, as shown by its ability to reduce fumarate or nitrate with electrons supplied from a cathode.[36] In this work, we explore the biotechnological potential for *E. coli* MFe444 by utilizing it as a host for glucose electro-fermentation and demonstrate control in both

directions over the ratio of oxidized and reduced *E. coli* fermentation products via an electrode.

METHODS

Strains and plasmids

Strains and plasmids used in this study are listed in **Table 14**.

Table 14. Strains and plasmids used for experiments described in Chapter 5.

Strains	Parent	Plasmids	Source
MFe408	C43(DE3)	pEC86, pSB1ET2	54
MFe444	C43(DE3)	pEC86, I5049	24

Plasmids	Genes	Antibiotic Resistance	Source
pEC86	*ccmA-H*	Chloramphenicol	55
pSB1ET2	none	Kanamycin	56
I5049	*cymA*, *mtrCAB*	Kanamycin	24

Culturing

MFe408 and MFe444 were precultured aerobically in 2 ml LB (Neogen) supplemented with 50 μg ml^{-1} kanamycin and 30 μg ml^{-1} chloramphenicol overnight at 30 °C with shaking at 250 rpm. To induce expression of the Mtr pathway and cytochrome *c* maturation proteins, MFe408 and MFe444 were subcultured in 50 ml of 2xYT (Difco) supplemented with 50 μg ml^{-1} kanamycin and 30 μg ml^{-1} chloramphenicol. 2xYT cultures were inoculated to an initial OD_{600} of 0.02 and were incubated aerobically at 30 °C with

shaking at 250 rpm. OD_{600} was monitored and IPTG was added to a final concentration of 10 μM when cultures reached an OD_{600} of 0.2-0.3. After approximately 18 hours, cells were harvested via centrifugation (9,000 rpm, 5 min, 22 °C), the supernatant was discarded, and cell pellets were washed with 25 ml of basal M5 high HEPES medium (1.29 mM K_2HPO_4, 1.65 mM KH_2PO_4, 7.87 mM NaCl, 1.70 mM NH_4SO_4, 475 μM $MgSO_4 \cdot 7H_2O$, 100 mM HEPES, 0.01% (w/v) casamino acids, pH 7.2). Cell pellets were resuspended in 25 ml basal M5 high HEPES medium and were inoculated into experimental cultures to an initial OD_{600} of 0.2.

Cultures for iron-reduction experiments were conducted in an anaerobic chamber with an atmosphere of 5% H_2 and 95% N_2. All media and culture tubes were placed into the chamber one day prior to inoculation. Iron-reduction medium contained basal M5 high HEPES medium supplemented with Wolfe's mineral solution, Wolfe's vitamin solution without riboflavin, 20 mM D-glucose, either 50 mM Fe(III)-NTA or 50 mM Fe_2O_3, and 50 μg ml^{-1} kanamycin. Where specified, 5 μM riboflavin was added.

Fe^{2+} quantification

Fe^{2+} quantification was performed using the ferrozine method.[37] Acidified samples and standards were prepared by adding 25 μl of standard or sample to 75 μl of anaerobic 2 M HCl in an anaerobic chamber. Samples and standards were removed from the chamber after acidification. A 10 μl aliquot of acidified sample or Fe^{2+} standard prepared from iron (II) chloride tetrahydrate was combined with 190 μl of 1 g L^{-1} FerroZine reagent in a 96-well plate. Absorbance was read at 562 nm on a H1M BioTek Plate Reader.

HPLC analysis

HPLC samples were prepared by centrifuging 700 µl aliquots at 16,100 rpm for 10 minutes in a Minispin Plus Eppendorf microcentrifuge. 600 µl of the supernatant was transferred to a 2 ml glass HPLC vial. Samples were refrigerated at 10 °C in the HPLC autosampler during the run.

HPLC analysis was performed on a Shimadzu 20A HPLC using an Aminex HPX-87H column (BioRad, Hercules, CA) with a Microguard Cation H^+ guard column (BioRad, Hercules, CA) at 50 °C. Analysis was conducted at a 0.6 ml min^{-1} flow rate in 5 mM sulfuric acid and a 30-minute run time. HPLC eluent was prepared by diluting 98% HPLC-grade sulfuric acid solution in Milli-Q water. The eluent was degassed at 37 °C for 3 to 5 days prior to use.

Bioelectrochemical system set-up

Bioelectrochemical measurements were performed using two-chamber bioelectrochemical reactors (Adams and Chittenden Scientific Glass Coop, custom design), separated by a cation exchange membrane (Membranes International, Catalog: CMI-7000S). The three-electrode system consisted of a carbon felt working electrode adhered to a titanium wire via CCC carbon adhesive (Electron Microscopy Sciences, Catalog: 12664), a graphite rod as the counter electrode (Electron Microscopy Science, Catalog: 07200), and an Ag/AgCl reference electrode in saturated KCl, with a magnesia stick frit (Sigma Aldrich, Catalog: 31408-1EA). The working chamber was filled with a final volume of 100 ml of M5 high HEPES medium prior to autoclaving. After autoclaving, the medium was supplemented with Wolfe's mineral solution, Wolfe's vitamin solution without riboflavin, 50 mg ml^{-1} kanamycin, 50 mM D-glucose, 10 µM IPTG, and 5 µM riboflavin. The

electrodes were connected to a potentiostat (VMP, BioLogic USA), and the working electrode was poised at +200 $mV_{Ag/AgCl}$ for anodic experiments or -500 $mV_{Ag/AgCl}$ for cathodic experiments. Current was measured every 1 second. Precultures were prepared as described above, and bioelectrochemical system working chambers were inoculated with washed cells to an initial OD_{600} of 0.2.

Data analysis

Data were analyzed using R version 4.3.1 and packages ggplot2 3.4.2, dplyr 1.1.2, TTR 0.24.3, viridis 0.6.4, grid 4.3.1, and gridExtra 2.3.[38–43] Moles of electrons to or from the electrode during electro-fermentations were calculated by integrating the area under the curve and converting to moles using Faraday's constant using **Equation 1**. Percent of electrons from glucose routed to the anode were calculated by dividing the moles of electrons by the total moles of electrons input using **Equation 2**. Percent of electrons from glucose routed to fermentation products during anodic electro-fermentation were calculated by dividing the total number of electrons in the fermentation products by the total number of electrons in glucose consumed following **Equation 3**. Percent of electrons from the cathode routed to fermentation products were calculated by dividing the total number of electrons in the fermentation products by the total amount of electrons input (from glucose and electrode) using **Equation 4**. Percent of carbon routed to fermentation products were calculated by dividing the moles of carbon in the fermentation products by the moles of carbon from glucose consumed using **Equation 5**.

$$\text{electrode } e^- \text{ moles} = \int \text{current mC s} \times 1\ \text{s} \times \frac{\text{C}}{1000\ \text{mC}} \times \frac{\text{mole}}{96{,}485\ \text{C}}$$

Equation 1. Conversion of mC s to moles of electrons.

$$\%\ \mathrm{e^-}\ \text{to anode} = \left(\frac{\text{electrode } \mathrm{e^-} \text{ moles}}{\left(0.08\ \mathrm{L} \times \frac{\Delta\text{glucose moles}}{\mathrm{L}}\right) \times 24\ \mathrm{e^-}} \right) \times 100$$

Equation 2. Percent of electrons routed to electrode in anodic electro-fermentation.

$$f(e) = e^-\ moles\ of\ product = \left(0.08\ \mathrm{L} \times \frac{\text{product moles}}{\mathrm{L}}\right) \times \mathrm{e^-}$$

Product	**e⁻**
Lactate	12
Formate	2
Acetate	8
Succinate	13
Ethanol	12

$$\%\ \mathrm{e^-}\ \text{to fermentation products} = \left(\frac{\Sigma_{i=1}^{n} f(e,i)}{\left(0.08\ \mathrm{L} \times \frac{\Delta\text{glucose moles}}{\mathrm{L}}\right) \times 24\ \mathrm{e^-}} \right) \times 100$$

Equation 3. Percent of electrons routed to fermentation products in anodic electro-fermentation.

$$e^-\ moles\ of\ product = \left(0.08\ \mathrm{L} \times \frac{\text{product moles}}{\mathrm{L}}\right) \times \mathrm{e^-}$$

Product	**e⁻**
Lactate	12
Formate	2
Acetate	8
Succinate	13
Ethanol	12

$$\%\ e^{-}\ \text{to fermentation products} = \left(\frac{\Sigma_{i=1}^{n}\ \textbf{equation 5}, i}{\left(\left(0.08\ \text{L} \times \frac{\Delta \text{glucose moles}}{\text{L}} \right) \times 24\ e^{-} \right) + \text{electrode}\ e^{-}\ \text{moles}} \right) \times 100$$

Equation 4. Percent of electrons routed to fermentation products in cathodic electro-fermentation.

$$f(c) = e^{-}\ moles\ of\ product = \left(0.08\ \text{L} \times \frac{\text{product moles}}{\text{L}} \right) \times \text{C}$$

Product	**C**
Lactate	3
Formate	1
Acetate	2
Succinate	4
Ethanol	2

$$\%\ \text{C to fermentation products} = \left(\frac{\Sigma_{i=1}^{n} f(c,i)}{\left(0.08\ \text{L} \times \frac{\Delta \text{glucose moles}}{\text{L}} \right) \times 6\ \text{C}} \right) \times 100$$

Equation 5. Percent of carbon routed to fermentation products.

RESULTS

The engineered electroactive *E. coli* strain MFe444 can use the non-fermentable electron donor lactate to reduce extracellular iron and electrodes.[24] Here, we tested whether MFe444 can also use a fermentable substrate to power electrode reduction and whether the presence of the electrode would alter the ratio of fermentation products. We

cultivated MFe444 (*E. coli* expressing *S. oneidensis* CymA, MtrCAB, and *E. coli* cytochrome *c* maturation proteins) and MFe408 (*E. coli* expressing only the cytochrome *c* maturation proteins) in a bioelectrochemical system with 50 mM D-glucose, 5 μM riboflavin, and an anode poised at +200 $mV_{Ag/AgCl}$. MFe444 produced a higher current than MFe408, indicating more electron transfer occurring in the Mtr-expressing strain (**Figure 40a**). OD_{600} in the working chamber of the bioelectrochemical system was monitored throughout the cultivation period. Both strains reached a similar maximum OD_{600} after one day of cultivation. MFe408 maintained a relatively consistent OD_{600} from days 1-6 whereas MFe444 displays a drop in OD_{600} after day 1 (**Figure 41**). This indicates that the difference in current between the strains is due to Mtr pathway activity and not a difference in cell density, as MFe444 displayed a higher current than MFe408 on day one when both strains had a similar OD_{600}. We measured the concentrations of fermentation products throughout the anodic electro-fermentation and observed that MFe444 produced 19.0% and 28.5% less of the more reduced fermentation products lactate and succinate, respectively. MFe444 produced 10.4% and 16.4% more of the oxidized fermentation products formate and acetate, respectively (**Figure 40b, Table 15**). Fumarate concentrations were not assessed because it is not a major fermentation product and due to low succinate production.[3,44,45]Previous studies have shown that riboflavin improves EET to solid electron acceptors in MFe444 oxidizing lactate.[24] To determine whether riboflavin was required for EET during glucose electro-fermentation, MFe408 and MFe444 were cultivated in bioelectrochemical systems with 50 mM D-glucose as the carbon source and electron donor and an anode poised at +200 $mV_{Ag/AgCl}$ as the extracellular electron acceptor. When the bioelectrochemical systems were inoculated, the reactors contained

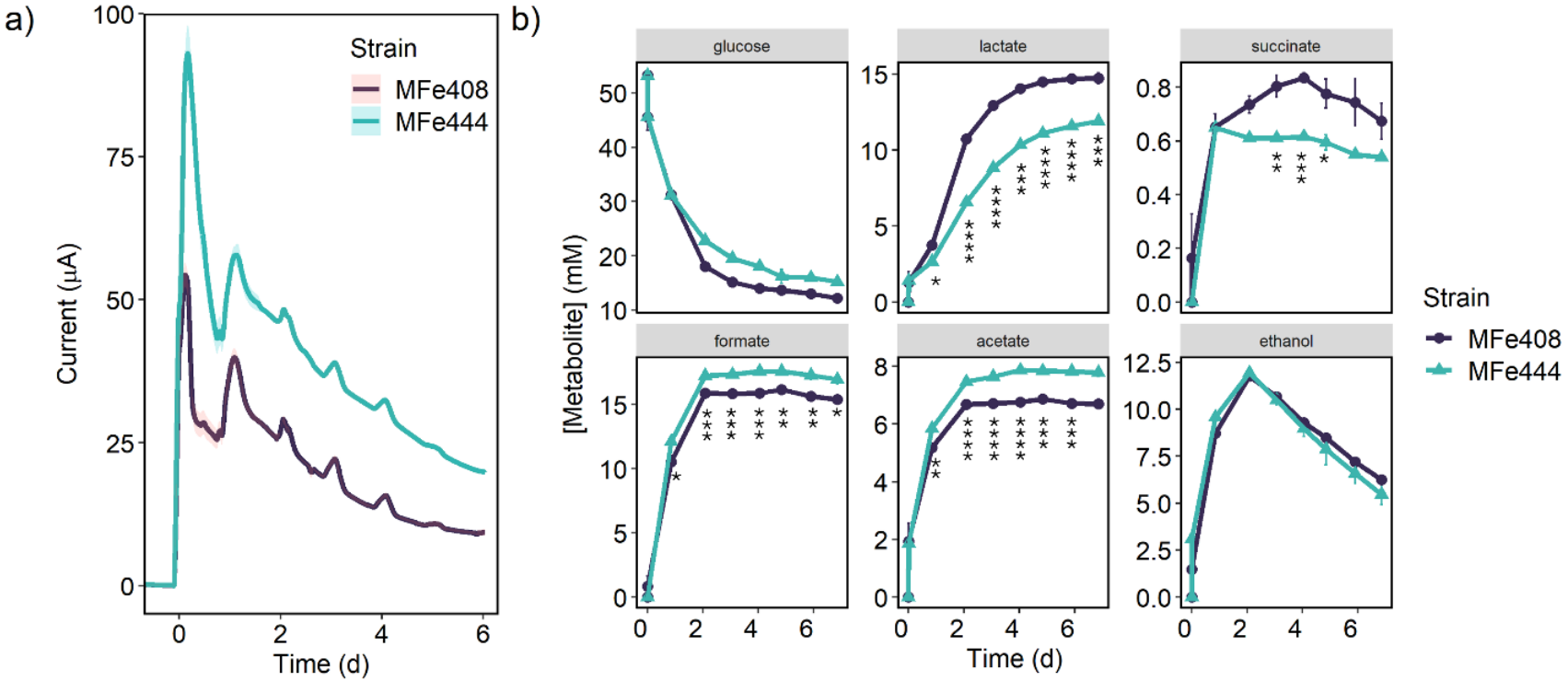

Figure 40. Current (A) and metabolite concentrations (B) of MFe408 and MFe444 during anodic electro-fermentation. Strains cultivated in a bioelectrochemical system with 50 mM D-glucose, 5 μM riboflavin, and an anode poised at +200 $mV_{Ag/AgCl}$. Inoculation occurred at time 0. P-values were calculated at each timepoint between the MFe408 and MFe444 conditions. * 0.05 < p < 0.1, ** 0.01 < p < 0.05, *** 0.001 < p < 0.01, **** p < 0.001. P values not calculated for glucose.

Table 15. Final concentrations and percent differences of metabolites from MFe408 and MFe444 anodic electro-fermentation depicted in Figure 40.

	Lactate (mM)	Succinate (mM)	Formate (mM)	Acetate (mM)	Ethanol (mM)
MFe408	14.7 ± 0.3	0.7 ± 0.1	15.4 ± 0.1	6.7 ± 0.1	6.2 ± 0.2
MFe444	11.9 ± 0.2	0.5 ± 0.0	17.0 ± 0.4	7.8 ± 0.1	5.5 ± 0.6
Percent difference	19.0%	28.5%	10.4%	16.4%	11.3%

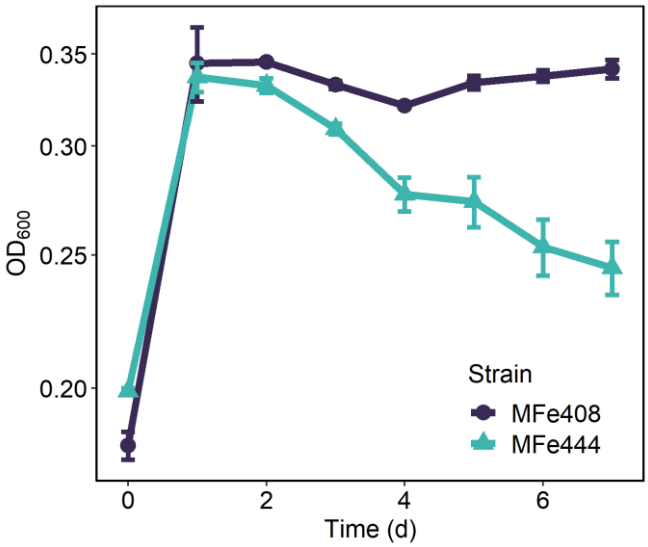

Figure 41. OD_{600} measurements of MFe408 and MFe444 during anodic electro-fermentation depicted in Figure 40. Strains cultivated in a bioelectrochemical system with 50 mM D-glucose, 5 µM riboflavin, and an anode poised at +200 $mV_{Ag/AgCl}$.

0.2 µM riboflavin. After ~24 hours, riboflavin was increased to a final concentration of 5 µM. With 0.2 µM riboflavin, current production by the two strains was similar. A divergence in current values was observed when the riboflavin concentration was increased, with MFe444 displaying a greater current than MFe408 (**Figure 42**).

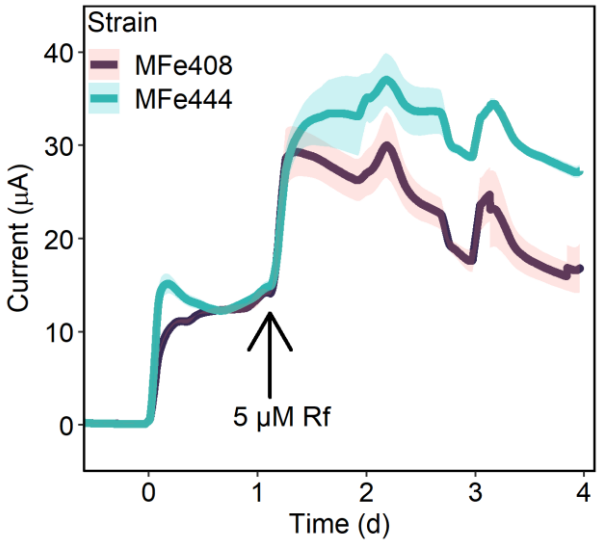

Figure 42. Current of MFe408 and MFe444 anodic electro-fermentation with different riboflavin concentrations. Strains were cultivated with 50 mM D-glucose and an anode poised at +200 $mV_{Ag/AgCl}$ with 0.2 or 5 µM riboflavin (Rf). Sufficient riboflavin concentration is required to support EET between the electroactive *E. coli* and the electrode. Inoculation occurred at time 0.

Since electro-fermentation requires specialized equipment, we tested whether we could achieve the same effect using a cheaper and more accessible method. To do this, we cultured MFe408 and MFe444 anaerobically in minimal medium containing 20 mM D-glucose as a carbon and electron source, either soluble iron (Fe(III)-NTA) or insoluble iron (Fe_2O_3) as an electron acceptor, with 5 µM riboflavin. Iron reduction was monitored as an indicator of extracellular electron transfer (**Figure 43a**). Under these conditions, MFe444 reduced 225% more Fe_2O_3 than the control strain (**Table 16**). Glucose was completely consumed, and fermentation product generation was complete within the first 24 hours of cultivation (**Figure 43b**). All fermentation product concentrations were 0 mM at the time of inoculation, and this measurement was omitted from the plots to ease visualization of differences. Consistent with the anodic electro-fermentation results, MFe444 produced 27.6% less lactate and 2.6% more acetate than the control strain (**Table 16**). Formate

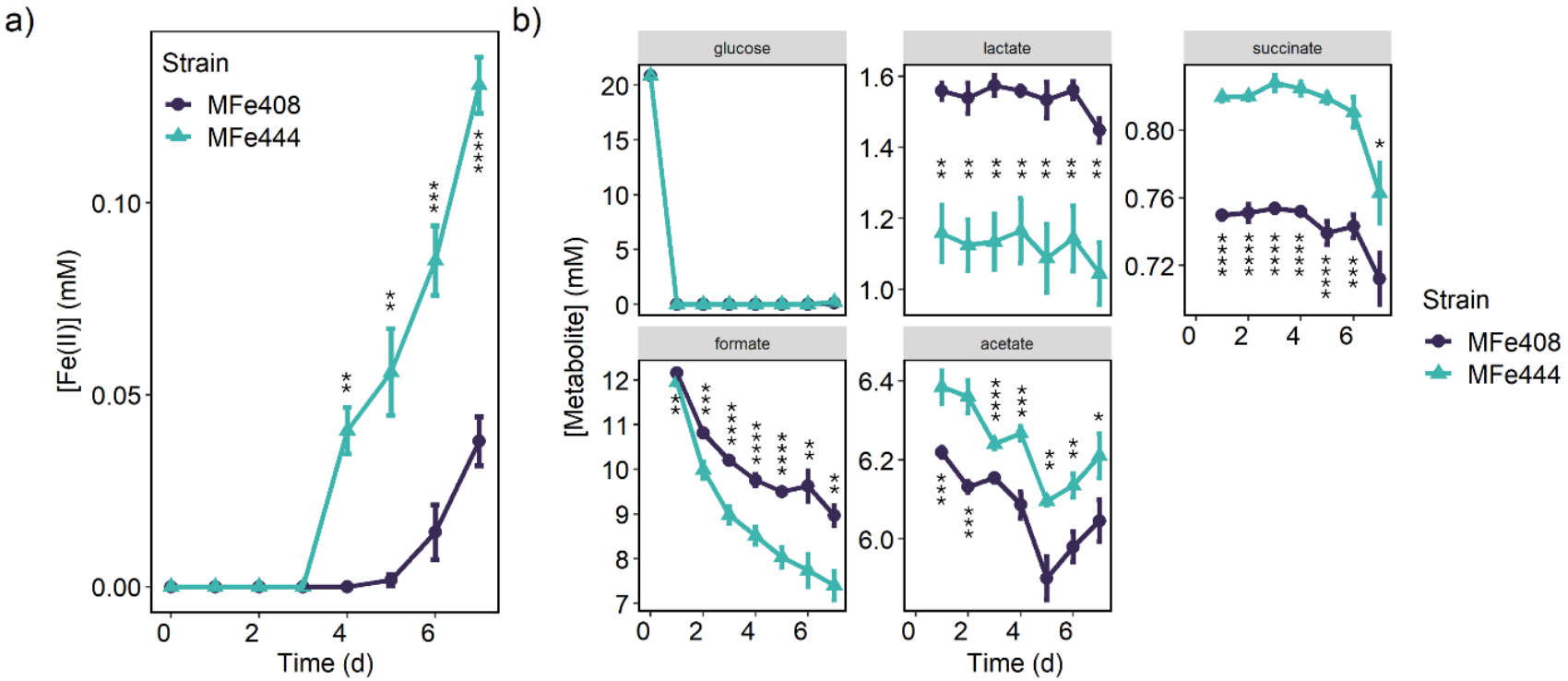

Figure 43. Metabolite concentrations during anaerobic cultivation of MFe408 and MFe444 with 20 mM D-glucose as the electron donor and 50 mM Fe_2O_3 as the electron acceptor. Note that y-axis scales differ between panels. Metabolite concentrations are reported starting at day 1 to promote ease of trend visualization. All fermentation product concentrations were measured and found to be 0 mM at the time of inoculation. P-values were calculated at each timepoint between the MFe408 and MFe444 conditions. * $0.05 < p < 0.1$, ** $0.01 < p < 0.05$, *** $0.001 < p < 0.01$, **** $p < 0.001$. P values for glucose were not determined.

Table 16. Metabolite concentrations of MFe408 and MFe444 cultivation with glucose, riboflavin, and Fe_2O_3 depicted in Figure 43.

	Fe(II) (mM)	Lactate (mM)	Succinate (mM)	Formate (mM)	Acetate (mM)
MFe408	0.04 ± 0.01	1.45 ± 0.03	0.71 ± 0.02	8.96 ± 0.22	6.05 ± 0.05
MFe444	0.13 ± 0.01	1.05 ± 0.09	0.76 ± 0.02	7.40 ± 0.32	6.21 ±0.06
Percent difference	225%	27.6%	7.0%	17.4%	2.6%

concentrations began to drop after the first day, while the other fermentation products (lactate, succinate, and acetate) remained at consistent levels. Because iron reduction does not occur until later timepoints where formate concentrations are decreasing, it is possible that electrons derived from formate oxidation participate in the iron reduction. With soluble iron provided as the electron acceptor, there was no difference between the two strains' iron reduction capabilities (**Figure 44**).

To determine if the fermentation product ratio could be influenced in the opposite direction, the strains were cultivated in bioelectrochemical systems with 50 mM D-glucose, 5 µM riboflavin, and a cathode poised at -500 $mV_{Ag/AgCl}$ as an extracellular electron donor. Under these conditions, MFe444 produced a greater negative current than MFe408 (**Figure 45a**). Similar to the anodic electro-fermentation, the two strains displayed similar OD_{600} measurements throughout the course of the cultivation, indicating that the difference in current between the strains is due to Mtr pathway activity and not a difference in cell density (**Figure 46**). MFe444 production of the reduced fermentation product succinate increased 5.2% during cathodic electro-fermentation, indicating that the electrons taken up by the Mtr pathway could be used toward production of more reduced fermentation products under these conditions (**Figure 45b, Table 17**).

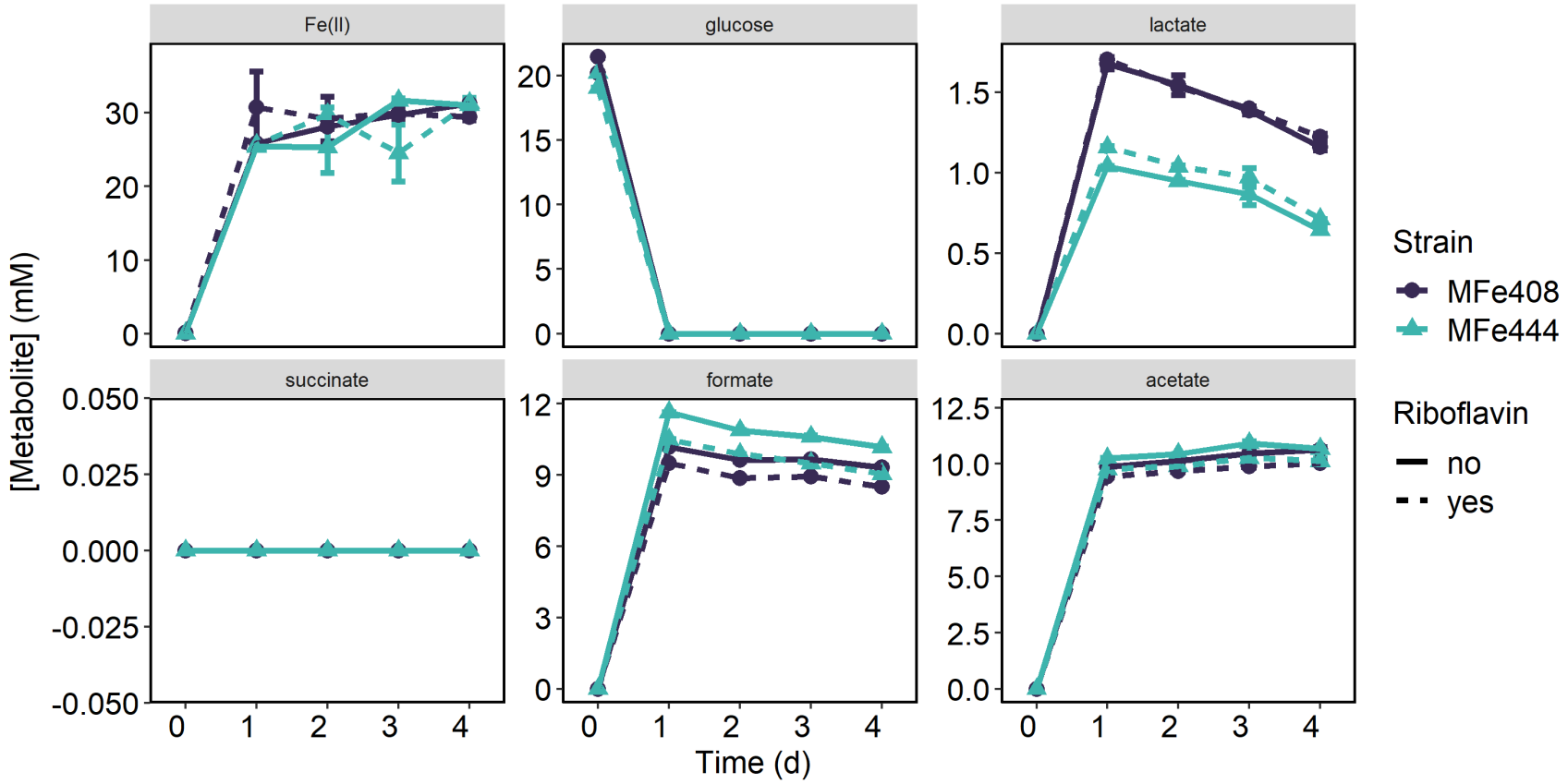

Figure 44. Fe^{2+} and metabolite concentrations during anaerobic cultivation of MFe408 and MFe444 with 20 mM D-glucose as the electron donor and 50 mM Fe(III)-NTA as the electron acceptor.

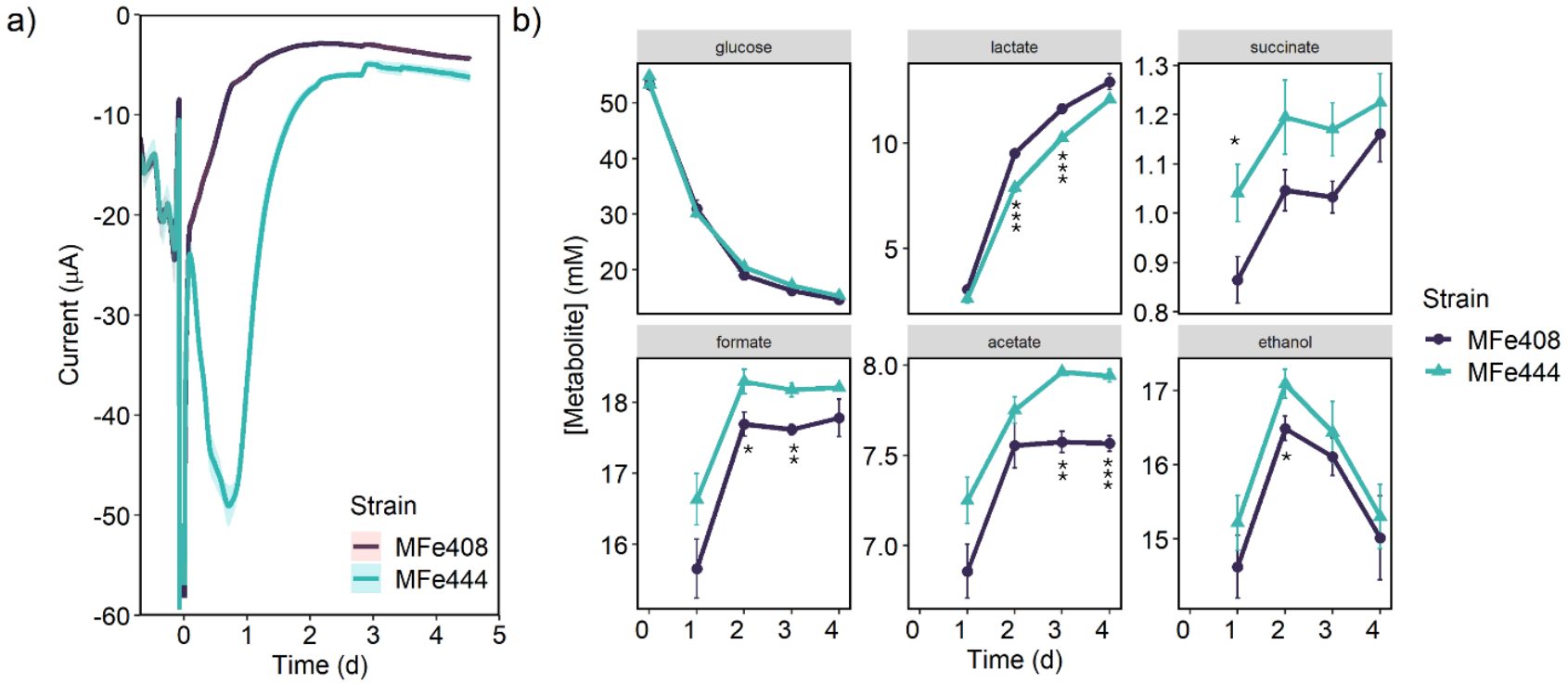

Figure 45. Current (A) and metabolite concentrations (B) of MFe408 and MFe444 during cathodic electro-fermentation. Strains cultivated in a bioelectrochemical system with 50 mM D-glucose, 5 μM riboflavin, and a cathode poised at -500 $mV_{Ag/AgCl}$. Inoculation occurred at time 0. Metabolite concentrations are reported starting at day 1 to promote ease of trend visualization. All fermentation product concentrations were measured and found to be 0 mM at the time of inoculation. P-values were calculated at each timepoint between the MFe408 and MFe444 conditions. * $0.05 < p < 0.1$, ** $0.01 < p < 0.05$, *** $0.001 < p < 0.01$, **** $p < 0.001$. P values for glucose not calculated.

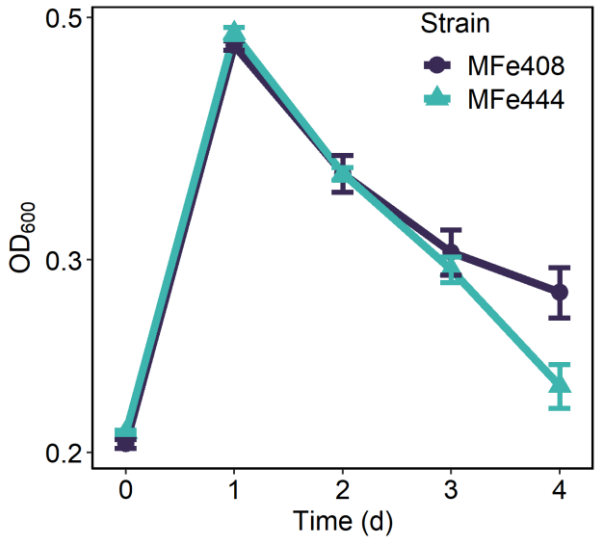

Figure 46. OD_{600} measurements of MFe408 and MFe444 during cathodic electro-fermentation depicted in Figure 45. Strains cultivated in a bioelectrochemical system with 50 mM D-glucose, 5 µM riboflavin, and a cathode poised at -500 $mV_{Ag/AgCl}$.

Table 17. Final concentrations and percent differences of metabolites from MFe408 and MFe444 cathodic electro-fermentation depicted in Figure 45.

	Lactate (mM)	Succinate (mM)	Formate (mM)	Acetate (mM)	Ethanol (mM)
MFe408	12.92 ± 0.37	1.16 ± 0.06	17.78 ± 0.26	7.57 ± 0.04	15.01 ± 0.57
MFe444	12.09 ± 0.01	1.22 ± 0.06	18.21 ± 0.02	7.94 ± 0.04	15.30 ± 0.43
Percent difference	6.4%	5.2%	2.4%	4.9%	1.9%

DISCUSSION

In this work, we demonstrate proof-of-concept that electro-fermentation can be used to influence *E. coli* fermentation product ratios, providing a potential mechanism for overcoming the redox balance restrictions of traditional fermentation. We show that an engineered *E. coli* strain MFe444 can use the fermentable sugar glucose for electro-fermentation and the electrode potential influences fermentation product ratios. The shift

in fermentation product ratios during anodic electro-fermentation toward oxidized products and away from reduced products is justified by the changes in electron transfer capabilities between the two strains. MFe444 increases electron transfer to the electrode by 104% over MFe408 with the Mtr pathway. This is accompanied by a 2.5% decrease in electrons routed towards fermentation products, but only a 0.9% decrease in carbon to fermentation products. The greater difference in electrons than carbon being directed to fermentation is directly observable in the fermentation product ratio, accounting for the decrease in lactate and succinate and concurrent increase in formate and acetate.

While the electrode clearly has influence over the fermentation product ratios, the difference of “lost” electrons in the fermentation pathway of MFe444 cannot be completely explained by extracellular electron transfer. MFe444 produces 2.7 mmol fewer electrons in the form of fermentation products’ chemical bonds than MFe408. The difference in electrons deposited on the anode is only 0.101 mmol, which accounts for only 3.7% of the electrons removed from the fermentation pathway. We hypothesize the anode may also be responsible for regulatory changes that provide additional mechanisms of altering fermentation pathway flux beyond the redirection of electrons to the anode. Changes in regulation were also observed in MFe444 when exposed to a cathode electrode previously.[36]

We also show that influence over the fermentation product ratios can be achieved by cultivating MFe444 anaerobically in culture tubes with solid iron as the terminal electron acceptor. This set up may be more accessible and reasonable to scale up than bioelectrochemical systems, making it a viable alternative method. Cultivating MFe444 with iron as the terminal electron acceptor generated lower amounts of the fermentation

products than during anodic electro-fermentation, except in the case of succinate. The fermentation product ratios in the iron reducing cultures resemble that of the anodic electro-fermentation for changes in lactate and acetate production, but not in succinate and formate production. In iron reduction cultures, MFe444 produces 27.6% less lactate and 2.6% more acetate, whereas during anodic electro-fermentation MFe444 produces 19.0% less lactate and 16.4% more acetate. These changes reflect the expected observation that less reduced products and more oxidized products would be produced more in a system where electrons are transported out of the cell.

Cultivation with iron as the terminal electron acceptor deviates from expectations for other metabolites, with MFe444 producing 7.0% more succinate and 17.4% less formate than MFe408. This is contrasted with the expected effect observed in the anodic electro-fermentation, where MFe444 produced 28.5% less succinate and 10.4% more formate. Another explanation for the differences between anodic electro-fermentation and iron reduction cultures could be the atmosphere in which they were cultivated. Bioelectrochemical systems were continually sparged with N_2 whereas the iron reduction cultures were incubated in an anaerobic chamber containing 95% N_2 and 5% H_2. H_2 and formate metabolism are linked through the quinone pool and through formate hydrogen lyase.[46,47] The presence of H_2 could therefore be a cause of altered formate metabolism. Additionally, the initial glucose concentrations were different between the conditions. The iron reduction cultures contained 20 mM D-glucose to create an electron-acceptor limited environment to encourage extracellular electron transfer to Fe_2O_3. D-glucose was included at 50 mM in the bioelectrochemical reactors because the anode acts as a limitless electron acceptor. The greater availability of glucose in the bioelectrochemical reactors provided

more carbon to the system and it is therefore reasonable that MFe444 produces a greater amount of fermentation products than in the iron-reducing cultures. The fine-tuning of aspects such as glucose concentrations and atmospheric composition could be useful tools in refining MFe444 fermentation.

MFe444 uses inward electron transfer to take up 90.3% more electrons from the cathode than MFe408. This is accompanied by a 0.3% increase in electrons and a 1.1% increase in carbon routed to fermentation products. While cathodic electro-fermentation displays operational inward electron transfer via the Mtr pathway, the effect on fermentation products is less pronounced. Overall, the maximum current, total charge transfer, and shift in metabolites was smaller for the cathodic electro-fermentation than for the anodic electro-fermentation. This is consistent with studies on the Mtr pathway in *S. oneidensis*, which generally indicate lower cathodic current than anodic current.[30,48–51] Inward electron transfer during *E. coli* cathodic electro-fermentation may be hindered by a limitation of proton-motive force. We have previously shown that in *S. oneidensis*, inward electron transfer to NAD^+ can occur but is dependent on proton-motive force because it requires reverse activity of respiratory NADH dehydrogenases.[29,52] Without a robust source of ATP or proton motive force generation, electron transfer from respiratory quinones to NAD^+ is limited.

Taken together, these data show that the fermentation products of electroactive *E. coli* can be influenced by the availability of reducing equivalents, and that this can be exploited for use in unbalanced fermentation. The Mtr pathway can operate in both the inward and outward electron transfer directions, which can allow the user to control production of more reduced or more oxidized products. Further strain and methodological

optimization could enhance control over fermentation product ratios. For example, expression of a periplasmic electron carrier such as *S. oneidensis* FccA could improve electron transfer rates between CymA and MtrCAB; and greater electrode potentials could create a stronger electron source or sink thus more greatly favoring reduced or oxidized fermentation products. Control over the availability of reducing equivalents during *E. coli* electro-fermentation could be a useful tool for optimizing biosynthesis of various products that are currently limited by the redox balance constraints of traditional fermentations.

FUNDING SOURCES

This work was supported by a 2018 Beckman Young Investigator Award and a National Science Foundation CAREER Award (1750785) to MT. CG was partially supported by the MSU Building Bridges Program.

REFERENCES

1. Müller, V. Bacterial Fermentation. in *eLS* (Wiley, 2008). doi:https://doi.org/10.1002/9780470015902.a0001415.pub2.

2. Folch, P. L., Bisschops, M. M. M. & Weusthuis, R. A. Metabolic energy conservation for fermentative product formation. *Microb Biotechnol* **14**, 829–858 (2021).

3. Clark, D. The fermentation pathways of *Escherichia coli*. *FEMS Microbiol Rev* **63**, 223–234 (1989).

4. Diaz, A. B., Blandino, A. & Caro, I. Value added products from fermentation of sugars derived from agro-food residues. *Trends Food Sci Technol* **71**, 52–64 (2018).

5. Iram, A., Ozcan, A., Turhan, I. & Demirci, A. Production of Value-Added Products as Food Ingredients via Microbial Fermentation. *Processes* **11**, 1715 (2023).

6. Tse, T. J., Wiens, D. J., Chicilo, F., Purdy, S. K. & Reaney, M. J. T. Value-Added Products from Ethanol Fermentation—A Review. *Fermentation* **7**, 267 (2021).

7. Martínez, J. L., Liu, L., Petranovic, D. & Nielsen, J. Pharmaceutical protein production by yeast: towards production of human blood proteins by microbial fermentation. *Curr Opin Biotechnol* **23**, 965–971 (2012).

8. Elander, R. P. Industrial production of β-lactam antibiotics. *Appl Microbiol Biotechnol* **61**, 385–392 (2003).

9. Seo, S.-O. & Jin, Y.-S. Next-Generation Genetic and Fermentation Technologies for Safe and Sustainable Production of Food Ingredients: Colors and Flavorings. *Annu Rev Food Sci Technol* **13**, 463–488 (2022).

10. Kracke, F., Lai, B., Yu, S. & Krömer, J. O. Balancing cellular redox metabolism in microbial electrosynthesis and electro fermentation – A chance for metabolic engineering. *Metab Eng* **45**, 109–120 (2018).

11. Yamada, S., Takamatsu, Y., Ikeda, S., Kouzuma, A. & Watanabe, K. Towards Application of Electro-Fermentation for the Production of Value-Added Chemicals From Biomass Feedstocks. *Front Chem* **9**, (2022).

12. Sravan, J. S., Butti, S. K., Sarkar, O. & Mohan, S. V. Electrofermentation. in *Microbial Electrochemical Technology* 723–737 (Elsevier, 2019). doi:10.1016/B978-0-444-64052-9.00029-7.

13. Xu, S., Jangir, Y. & El-Naggar, M. Y. Disentangling the roles of free and cytochrome-bound flavins in extracellular electron transport from *Shewanella oneidensis* MR-1. *Electrochim Acta* **198**, 49–55 (2016).

14. Marsili, E. *et al. Shewanella* secretes flavins that mediate extracellular electron transfer. *PNAS* **105**, 3968–3973 (2008).

15. Brutinel, E. D. & Gralnick, J. A. Shuttling happens: soluble flavin mediators of extracellular electron transfer in *Shewanella*. *Appl Microbiol Biotechnol* **93**, 41–48 (2012).

16. Okamoto, A., Nakamura, R. & Hashimoto, K. In-vivo identification of direct electron transfer from *Shewanella oneidensis* MR-1 to electrodes via outer-membrane OmcA–MtrCAB protein complexes. *Electrochim Acta* **56**, 5526–5531 (2011).

17. Hartshorne, R. S. *et al.* Characterization of *Shewanella oneidensis* MtrC: a cell-surface decaheme cytochrome involved in respiratory electron transport to extracellular electron acceptors. *J Biol Inorg Chem* **12**, 1083–1094 (2007).

18. Firer-Sherwood, M., Pulcu, G. S. & Elliott, S. J. Electrochemical interrogations of the Mtr cytochromes from *Shewanella*: opening a potential window. *J Biol Inorg Chem* **13**, 849–854 (2008).

19. Idalia, V.-M. N. & Bernardo, F. *Escherichia coli* as a Model Organism and Its Application in Biotechnology. in *Escherichia coli - Recent Advances on Physiology, Pathogenesis and Biotechnological Applications* (ed. Samie, A.) 253–274 (IntechOpen, Rijeka, 2017). doi:10.5772/67306.

20. Lee, Y., Lee, J. & Kim, S. Direct extracellular electron transfer from *Escherichia coli* through modified carbon nanoparticles. *Electrochim Acta* **437**, 141497 (2023).

21. Pitts, K. E. *et al.* Characterization of the *Shewanella oneidensis* MR-1 Decaheme Cytochrome MtrA. *J Biol Chem* **278**, 27758–27765 (2003).

22. Gescher, J. S., Cordova, C. D. & Spormann, A. M. Dissimilatory iron reduction in *Escherichia coli* : identification of CymA of *Shewanella oneidensis* and NapC of *E. coli* as ferric reductases. *Mol Microbiol* **68**, 706–719 (2008).

23. Schuetz, B., Schicklberger, M., Kuermann, J., Spormann, A. M. & Gescher, J. Periplasmic Electron Transfer via the *c* -Type Cytochromes MtrA and FccA of *Shewanella oneidensis* MR-1. *Appl Environ Microbiol* **75**, 7789–7796 (2009).

24. Jensen, H. M., TerAvest, M. A., Kokish, M. G. & Ajo-Franklin, C. M. CymA and Exogenous Flavins Improve Extracellular Electron Transfer and Couple It to Cell Growth in Mtr-Expressing *Escherichia coli*. *ACS Synth Biol* **5**, 679–688 (2016).

25. Marritt, S. J. *et al.* A functional description of CymA, an electron-transfer hub supporting anaerobic respiratory flexibility in *Shewanella*. *Biochem J* **444**, 465–474 (2012).

26. Myers, C. R. & Myers, J. M. Cloning and sequence of cymA, a gene encoding a tetraheme cytochrome *c* required for reduction of iron(III), fumarate, and nitrate by Shewanella putrefaciens MR-1. *J Bacteriol* **179**, 1143–1152 (1997).

27. Coursolle, D. & Gralnick, J. A. Reconstruction of Extracellular Respiratory Pathways for Iron(III) Reduction in *Shewanella oneidensis* Strain MR-1. *Front Microbiol* **3**, (2012).

28. Coursolle, D., Baron, D. B., Bond, D. R. & Gralnick, J. A. The Mtr Respiratory Pathway Is Essential for Reducing Flavins and Electrodes in *Shewanella oneidensis*. *J Bacteriol* **192**, 467–474 (2010).

29. Tefft, N. M. & Teravest, M. A. Reversing an Extracellular Electron Transfer Pathway for Electrode-Driven Acetoin Reduction. *ACS Synth Biol* **8**, 1590–1600 (2019).

30. Ross, D. E., Flynn, J. M., Baron, D. B., Gralnick, J. A. & Bond, D. R. Towards Electrosynthesis in *Shewanella*: Energetics of Reversing the Mtr Pathway for Reductive Metabolism. *PLoS One* **6**, e16649 (2011).

31. Rowe, A. R. *et al.* Identification of a pathway for electron uptake in *Shewanella oneidensis*. *Commun Biol* **4**, 957 (2021).

32. Rowe, A. R. *et al.* Tracking Electron Uptake from a Cathode into *Shewanella* Cells: Implications for Energy Acquisition from Solid-Substrate Electron Donors. *mBio* **9**, (2018).

33. TerAvest, M. A. & Ajo-Franklin, C. M. Transforming exoelectrogens for biotechnology using synthetic biology. *Biotechnol Bioeng* **113**, 687–697 (2016).

34. Lienemann, M. *et al.* Towards patterned bioelectronics: facilitated immobilization of exoelectrogenic *Escherichia coli* with heterologous pili. *Microb Biotechnol* **11**, 1184–1194 (2018).

35. TerAvest, M. A., Zajdel, T. J. & Ajo-Franklin, C. M. The Mtr Pathway of *Shewanella oneidensis* MR-1 Couples Substrate Utilization to Current Production in *Escherichia coli*. *ChemElectroChem* **1**, 1874–1879 (2014).

36. Baruch, M., Tejedor-Sanz, S., Su, L. & Ajo-Franklin, C. M. Electronic control of redox reactions inside *Escherichia coli* using a genetic module. *PLoS One* **16**, e0258380 (2021).

37. Stookey, L. L. Ferrozine---a new spectrophotometric reagent for iron. *Anal Chem* **42**, 779–781 (1970).

38. R Core Team. R: A language and environment for statistical computing. *R Foundation for Statistical Computing* Preprint at https://www.R-project.org/ (2021).

39. H. Wickham. ggplot2: Elegant Graphics for Data Analysis. Preprint at (2016).

40. Hadley Wickham, Romain François, Lionel Henry & Kirill Müller. dplyr: A Grammar of Data Manipulation. *R package version 1.0.9* Preprint at https://CRAN.R-project.org/package=dplyr (2022).

41. Garnier, S. *et al.* viridis(Lite) - Colorblind-Friendly Color Maps for R. (2023).

42. Ulrich, J. TTR: Technical Trading Rules. (2021).

43. Auguie, B. gridExtra: Miscellaneous Functions for 'Grid' Graphics. Preprint at (2017).

44. Förster, A. H. & Gescher, J. Metabolic Engineering of *Escherichia coli* for Production of Mixed-Acid Fermentation End Products. *Front Bioeng Biotechnol* **2**, (2014).

45. Song, C. W., Kim, D. I., Choi, S., Jang, J. W. & Lee, S. Y. Metabolic engineering of *Escherichia coli* for the production of fumaric acid. *Biotechnol Bioeng* **110**, 2025–2034 (2013).

46. Meshulam-Simon, G., Behrens, S., Choo, A. D. & Spormann, A. M. Hydrogen Metabolism in *Shewanella oneidensis* MR-1. *Appl Environ Microbiol* **73**, 1153–1165 (2007).

47. Kane, A. L. *et al.* Formate Metabolism in *Shewanella oneidensis* Generates Proton Motive Force and Prevents Growth without an Electron Acceptor. *J Bacteriol* **198**, 1337–1346 (2016).

48. Yang, Y. *et al.* Enhancing Bidirectional Electron Transfer of *Shewanella oneidensis* by a Synthetic Flavin Pathway. *ACS Synth Biol* **4**, 815–823 (2015).

49. Coursolle, D., Baron, D. B., Bond, D. R. & Gralnick, J. A. The Mtr Respiratory Pathway Is Essential for Reducing Flavins and Electrodes in *Shewanella oneidensis*. *J Bacteriol* **192**, 467–474 (2010).

50. Ford, K. C. & TerAvest, M. A. The electron transport chain of *Shewanella oneidensis* MR-1 can operate bidirectionally to enable microbial electrosynthesis. *Appl Environ Microbiol* **90**, (2024).

51. Madsen, C. S. & TerAvest, M. A. NADH dehydrogenases Nuo and Nqr1 contribute to extracellular electron transfer by *Shewanella oneidensis* MR-1 in bioelectrochemical systems. *Sci Rep* **9**, 14959 (2019).

52. Ford, K. C. & TerAvest, M. A. The electron transport chain of *Shewanella oneidensis* MR-1 can operate bidirectionally to enable microbial electrosynthesis. *Appl Environ Microbiol* **90**, (2024).

53. Lee, S. H. S. Importance of redox balance on the production of succinic acid by metabolically engineered *Escherichia coli*. *Appl Microbiol Biotechnol* **58**, 286–290 (2002).

54. Goldbeck, C. P. *et al*. Tuning Promoter Strengths for Improved Synthesis and Function of Electron Conduits in *Escherichia Coli*. *ACS Synth Biol 2* (3), 150–159 (2013).

55. Arslan, E. *et al*. Overproduction of The *Bradyrhizobium Japonicum* C-Type Cytochrome Subunits of Thecbb3Oxidase In *Escherichia coli*. *Biochem Biophys Res Commun 251* (3), 744–747 (1998).

56. Jensen, H. M. *et al*. Engineering of a Synthetic Electron Conduit in Living Cells. *PNAS 107* (45), 19213-19218, (2010).

CHAPTER 6:

CONCLUSION

OBJECTIVES

This dissertation presents original work toward developing *S. oneidensis* and *E. coli* as improved hosts for MES. Both organisms have strengths that make them attractive options for creating improved MES strains (pages 9 and 20). Currently, MES strains comprised of acetogens or mixed cultures are limited in their product scope, off-target production, and small genetic toolbox.[1–3] Acetate remains the main product for both biocatalysts, and off-target methane production plagues mixed-culture MES due to methanogen populations.[1] Since these organisms are not as well understood as model organisms like *S. oneidensis* and *E. coli*, there remain open questions for how to divert production away from acetate and toward more valuable products. Additionally, their limited tools for genetic engineering cause roadblocks for implementing what little insights do exist for improving product production and scope.[1–6]

S. oneidensis is a promising MES host as it is a model organism for EET, having well characterized metabolome, proteome, transcriptome, and genome.[7–12] The Mtr pathway which drives both OET and IET has been the subject of many characterization and practical studies.[13–21] Researchers have a good understanding of how to manipulate EET in *S. oneidensis* to provide desired system modifications. Additionally, there is some evidence that *S. oneidensis* has reversible formate dehydrogenases which can catalyze CO_2 reduction under cathodic potentials.[22] This is important because it suggests that if formate assimilation can be engineered in this organism, it could use CO_2 as a carbon and energy source. The objective of Chapter 2 was to engineer a formate-tolerant strain of *S. oneidensis* as a first step toward developing formatotrophy in this organism. Chapter 3 aimed to characterize Rnf, an important enzyme which connects the ferredoxin and NADH

pools that could be a source of low potential electrons for CO_2 fixation. Finally, the influence of a common inducer molecule used in strain development was characterized in Chapter 4.

E. coli is a model organism with a vast number of pathways engineered for fermentative biosynthesis of value-added product production,[23–27] which could be expressed in a MES-compatible strain. This would immediately greatly expand the product scope of MES. *E. coli* has previously been engineered to fix CO_2, showing that this feat is achievable in this organism.[28–30] Additionally, EET was introduced in strain MFe444.[31] Together these two engineering strategies could be used to generate an MES-compatible *E. coli* host. Chapter 5 investigates the potential for MFe444 to be used in a BES using a fermentable carbon source.

CONTRIBUTION OF PRESENTED WORK TOWARD DEVELOPMENT OF *S. ONEIDENSIS* AS A MES HOST

This dissertation contributes toward the development of *S. oneidensis* as a MES host by describing the evolution of a formate-tolerant strain, characterization of electron transfer enzyme Rnf, and phenotype assessment of IPTG on the wild-type strain.

In Chapter 2, a formate-tolerant strain of *S. oneidensis* is described. As formate is toxic to this organism, a formate-tolerant strain could improve future efforts at development of formatotrophy. The formate tolerant strains were generated through adaptive laboratory evolution in minimal lactate medium with increasing concentrations of formate. After just 30 days, eight strains were obtained which were tolerant to 100 mM formate. The sequencing of individual colonies from each evolution line revealed that two mutations appeared to be aiding in formate tolerance. The first was a substitution in sodium-

dependent bicarbonate transporter encoded by SO_3758. This transporter had a substitution in the binding pocket which brought the predicted binding affinity of formate much closer to the predicted binding affinity of the native substrate bicarbonate. This points to the role of this alteration being improved formate efflux, thus preventing toxic accumulation of formate in the cells. Another gene whose mutation improved formate tolerance was SO_1320. This gene had different mutations in different strains affecting protein residues V106I, V106F, and S52I. As a protein of unknown function, it is unclear what benefit these substitutions provide. The protein product is expected to localize to the cell membrane, which could indicate transporter activity or aid in membrane integrity. This first step toward developing a formate tolerant strain of *S. oneidensis* could pave the way for further development as a formatotroph. Development of an MES host could come from a formatotrophic strain through the CO_2 reductase activity of formate dehydrogenase or through the electrochemical reduction of CO_2 in the MES reactor.

The *S. oneidensis* Rnf complex was characterized in Chapter 3, as the Rnf complex is a respiratory enzyme with potential ties to the EET pathways. The Rnf complex connects the ferredoxin and NADH pools and could be an important source of low-potential electrons for CO_2 fixation. [32] This study found that in *S. oneidensis* growing on minimal lactate medium, Rnf operates in the reduced ferredoxin-forming direction and is powered by PMF. Importantly, a connection between Rnf and the iron-sulfur cluster formation and repair enzyme cysteine desulfurase, IscS, was established. IscS is a reduced ferredoxin-dependent enzyme which contributes to the synthesis and repair of cellular iron-sulfur clusters. This is activity which influences numerous enzymes, and the effects propagate throughout the cell. This work explored the metabolomic profile of Rnf and IscS CRISPRi

knockdown strains and found that they similarly accumulate MEP pathway metabolites. As the MEP pathway requires both ISC proteins (IspG and IspH) and reduced ferredoxins, it is a great example for how Rnf activity affects ISC biosynthesis and repair. We posit that the effect of Rnf is two-pronged across species. First is that Rnf generates reduced ferredoxins for enzymes requiring it as a cofactor. This includes both ISC proteins such as Nif, SoxR, and IspG and non-ISC proteins such as Fpr and IscS. The second prong is that Rnf provides reduced ferredoxins for ISC biosynthesis and repair. Disruption to this process is propagated throughout the cell, impacting activities of both ferredoxin-dependent ISC proteins such as Nif, SoxR, and IspG, as well as non-ferredoxin-dependent ISC proteins such as Nth, Nuo, and Acn. This connection of Rnf to multiple pathways can explain how its activity has been attributed to the function of many seemingly unrelated enzymes in the literature. These findings indicate that Rnf could be an important source of reduced ferredoxins for the EET pathway as well, as some evidence exists for reduction of the quinone pool by reduced ferredoxin-dependent enzymes in other species.[33,34]

The effect of IPTG on the growth of wild-type *S. oneidensis* on NAG was discussed in Chapter 4. *S. oneidensis* cannot use most six carbon sugars, including glucose, as a substrate because of missing genes for glucose permease, glucose kinase, and 6-phosphofructokinse.[35,36] However, NAG is one of the few six carbon sugars that can be metabolized by this organism through conversion of the sugar to fructose 6-phosphate which enters metabolism at glycolysis. [37] Because of this, NAG is commonly used as a sugar substrate for *S. oneidensis* during phenotype assessments of engineered strains. The work described in Chapter 4 shows that the common inducer molecule IPTG enhances growth of wild-type *S. oneidensis* on NAG. This is an important effect for all

researchers developing engineered *S. oneidensis* strains because it could lead to false positive correlations between a heterologous protein and the desired outcome. This is especially important when developing an MES strain because one of the main goals for MES is to generate high titers of value-added products. Expression of heterologous genes from an IPTG-inducible promoter is an inefficient method for scaled-up MES processes because plasmid maintenance through the addition of antibiotics and induction of gene expression through the addition of IPTG can dramatically raise costs. For design and screening purposes, this is the most efficient way to test the utility of various genomic additions. However, a strain suitable for scale-up would require the transfer of the gene to the genome and preferably under the control of a constitutive promoter. If a false positive correlation between the preliminary engineered strain and improved titers is due to the inducer, both time and funding will be spent on the development of an inducer-free strain, which would not yield the same results. Therefore, it is imperative to understand the interactions of inducers on the native system.

IPTG does impact growth of *S. oneidensis* on NAG under both aerobic and anaerobic conditions, although the effect is more pronounced under anaerobic conditions. However, IPTG does not appear to affect the strain's growth on other common substrates such as lactate and acetate.

FUTURE DIRECTIONS FOR DEVELOPING *S. ONEIDENSIS* AS A MES HOST

The analysis of the formate tolerant strains indicates that short-term evolution in increasing formate concentrations may not be enough to evolve a formate-assimilating mechanism. Rather, because improved formate efflux grants the cells greater tolerance, it appears that these strains highlight the toxicity of formate to *S. oneidensis*. A longer

evolution with smaller steps in formate concentration may be required for the evolution of a strain with formate-consuming ability. Alternatively, creating an *S. oneidensis* strain which requires formate for growth could be a promising approach. A formate-dependent strain could be evolved to improve its formate utilization to the point of supporting biomass production form the once-toxic molecule.

Replication of Davies' results[22] that *S. oneidensis* formate dehydrogenases can catalyze CO_2 reduction under cathodic potentials is an important next step for developing a MES-compatible strain. If formatotrophy can be evolved or engineered in *S. oneidensis*, the conversion of the formatotrophic strain to an autotrophic strain relies upon the capability of reducing CO_2 to formate. Anaerobic pre-culturing of the formatotrophic strain would be imperative as formate dehydrogenases have been shown to be oxygen sensitive. Formate production from CO_2 would require cultivation under cathodic potentials, thus providing electrons for the reduction reaction. An increase in current upon flushing the BES with CO_2 would indicate that CO_2 reduction is occurring and could be confirmed by monitoring formate levels via HPLC during the course of the experiment.

Should a formatotrophic or autotrophic strain of *S. oneidensis* be successfully created in the future, it is imperative to test for IPTG-correlated changes in metabolism once again. This is necessary to determine if IPTG is a suitable inducer to test strains engineered for value-added product production from formate and CO_2.

Additional studies on the Rnf complex and participation of reduced ferredoxins in EET could be beneficial for generating a more complete picture of electron transfer in *S. oneidensis*. Since the *S. oneidensis* electron transport chain is a branched pathway, it would be unsurprising to find a yet unidentified link connecting low-potential electrons from

ferredoxin to the EET pathway. In this work, Rnf activity was characterized during aerobic growth on minimal lactate medium. For a more comprehensive understanding of this complex, additional characterization using other minimal media substrates, rich media, and anoxic conditions can be done. Rnf activity is expected to be reversible, and this characteristic could be observed through the oxidation of ferredoxin under different conditions. Our examination of Rnf began with the hypothesis that it could be beneficial for engineering autotrophy in this organism. Therefore, additional experiments should be conducted which examines the feasibility of using reduced ferredoxins to drive CO_2 reduction in *S. oneidensis*.

Repetition of experiments described in this work for Rnf characterization should also be performed in *E. coli*. To date, the only function Rnf is known to have in *E. coli* is for its participation in SoxR reduction. In this work, we present a model for Rnf activity across species in that it is essential for ISC biosynthesis and repair. Testing of this model in other organisms is essential for confirmation of this model.

CONTRIBUTAION OF PRESENTED WORK TOWARD DEVELOPMENT OF *E. COLI* AS A MES HOST

As one of the most well-studied microbial production hosts, conversion of *E. coli* to a MES host would bring along a plethora of pathways for implementing CO_2 conversion to value-added products.[23–27] *E. coli* strain MFe444 was previously engineered to participate in EET via heterologous expression of the Mtr pathway.[31] Testing of this strain has only been carried out with lactate, a non-fermentable carbon and electron source, in order to display proof-of-concept that the pathway is functional.[31] Without electron acceptors, *E. coli* ferments glucose. Fermentation balances redox reactions to gain energy in an

environment which makes respiration impossible. This careful balance of fermentation products is a major constraint in *E. coli* fermentative biosynthesis reactions. Therefore, EET in *E. coli* serves two functions. The first is to allow for unbalanced fermentation, relieving redox balance constraints and opening avenues for greater product yields. The second is to connect the cells to an electrode, a necessary step for engineering this host for MES. Chapter 5 discusses work that explores the biotechnological potential of the strain by using the fermentable sugar glucose as a carbon and electron donor in both anodic and cathodic electro-fermentation in BESs.

This work demonstrates that MFe444 can use an anode as an electron sink via OET, drawing electrons away from the production of reduced fermentation products lactate and succinate and toward production of oxidized fermentation products formate and acetate. Alternatively, MFe444 can use a cathode as an electron donor via IET, influencing the fermentation product ratios toward the reduced products and away from the oxidized products. This control of fermentation product ratios could be an important tool in optimizing *E. coli* as an MES host because it removes the redox balance constraint which is present in standard *E. coli* fermentative biosynthesis reactions. This could make MES attractive not only for its conversion of CO_2 and clean electricity, but also for potentially higher titers than the same molecule production by traditional fermentation.

FUTURE DIRECTIONS FOR DEVELOPING *E. COLI* AS A MES HOST

MFe444 appears to be a promising host for electro-fermentation. However, it does not have CO_2-fixing capabilities, making it ill-suited for MES at this stage. To create an MES-compatible *E. coli* strain, it is necessary to connect the EET capabilities of MFe444 to the CO_2 fixing capabilities of other engineered strains. One possible way to accomplish

this is to add the Mtr and Ccm vectors from MFe444 to previously engineered CO_2-fixing *E. coli*. This would be the quickest and most efficient way to test whether the combination of these activities allows for product production from CO_2 in a BES. This approach would be more efficient than engineering CO_2 production in *E. coli*, because as discussed in Chapter 5, the engineering of CO_2 fixation in a heterotrophic organism is a challenging feat. On the contrary, EET can be transferred to *E. coli* by transforming two vectors into the host.

Should the transfer of EET via expression of MtrCAB, CymA, and Ccm proteins create a strain capable of MES, the next step would be integration of these proteins in the genome. This would create a more stable strain with no antibiotic requirements, thus keeping production costs down. As the cytochrome maturation proteins used in MFe444 are those from *E. coli*, replacing the native promoter on the genome with a stronger constitutive promoter could eliminate the need for another copy of the genes elsewhere in the genome.

CONCLUDING REMARKS

MES could be a powerful technology for aiding in the turn away from fossil fuels. While current biocatalysts are limited in their product scope and potential for genetic engineering, development of additional strains could be the answer this technology needs to become industrially relevant. This dissertation outlines the progress toward development of more versatile and robust MES biocatalysts from *S. oneidensis* and *E. coli*. Future building upon this work could have great potential for aiding in the fight against climate change.

REFERENCES

1. Prévoteau, A., Carvajal-Arroyo, J. M., Ganigué, R. & Rabaey, K. Microbial electrosynthesis from CO_2: forever a promise? *Curr Opin Biotechnol* **62**, 48–57 (2020).

2. Rosenbaum, M. A. & Henrich, A. W. Engineering microbial electrocatalysis for chemical and fuel production. *Curr Opin Biotechnol* **29**, 93–98 (2014).

3. Schiel-Bengelsdorf, B. & Dürre, P. Pathway engineering and synthetic biology using acetogens. *FEBS Lett* **586**, 2191–2198 (2012).

4. Arends, J. B. A., Patil, S. A., Roume, H. & Rabaey, K. Continuous long-term electricity-driven bioproduction of carboxylates and isopropanol from CO_2 with a mixed microbial community. *J CO_2 Util* **20**, 141–149 (2017).

5. Ganigué, R., Puig, S., Batlle-Vilanova, P., Balaguer, M. D. & Colprim, J. Microbial electrosynthesis of butyrate from carbon dioxide. *Chem Comm* **51**, 3235–3238 (2015).

6. Raes, S. M. T., Jourdin, L., Buisman, C. J. N. & Strik, D. P. B. T. B. Continuous Long-Term Bioelectrochemical Chain Elongation to Butyrate. *ChemElectroChem* **4**, 386–395 (2017).

7. Pinchuk, G. E. *et al.* Pyruvate and Lactate Metabolism by *Shewanella oneidensis* MR-1 under Fermentation, Oxygen Limitation, and Fumarate Respiration Conditions. *Appl Environ Microbiol* **77**, 8234–8240 (2011).

8. Beliaev, A. S. *et al.* Global Transcriptome Analysis of *Shewanella oneidensis* MR-1 Exposed to Different Terminal Electron Acceptors. *J Bacteriol* **187**, 7138–7145 (2005).

9. Leaphart, A. B. *et al.* Transcriptome Profiling of *Shewanella oneidensis* Gene Expression following Exposure to Acidic and Alkaline pH. *J Bacteriol* **188**, 1633–1642 (2006).

10. Pinchuk, G. E. *et al.* Constraint-Based Model of *Shewanella oneidensis* MR-1 Metabolism: A Tool for Data Analysis and Hypothesis Generation. *PLoS Comput Biol* **6**, e1000822 (2010).

11. Cao, X., Qi, Y., Xu, C., Yang, Y. & Wang, J. Transcriptome and metabolome responses of *Shewanella oneidensis* MR-1 to methyl orange under microaerophilic and aerobic conditions. *Appl Microbiol Biotechnol* **101**, 3463–3472 (2017).

12. Heidelberg, J. F. *et al.* Genome sequence of the dissimilatory metal ion–reducing bacterium *Shewanella oneidensis*. *Nat Biotechnol* **20**, 1118–1123 (2002).

13. Brutinel, E. D. & Gralnick, J. A. Shuttling happens: soluble flavin mediators of

extracellular electron transfer in *Shewanella*. *Appl Microbiol Biotechnol* **93**, 41–48 (2012).

14. Kouzuma, A. Molecular mechanisms regulating the catabolic and electrochemical activities of *Shewanella oneidensis* MR-1. *Biosci Biotechnol Biochem* **85**, 1572–1581 (2021).

15. Richardson, D. J. *et al.* The 'porin–cytochrome' model for microbe-to-mineral electron transfer. *Mol Microbiol* **85**, 201–212 (2012).

16. Beblawy, S. *et al.* Extracellular reduction of solid electron acceptors by *Shewanella oneidensis*. *Mol Microbiol* **109**, 571–583 (2018).

17. Kane, A. L. *et al.* Formate Metabolism in *Shewanella oneidensis* Generates Proton Motive Force and Prevents Growth without an Electron Acceptor. *J Bacteriol* **198**, 1337–1346 (2016).

18. Madsen, C. S. & TerAvest, M. A. NADH dehydrogenases Nuo and Nqr1 contribute to extracellular electron transfer by *Shewanella oneidensis* MR-1 in bioelectrochemical systems. *Sci Rep* **9**, 14959 (2019).

19. Ford, K. C. & TerAvest, M. A. The electron transport chain of *Shewanella oneidensis* MR-1 can operate bidirectionally to enable microbial electrosynthesis. *Appl Environ Microbiol* **90**, (2024).

20. Tefft, N. M. & Teravest, M. A. Reversing an Extracellular Electron Transfer Pathway for Electrode-Driven Acetoin Reduction. *ACS Synth Biol* **8**, 1590–1600 (2019).

21. Tefft, N. M., Ford, K. & TerAvest, M. A. NADH dehydrogenases drive inward electron transfer in *Shewanella oneidensis* MR-1. *Microb Biotechnol* **16**, 560–568 (2023).

22. Davies, J. Characterisation of the reversible formate dehydrogenases of *Shewanella*. (University of East Anglia, 2017).

23. Pontrelli, S. *et al. Escherichia coli* as a host for metabolic engineering. *Metab Eng* **50**, 16–46 (2018).

24. Hoesl, M. G. & Budisa, N. Recent advances in genetic code engineering in *Escherichia coli*. *Curr Opin Biotechnol* **23**, 751–757 (2012).

25. Idalia, V.-M. N. & Bernardo, F. *Escherichia coli* as a Model Organism and Its Application in Biotechnology. in *Escherichia coli - Recent Advances on Physiology, Pathogenesis and Biotechnological Applications* (ed. Samie, A.) 253–274 (IntechOpen, Rijeka, 2017). doi:10.5772/67306.

26. Huang, T. & Ma, Y. Advances in biosynthesis of higher alcohols in *Escherichia coli*.

World J Microbiol Biotechnol **39**, 125 (2023).

27. Yang, D., Park, S. Y., Park, Y. S., Eun, H. & Lee, S. Y. Metabolic Engineering of *Escherichia coli* for Natural Product Biosynthesis. *Trends Biotechnol* **38**, 745–765 (2020).

28. Antonovsky, N. *et al.* Sugar Synthesis from CO_2 in *Escherichia coli*. *Cell* **166**, 115–125 (2016).

29. Herz, E. *et al.* The genetic basis for the adaptation of *E. coli* to sugar synthesis from CO_2. *Nat Commun* **8**, 1705 (2017).

30. Gleizer, S. *et al.* Conversion of *Escherichia coli* to Generate All Biomass Carbon from CO_2. *Cell* **179**, 1255-1263.e12 (2019).

31. Jensen, H. M., TerAvest, M. A., Kokish, M. G. & Ajo-Franklin, C. M. CymA and Exogenous Flavins Improve Extracellular Electron Transfer and Couple It to Cell Growth in Mtr-Expressing *Escherichia coli*. *ACS Synth Biol* **5**, 679–688 (2016).

32. Biegel, E., Schmidt, S., González, J. M. & Müller, V. Biochemistry, evolution and physiological function of the Rnf complex, a novel ion-motive electron transport complex in prokaryotes. *CMLS* **68**, 613–634 (2011).

33. St. Maurice, M. *et al.* Flavodoxin:Quinone Reductase (FqrB): a Redox Partner of Pyruvate:Ferredoxin Oxidoreductase That Reversibly Couples Pyruvate Oxidation to NADPH Production in *Helicobacter pylori* and *Campylobacter jejuni*. *J Bacteriol* **189**, 4764–4773 (2007).

34. Bojko, M. & Wieckowski, S. NADPH and ferredoxin:NADP+ oxidoreductase-dependent reduction of quinones and their reoxidation11Preliminary results were presented at the 10th FESPP Congress, Florence, Italy (Plant Physiol. Biochem., Special issue, 1996, p. 99). *Phytochemistry* **50**, 203–208 (1999).

35. Chubiz, L. M. & Marx, C. J. Growth Trade-Offs Accompany the Emergence of Glycolytic Metabolism in *Shewanella oneidensis* MR-1. *J Bacteriol* **199**, (2017).

36. Rodionov, D. A. *et al.* Genomic encyclopedia of sugar utilization pathways in the *Shewanella* genus. *BMC Genomics* **11**, 494 (2010).

37. Yang, C. *et al.* Comparative Genomics and Experimental Characterization of N-Acetylglucosamine Utilization Pathway of *Shewanella oneidensis*. *J Biol Chem* **281**, 29872–29885 (2006).